Journal of the
OPTICAL SOCIETY
of AMERICA

VOLUME 39, NUMBER 1 JANUARY, 1949

Camera Shutters*

AMROM H. KATZ
Photographic Laboratory, Engineering Division, Air Materiel Command, Wright Field, Dayton, Ohio
(Received June 30, 1948)

An extensive program of research into characteristics of shutters, begun in 1941, has resulted in a series of definitions and test methods for between-lens and focal-plane type shutters which have been adopted by the ASA. The characteristics of these two types of shutters, and of louvre shutters, are reviewed, and the important distinction between effective exposure time and actual (or motion-stopping) exposure time in these two shutter types is clarified. The oscillographic test method for between-lens shutters is described and depicted *via* photograph and schematic diagram. The strobotac and drum tester method for focal plane shutters are summarized, as is a method for testing louvre shutters.

The effect of inefficient between-lens shutters on optical performance, effect of a glass pressure plate on efficiency of focal-plane shutters, and equations for the two types of distortion caused by focal plane shutters are discussed. The utilization and advantage of shutter speed in aerial cameras to reduce the deteriorative effects upon definition caused by forward aircraft speed, angular motion of the aircraft about its axis, and camera vibration are discussed.

The shutterless strip camera and the corollary principle of image speed compensation with moving-film magazines in conventional cameras, and the potentialities of this important new development, are described.

The impetus of wartime necessity resulted in development of several new shutters, improvements in others, and consideration of many more types. The Langer multiple-slit focal plane shutter, shutters based on birefringent phenomena, multiple-disk between-lens shutters are considered. Shutter leaves of Be-Al alloy were tried, with conspicuous success. The work done by Mitchell in doubling the speed of the 6-in. K-17 shutter and a detailed analysis of research results obtained in improving the K-22 focal plane shutter are presented.

A louvre-shutter for the 48-in. f:6.3×18 lens was built at the Photographic Laboratory. Photographs and a schematic diagram of this high performance shutter are included. A doctrine of tactical usage and development for shutters has been formulated; mapping cameras will continue to use between-lens shutters, as will night cameras, but the very large day reconnaissance camera will use focal plane shutters exclusively. A list of seventeen memorandum reports, which cover in detail the work summarized in this paper, is appended.

I. Introduction
II. Characteristics of conventional between lens shutters
III. Characteristics of focal plane shutters
IV. Characteristics of louvre shutters
V. Test method for between lens shutters
VI. Test method for focal plane shutters
VII. Test method for louvre shutters
VIII. The effect of shutters on optical performance
IX. The effect of shutters on resolving power of aerial cameras
X. The shutterless strip camera and forward image motion compensation
XI. Wartime progress in shutters
XII. General comparison of shutter types

* Invited paper presented at Symposium on Resolution and Shutters, Boston University Optical Research Laboratory, July 18, 1947.

I. INTRODUCTION

SHUTTERS have been and will continue to be extremely important components of aerial cameras, despite the advent and great potential use of shutterless strip cameras.

As late as 1941 there existed within the struc-

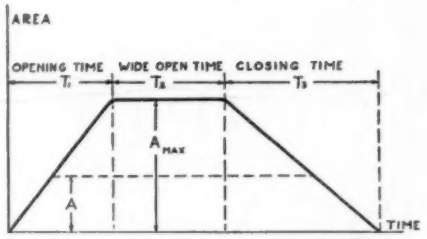

FIG. 1. Efficiency curve of a between-lens shutter.

ture of the photographic industry, here and abroad, no integrated and accepted system of definitions, test methods, and optical theory applicable to either ground or aerial camera shutters. It was clear that advances in shutter design and application to aerial photographic problems had to be preceded by the formulation and dissemination of a consistent and accurate theory of shutters.

Shutter research initiated by Colonel G. W. Goddard, Chief of the Photographic Laboratory of the Air Materiel Command, and conducted by the writer, has led to the development of a series of definitions, test apparatus, and methods applicable to both between-lens and focal plane shutters which have been adopted *in toto* by the American Standards Association as war standards (Z52.62, Z52.63, Z52.64, Z52.65) and are now in the process of being adopted as peacetime permanent standards (Z38.4.22, Z38.4.23, Z38.4.24, Z38.4.25).

Further studies of shutter effects, materials, and use of shutters led to the development of new and improved shutters, modifications to old shutters, and to the development of a general doctrine relating to Air Forces shutters and the direction of future developments.

Except for certain as yet unpublished reports, most of the work to be discussed is found in the appended list of references. These reports are on file at the Air Materiel Command, Wright Field, Ohio, and, in general, are available upon request.

II. CHARACTERISTICS OF CONVENTIONAL BETWEEN-LENS SHUTTERS

The conventional between-lens shutter consists of one or more blades (usually four or five) which are mounted as close to the diaphragm position as possible. In operation, this type of shutter admits light through the center of the lens before it admits light through the peripheral areas of the lens. When fully open, no part of the shutter blades remains in the path of the light through the lens.

The three characteristics of between-lens shutters which are of interest are actual time open, efficiency, and effective speed. A shutter operates in finite time, and, being a mechanism driven neither by infinite power nor having zero mass or moment of inertia, the shutter requires part of its total operating time to open and to close. Consequently, the illumination received in the focal plane varies with the open area of the shutter. Since the amount of light transmitted by the lens-shutter combinations is proportional to the shutter area open, except for small corrections, it is permissible to use the area *vs.* time curve of a shutter interchangeably with the intensity-time curve of the same shutter, and call either one the operating characteristic or efficiency curve. Such a curve is shown in Fig. 1.

Definitions applicable to the three characteristics of the between-lens shutter are:

(a) *Actual time open* or *total open time* of a between-lens shutter is the time interval from the beginning of the opening period to the end of the closing period.

(b) *Efficiency* of a between-lens shutter at a particular diaphragm opening and exposure setting is the ratio of the amount of light transmitted by the shutter to the amount that would have been transmitted had the shutter been wide open for the entire exposure.

(c) *Effective speed* or *effective exposure time* of a between-lens shutter with characteristics of efficiency E, and total open time T, as defined above, is defined as that time of exposure which would permit a quantity of light equal to that actually transmitted by the shutter to pass through the full aperture.

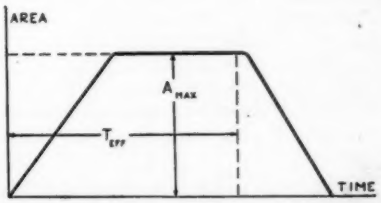

FIG. 2. Basis for definition of effective speed.

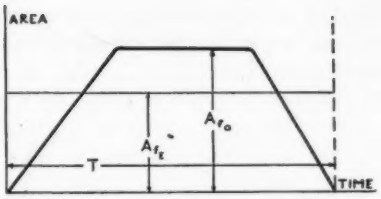

FIG. 3. Basis for definition of effective f/stop.

There is an immediate interest in both the actual time open and effective speeds:

1. From the standpoint of correct exposure, it is necessary to know the effective speed.

2. From the standpoint of "stopping motion," i.e., avoiding blur of the image due to relative movement of camera and subject during exposure, it is necessary to know the actual time open.

From the definition of efficiency given above, it is seen that efficiency E is given by:

$$E=\int_0^T A\,dt/A_{\max}\cdot T. \tag{1}$$

Fortunately, for purposes of both calculation and further analysis, the efficiency curve may be represented rather simply. Thousands of tests made on a great variety of shutters, and using the oscillographic method to be described below, indicate that the opening and closing portions of the efficiency curve are essentially linear. Departures from linearity are, in general, of the second order; of course, for those shutters whose efficiency curves are decidedly non-linear, the basic formula for E (Eq. (1) above) must be used. In the case of linear open and closing portions of the efficiency curve (see Fig. 1) the efficiency is given by

$$E=1-(T_1+T_3)/2T. \tag{2}$$

Consideration of the efficiency curve (Fig. 1) indicates that efficiency increases as a lens is stopped down, for as a lens is stopped down, the opening and closing times are a smaller fraction of the total open time. The exact relationship between efficiency and diaphragm stop will now be derived.

In this discussion, the quantities E_0, T_1, T_2, $A_{\max}$ refer to the constants for the lens-shutter combination when the lens is opened to its maximum area, at stop f_0; E_f and A refer to the corresponding quantities at stop f.

$$A=K/f^2, \quad A_{\max}=K/f_0^2, \tag{3}$$

and

$$E=1-(T_1+T_3)/2T. \tag{2}$$

When the area open is A and not $A_{\max}$, the opening and closing times are a corresponding fraction of T_1 and T_3, so that

$$E=1-(T_1+T_3)/2T\cdot A/A_{\max}. \tag{4}$$

Whereupon, upon substitution from (3) into (4),

$$E=1-(T_1+T_3)/2T\cdot(f_0/f)^2. \tag{5}$$

Hence, if a shutter lens combination is tested at its maximum diaphragm stop f_0 and the efficiency is found to be E_0, which may be written

$$E=1-K, \tag{6}$$

then at any other stop f the efficiency is given by

$$E_f=1-K(f_0/f)^2. \tag{7}$$

It should be noted that knowledge of the efficiency at any f stop enables calculation of the efficiency at any other stop, either greater or smaller.

Consideration of Eqs. (6) and (7) yields a simple working rule: *As a lens is stopped down one full stop the efficiency of the shutter advances halfway to 100 percent from its original value.*

As an example of the foregoing rule, take the case of a lens-shutter combination which has an efficiency of 60 percent at f:4.0. Then at f:5.6 the efficiency is 80 percent, at f:8 it is 90 percent, and f:11 it is 95 percent. This simple rule eliminates the necessity for construction of detailed charts for efficiency as a function of f/stop.

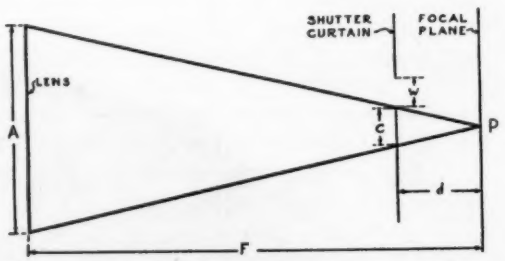

FIG. 4. Schematic drawing of film, lens, and focal plane shutter. A = lens aperture, and F = focal length.

The concept and use of effective speed is firmly ingrained among photographers. This is unfortunate in several respects. First, because manufacturers tend to mark shutters with the effective speed calculated for the maximum opening, this system of marking puts a premium upon inefficiency. As an example, were two shutters with the same actual time open of 1/100 second to have efficiencies of 50 percent and 100 percent respectively, the former and inefficient shutter would be marked 1/200 second, and the latter would be marked 1/100 second. Even using this system, the highest marked speeds on commercial shutters, both of foreign and domestic manufacture, usually exceed the measured effective speeds calculated at full aperture.

Another and more serious difficulty with the marking of shutters in effective speed calculated at the maximum aperture is that a lens-shutter combination is not always used at maximum aperture. For the case of ground cameras, it has been variously and conservatively estimated that no more than 1 percent of all photography, color, black and white, indoor and outdoor, is done at maximum aperture. The formula for efficiency as a function of f stop shows that the effective speed at one stop or more below full aperture is as close or closer to the actual time open as is the effective speed at the maximum aperture. Consequently, if shutters were marked with actual time open, the photographer could use this rating for the effective exposure and at least 99 percent of the time be closer to the true value than were he to use the effective speed calculated at maximum aperture.

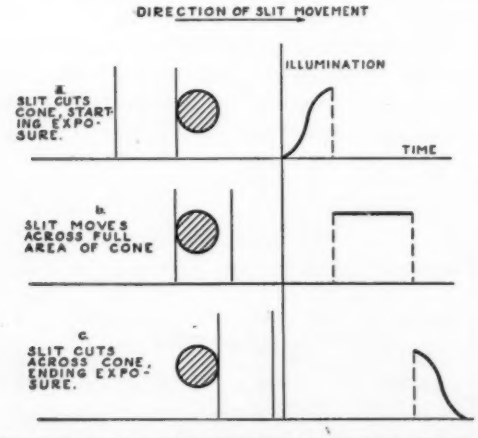

FIG. 5. Variation of illumination in focal plane slit crosses cone of light.

Were not the concept of effective speed so firmly entrenched in photographic literature and practice, the following concept of "effective f stop," first proposed in 1941, would be more vigorously advanced as a better expression of shutter performance.

The bases for the definitions of effective speed and effective f stop are shown in Figs. 2 and 3.

The equation for effective speed is

$$T_{\text{eff}} = \int_0^T A\,dt / A_{\max} \tag{8}$$

and represents a length along the time axis which would block off a rectangle as shown whose area is that of the area under the curve. The averaging in this case is with respect to area.

If now the area under the curve is averaged with respect to time, the average area A_{fE} is

$$A_{fE} = \int_0^T A\,dt / T, \tag{9}$$

and it is clear that the f stop f_E corresponding to this average area will serve as a measure of the efficiency of the shutter at the stop used.

The definition follows:

The "effective f stop" of a lens-shutter combination is that f stop which would allow as much light to pass during the total time of exposure as is passed by the lens and shutter during the exposure.

From Fig. 3, and Eq. (9),

$$A_{fE} = E \cdot A_{f0}. \tag{10}$$

The relationship

$$A_{fE}/A_{f0} = (f_0/f_E)^2 \tag{11}$$

and Eq. (10) yield at once

$$f_E = f_0 E^{-\frac{1}{2}}. \tag{12}$$

An example using both systems of describing shutter performance follows. Consider a shutter and lens combination marked 1/100 second. If tested at f:4.5, the characteristics of this shutter described conventionally might be as follows:

Nominal speed at f:4.5..... 1/100 second
Actual time open..... 1/60 second
Efficiency..... 60 percent
Effective speed at f:4.5..... 1/100 second.

On this system, using the concept of "effective f stop," the description would be:

Nominal speed at f:4.5..... 1/100 second
Actual time open..... 1/60 second
Efficiency..... 60 percent
Effective f stop at f:4.5..... $4.5/(0.6)^{\frac{1}{2}}=5.6$.

Further advantages to this system will be discussed in the section on optical effects of shutters.

III. CHARACTERISTICS OF FOCAL PLANE SHUTTERS

The focal plane shutter usually consists of an opaque cloth curtain containing a narrow open slit. This shutter, mounted in the vicinity of the focal plane, moves across the focal plane, exposing successive strips of the film through the open slit. As in the case of between-lens shutters, the three characteristics of interest are actual time open, efficiency, and effective speed. In Fig. 4, P is the image of a point in the object-space. The shutter curtain moving down across the cone of light takes longer to cut this cone at C than it would were the curtain and slit directly in the focal plane.

A = lens aperture,
F = focal length,
d = distance from shutter to focal plane,
W = width of shutter aperture,
C = diameter of cone of light at shutter position.

The discussion above leads to the following definitions for the focal plane shutter:

(a) *Actual time open or total open time* of a focal plane shutter, operating in a camera and with a lens, for a given point in the focal plane is the total time of exposure of that point.

(b) *Efficiency* of a focal plane shutter is the ratio of the actual time of exposure, were the shutter in the focal plane, to the actual time of exposure as defined above.

(c) *Effective speed* or *effective exposure time* of a focal plane shutter is that time of exposure which, at maximum illumination by the lens, would yield the same exposure as that obtained in the actual time open. It is equal to actual time open T times efficiency E. (Note: That the effective exposure time is equal to the efficiency times the actual time open will be proved below.)

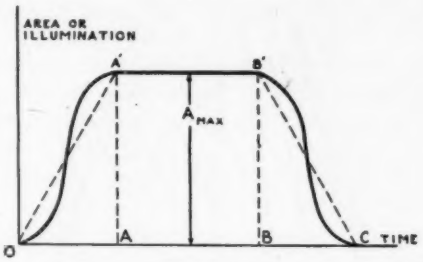

FIG. 6. Area of cone section exposed *versus* slit position ($W>C$).

An additional characteristic of focal plane shutters, due to non-uniformity of curtain velocity in the focal plane, has historically been called acceleration. The development of different-acting types of focal plane shutters makes this term obsolete, the term now used being defined below:

Exposure variation: The exposure variation characteristic of a focal plane shutter is defined as the difference between maximum and minimum curtain velocities in the focal plane, divided by the minimum curtain velocity.

In considering the manner in which the focal plane shutter slit cuts the cone of light (Fig. 4), it is necessary to investigate the shape and size of that part of the cone which is cut in different parts of the film plane. It is easily shown that, except for vignetting effects, the section of this light cone where it is cut by the shutter is a circle whose diameter is constant at a given f stop for all positions of the cone. Hence, efficiency of the shutter is essentially constant over its area of operation. Reference to Fig. 4 will show that in order for the shutter slit, of width W, to completely transverse the cone of light, of diameter C, the shutter must move a distance $C+W$. Were the shutter exactly in the focal plane, it would have to move only the slit width W to completely enter and leave the cone apex. Referring to Fig. 4, and the definition of efficiency given above, the efficiency is found to be

$$\begin{aligned} E &= W/(W+C) \\ &= W/(W+dA/F) \\ &= W/(W+d/f), \end{aligned} \tag{13}$$

where f is the f stop of the lens.

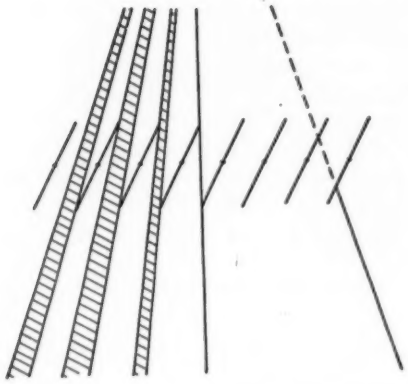

FIG. 7. Passage of light through a louvre shutter.

There remains the consideration of the time-illumination curve of a point in the focal plane as the cone of light is cut by the slit.

The three stages in the passage of the slit across the cone of light may be shown below in Fig. 5.

The graph of illumination as a function of time, which is identical with the curve representing area of cone section exposed as a function of slit position (assuming uniform motion of the shutter) is plotted below as Fig. 6. OA and BC are equal to the cone diameter, and OB is equal to the slit width. Considerations of mathematical and physical symmetry yield the result that the areas under OA' and $B'C$ are the same and equal to the areas of triangles $OA'A$ and $BB'C$. Therefore, the area under the curve $= A_{\max} \cdot (OB)$.

This area corresponds to the exposure that a point would receive were the shutter operating in the focal plane—for in that case the curve would be rectangular, of height $A_{\max}$ and base length OB. It is therefore clear that the effective speed of a focal plane shutter, by the first part of the definition of effective speed, is the fraction OB/OC of the actual time open. In terms of the quantities shown in Fig. 4,

$$OB = W \quad \text{and} \quad OC = W + C.$$

Effective speed

$$= W/(W+C) \cdot (\text{actual time open}) = E \cdot T. \tag{14}$$

Equation (14) shows that the definitions of efficiency, actual time open, and effective speed are consistent, and that the definition of efficiency from the standpoint of actual exposure time yields the same equation for efficiency as does the formulation of the efficiency concept on the basis of effective exposure. A somewhat more tedious proof of the same equivalence for the case $W < C$ can be readily constructed.

It should be noted that the efficiency of a focal plane shutter depends solely upon the geometry of the camera, the slit width, and the f stop, and is therefore easily calculated without any test apparatus other than a machinist's scale.

IV. CHARACTERISTICS OF LOUVRE SHUTTERS

The louvre shutter, in its usual form, consists of a series of narrow, thin, rectangular blades, arranged so they overlap much as does a venetian blind. A suitable mechanism, usually spring-powered, drives these blades open and closed, completing a photographic cycle.

Because this type shutter does not act like a varying aperture diaphragm, but rather like a variable neutral density filter, it may be placed

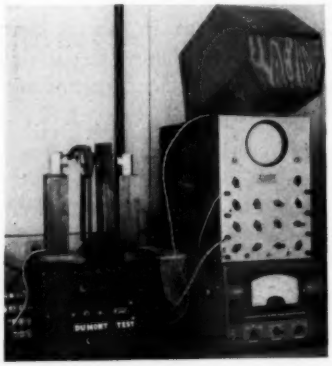

(a)

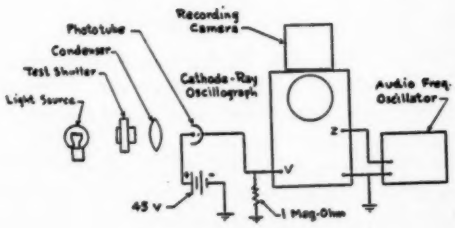

(b)

FIG. 8. Schematic diagram of oscillographic test method.

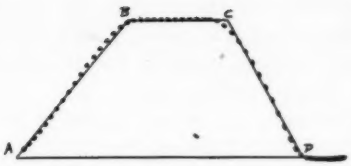

FIG. 9. Typical oscillogram of shutter action and accompanying calculations.

$T_n = \frac{1}{200}$th second.

$f = 4000$ dots per second.

$T_a = \frac{N_{ad}}{f} = \frac{44}{4000} = \frac{1}{91}$ second.

$E = \frac{N_{ad}/2 + N_{bc} + N_{cd}/2}{N_{ad}} = \frac{18/2 + 14 + 12/2}{44} = 66$ percent.

$T_e = E \cdot T_a = \frac{0.66}{91} = \frac{1}{138}$ second.

T_n = nominal (marked) speed.

f = frequency of dots.

T_a = actual time open (motion-stopping speed).

E = efficiency.

T_e = effective (exposure) speed.

N_{ad} = number of spaces from A to D.

anywhere in the optical system, at the discretion and convenience of the designer.

Used almost exclusively by the Germans in their long focal length reconnaissance cameras, their louvre shutter was placed between the lens elements. On some British cameras the louvre shutter was mounted behind the rear element. The single wartime American-made louvre shutter, to be described in detail below, was mounted in a 48-in. f:6.3 telephoto lens; it was located at the point of minimum cross section of the complete bundle traversing the optical system.

The three concepts of actual time open, efficiency, and effective speed are of the same relevance and importance for the louvre shutter as for the between-lens and focal plane types. However, the definitions of efficiency must be slightly modified, to take account of the fact that the shutter blades remain in the light bundle during the exposure. We have, therefore: The *efficiency* of a louvre shutter is the ratio of the amount of light transmitted by the shutter to the amount that would have been transmitted had the shutter been removed for the actual time of exposure.

Because of the way in which the louvres open, exposure is not simultaneous for a bundle of light incident on the lens at a given angle. Figure 7 illustrates this phenomenon for the case of an axial bundle.

It is seen that both the actual speed, efficiency, and effective speed depend not only on the f stop of the lens, but on the exact location of the shutter within or without the lens and the angle of incidence of the beam. For bundles of high convergence, the shutter will always present a considerable obstacle, thus making this type of shutter extremely impractical for high aperture ratio or fast lenses. The advantages and disadvantages of the louvre shutter, and comparison with other types, will be discussed in a subsequent section.

V. TEST METHOD FOR BETWEEN-LENS SHUTTERS

The oscillographic shutter tester, proposed in January 1941, by the writer, and developed jointly by D. W. Kerns, formerly of the Photographic Laboratory, Dr. Ernst Krause of the Naval Research Laboratory, and the writer, has been subsequently adopted by all the armed services, and the photographic industry, and now constitutes the ASA standard for testing between-lens shutters. A schematic diagram and photograph of the test apparatus is shown in Fig. 8. The photo-cell circuit shown below differs but slightly from that in the ASA standard; circuit constants and tube combinations which yield linear output, with maximum voltage about one or two volts, are equally acceptable.

Essential to the success of this test method is an oscillograph containing a single-sweep circuit, provision for z axis beam modulation, and linear vertical and horizontal deflection amplifiers. The DuMont type 247 oscillograph is ideal for this purpose. This test method was originally devised and built around the DuMont 175A oscillograph;

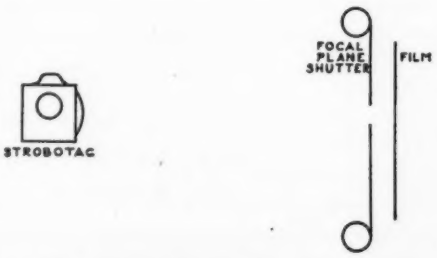

FIG. 10. Schematic diagram, strobotac test method.

now obsolete, the type 175A oscillograph has been replaced by the type 247.

The light source (preferably a small frosted lamp operated on d.c. to eliminate 60-cycle ripple), shutter under test, condenser, and vacuum photo-tube, are arranged as shown in Fig. 8. The optical system is arranged so that all the light passing through the shutter strikes the light-sensitive surface of the photo-tube. The potential drop across the high resistance is applied to the vertical deflection plates of the oscillograph through a vertical deflection amplifier. The output of the audiofrequency oscillator, connected to the grid of the cathode-ray tube, modulates the beam so that the otherwise continuous trace is broken up by timing dots.

When the single sweep and synchronization circuits of the oscillograph are properly adjusted, and the shutter tripped, a luminous intensity *vs.* time curve is produced on the screen of the oscillograph. Easily photographed, this efficiency curve can then be analyzed at the convenience of the technician. Use of a *CR* tube with a long persistent surface permits visual observation and counting of timing dots.

A typical oscillograph record and accompanying calculations is shown in Fig. 9.

The timing frequency impressed upon the grid of the cathode-ray tube is usually chosen so as to yield about 30 dots in the pattern being studied.

Actual time open is readily calculated from a direct count of the timing dots. If the total number of spaces is N_{ad} and the frequency is n, then total time open is

$$T = N_{ad}/n. \tag{15}$$

Efficiency E is given by

$$E = [N_{bc} + (N_{ab} + N_{cd})/2]/N_{ad}. \tag{16}$$

Effective speed is, as before,

$$T_e = E \cdot T. \tag{17}$$

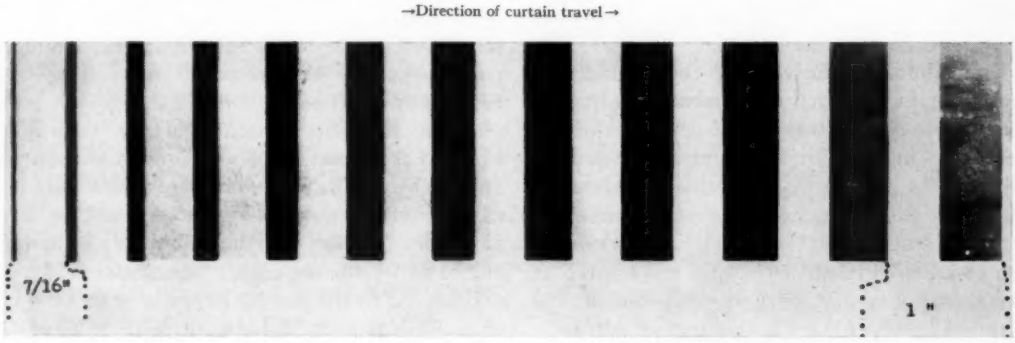

FIG. 11. Sample focal plane shutter test record (strobotac test method) and calculation of shutter characteristics.

Computation of efficiency at f:5.0:efficincy $= \dfrac{W}{W + d/f}$,

Where $\begin{cases} w = \text{width of slit.} \\ d = \text{distance of film from shutter,} \\ f = f \text{ stop of lens used.} \end{cases}$ In this case $\begin{cases} w = 0.406'', \\ d = 0.75'', \\ f = 5.0. \end{cases}$

$$\text{Efficiency} = \frac{0.406}{0.406 + 0.75/5.0} = 73 \text{ percent.}$$

Strobotac frequency for this test was 12,000 per minute = 200/sec.
The white bands are pictures of the slit as it moves across the focal plane.

$$\text{Acceleration} = \frac{\text{Final velocity} - \text{initial velocity}}{\text{initial velocity}} = \frac{1 - 7/16}{7/16} = 9/7 = 129 \text{ percent.}$$

$$\text{Effective speed at beginning} = t_B \quad \frac{t_B}{0.406} = \frac{1/200}{7/16} \quad \therefore \quad t_B = 1/217 \text{ sec.}$$

$$\text{Effective speed at end} = t_E \quad \frac{t_E}{0.406} = \frac{1/200}{1} \quad \therefore \quad t_E = 1/493 \text{ sec.}$$

Average effective speed = 1/358

	beginning of travel	end of travel	average
Effective (exposure) speed	1/217	1/493	1/358
Actual (motion stopping) speed	1/158	1/360	1/261

Calculation of focal plane shutter characteristics from strobotac test.

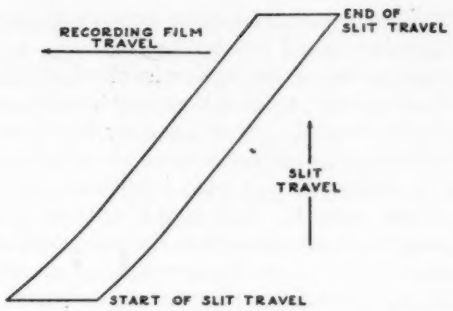

FIG. 12. Sample focal plane shutter test record produced on drum tester (fixed shutter slit).

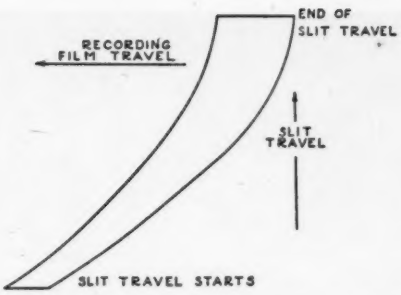

FIG. 13. Sample focal plane shutter test record produced on drum tester (variable shutter slit).

By this method, with no modifications, speeds ranging from 2 seconds to a fraction of a millisecond may be quickly, accurately, and precisely determined. Flash-bulb characteristics, characteristics of internally synchronized shutters, synchronization between flash-bulb and shutter, and similar phenomena are easily and quickly studied with this oscillographic test method.

It is of interest and importance to note the hierarchy of measurements for the between-lens shutter.

Actual time open and efficiency are measured directly, while effective speed is calculated from the two preceding parameters.

Actual time open is a characteristic of the between-lens shutter which is independent of lens or aperture stop. As the diaphragm stop is varied, efficiency and, therefore, effective speed, vary. The fundamental importance of the actual time open characteristic for between-lens shutter should be borne in mind when a different fundamental parameter is found for the focal-plane shutter.

VI. TEST METHODS FOR FOCAL PLANE SHUTTERS

Two methods have been developed for testing focal plane shutters. The first, the strobotac test method, is simple to perform, yields an easily interpreted graphic record of shutter performance, but is not adaptable to low shutter speeds, or to shutters of the Leica or Contax type utilizing a variable aperture shutter which at speeds of about 1/50 second and slower expose the whole focal plane for part of the exposure.

The schematic diagram of Fig. 10 illustrates this strobotac test method.

The strobotac is an electronic stroboscope, developed as a product of the researches of Edgerton, Germeshausen, and Grier. Manufactured and marketed by the General Radio Corporation, the strobotac is calibrated for flashing rates from 600 to 14,400 per minute. The duration of the flash is about 1/2000 second, with about 90 percent of the light being emitted in 1/4000 second. If the strobotac is operated off a controlled frequency 60-cycle a.c. line, its calibration may be checked by use of a vibrating reed enclosed within the instrument, which is also run off line frequency directly.

In this test method the strobotac is placed several feet (4 to 12 feet) from the shutter. With the lens removed from the camera under test, and a sheet of film placed immediately behind the shutter, the shutter is tripped. The photographic record produced is a series of dark bands, which are successive projections of the slit as it traverses the focal plane. From knowledge of the flashing rate, the linear curtain speed may be calculated. Acceleration or exposure variation is calculable independent of strobotac frequency. An actual test record, and accompanying calculation, are shown below in Fig. 11.

Certain experimental techniques need be followed to insure optimum results. If a sheet of onion-skin paper or a ground glass is placed behind the shutter, and the shutter tripped, a visual record will be obtained. Adjustment of the flashing rate of the strobotac is made to yield a convenient number of non-overlapping bands. In the case of very wide slits and/or low velocity curtains as found in slow shutters, it is necessary to restrict a portion of the slit by covering it

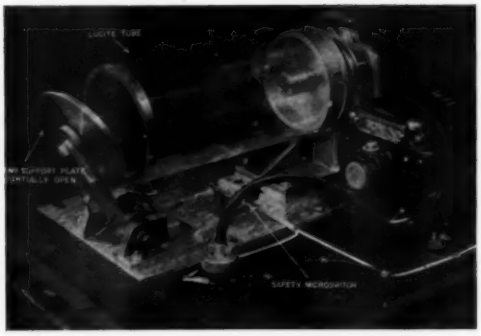

FIG. 14. Drum tester for focal plane shutters, showing details of Lucite drum and support mechanism.

with a piece of tape in which a small hole is punched. When there is insufficient room to place the strobotac several feet from the shutter, or when excessive vignetting results, a field stop with an inch to inch-and-a-half aperture should be placed over the cover glass of the strobotac. The purpose of these techniques is to minimize the shadow or penumbral effects resulting from separation of the recording film and the shutter.

It may be easily shown that the magnitude of this shadow effect is independent of slit position in the focal plane. Manifesting itself as an apparent increase in slit width, the magnitude of the effect is given by:

$$\text{Apparent increase in slit width} = d(D+W)/H, \quad (18)$$

where d = separation of shutter and film,
H = distance from Strobotac to shutter,
D = effective aperture of Strobotac, and
W = actual width of slit.

If fast panchromatic film and a high energy developer are used, H may be increased to 12 or 15 feet, reducing the shadow effect to an entirely negligible quantity.

A slight error is made in estimating the position of the slit because of the projection effect and the separation of film and shutter. The relative error in overestimating the total travel of the slit is given by the following formula, from which second-order terms are dropped:

$$\text{Relative error in estimating total travel} = d/H. \quad (19)$$

This quantity can be made very small, and certainly less than 1 percent.

Consideration of the errors involved in this test method indicates that they may be made as small as is desired. The major error that must be avoided is misinterpretation of the record. It must be recognized that what is being measured is curtain velocity, not actual (or motion-stopping) exposure time. From the measurement of curtain velocity and measurement of the slit width, the time necessary for the slit to move its own width may be determined. It is important to recognize this time as the effective exposure time. The efficiency of the shutter may be calculated from the formula derived in the preceding section (Eq. (13)).

The actual time open (or motion-stopping speed) is then calculated from

$$\text{Actual time open} = \text{effective speed/efficiency}. \quad (20)$$

It will be remembered that the fundamental constant for between-lens shutters is actual time open, which is independent of efficiency; the fundamental constant for the focal plane shutter, however, is the effective exposure time, which is independent of efficiency. In this case, actual time open varies with the efficiency.

The second focal plane shutter test method developed by the Photographic Laboratory is adaptable to all types of focal plane shutters, large and small, slow and fast. It has been adopted as the standard test for focal plane shutters by the American Standards Association.

Actual design and construction of the instrument to be described was accomplished by Lieutenant Edward Rich and Mr. Hugh Mohr, under the general supervision of the writer. A piece of film 9½″ wide and about 16″ long is supported by centrifugal force against the inside of a cylindrical Lucite drum. This drum is revolved at high speed past a narrow slit, through which light may be admitted to the film. The shutter to be tested is supported so that the direction of slit travel is parallel to the axis of the cylinder. A light source, preferably a clear 200-watt bulb, is mounted about 6 or 8 feet above the shutter. The resulting test record is a diagonal trace, readily interpretable, with time proportional to linear distance on the film and

inversely proportional to the linear speed of the film past the exposing slot. Sample test records produced by fixed and variable slit shutters are sketched below in Figs. 12 and 13.

The instrument as at present constituted is capable of 6 speeds, ranging from 405 to 7250 r.p.m., corresponding to a linear speed of from 108 to 1933 inches/sec. An addition to the instrument of a small supplementary motor to frictionally drive the drum at 1 r.p.s. will be completed shortly, extending the range of the apparatus.

The construction and engineering details pertaining to this instrument are fully described in reference 16. Figures 14 and 15 are photographs of the test instrument, which has also been adopted as an ASA standard for focal plane shutters.

VII. TEST METHODS FOR LOUVRE SHUTTERS

As noted above, the characteristics of a louvre shutter depend to a great extent on both the particular lens used, the angle of incidence of the entering bundle, and the position of the shutter within the optical system. For these reasons, it is impossible to accurately test a louvre shutter except when it is mounted in the lens with which it is being used. For the same reasons, a collimator is necessary. The actual testing employs the oscillograph shutter tester previously described, with the photo-tube pick-up mounted close to the focal plane of the lens.

A complete test involves at least three or four test positions in the focal plane, and several diaphragm positions for each of the focal plane positions. Because some portion of the louvres always remain in the beam cross section, it is necessary to completely remove the shutter to measure maximum possible light transmission. This is easily accomplished on the oscillograph, because only relative values with and without the shutter are required. The efficiency is then calculated from the applicable definition, which is given in Section IV.

VIII. THE EFFECT OF SHUTTERS ON OPTICAL PERFORMANCE

Lenses are, in general, tested apart from and without the shutters with which they will be used. This procedure has considerable merit for the optical designer, or for one interested in comparing lenses. Photographic lenses, however, are usually used to make photographs, and hence cannot be divorced completely from the accessories used with the lens.

It is well known that the resolving power of a lens varies with the f stop. This variation is not the same for all lenses; some lenses yield maximum resolution at the maximum aperture, while others have their worst resolving power at maximum aperture. The shutter efficiency curve shows that an exposure at the wide open stop is in reality a succession of exposures at various stops.

Between-lens shutters of, say, 55–60 percent efficiency, at maximum aperture, are common for high speed settings. In this case, the exposure at maximum aperture is only about $\frac{1}{3}$th of the total exposure. It is, therefore, clear that measurements of resolving power of a lens at its wide open stop may be a poor index to its performance when an inefficient shutter is used. The performance of a lens may, therefore, vary with the shutter with which it is used; hence statements of lens-resolving power at maximum aperture, if the lens is tested independently of the shutter, may be far from the actual performance of the lens-shutter combination.

Although, as noted in the section on between-lens shutters, the shutter is usually mounted close

FIG. 15. Drum tester for focal plane shutters.

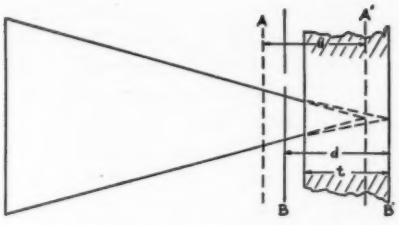

FIG. 16. Effect of glass plate in focal plane upon efficiency of a focal plane shutter.

to the diaphragm, it is not coincident with the diaphragm, and an exposure with an inefficient shutter may be regarded as a succession of exposures made with a displaced diaphragm stop.

The effect on lens aberrations resulting from a displaced diaphragm stop are well known, and may be briefly summarized. Spherical aberration is unaffected, but if spherical aberration is present, coma is increased. In the presence of either spherical aberration or coma, astigmatism is increased. The equations governing these changes are reproduced from Kingslake's article in the *Handbook of Photography*. K in these equations is the displacement of the diaphragm stop, which for purposes of this discussion is the distance between shutter and diaphragm.

$$\left.\begin{aligned}&\text{Change in coma} = K(\text{spherical aberration}).\\&\text{Change in astigmation} = 2K(\text{coma})\\&\qquad\qquad + K^2(\text{spherical aberration}).\end{aligned}\right\} \quad (21)$$

This same point is especially important for the case of mapping cameras; mapping lenses, designed to be distortion-free, depend upon accurate location of the diaphragm stop to ensure negligible distortion. Air Force mapping lenses are calibrated for distortion on an outdoor test range, using the lens in its camera and shutter, and thus eliminating the possible source of error from the shutter.

Another effect, which is a by-product of using an inefficient between-lens shutter, is the increased depth of field which, of course, results from taking the photograph at a whole series of stops rather than at the wide open stop. This discussion emphasizes the desirability of using the concept of "effective f stop" rather than effective exposure speed.

The focal plane shutter has long been held before the amateur photographer as an example of a highly efficient shutter. This could easily be true, were the basic formula for efficiency widely understood and applied to the construction of shutters. In actual practice, the high efficiency of focal plane shutters is largely a myth, for the design of most commercial focal plane shutters does not take advantage of the potentialities inherent in Eq. (13).

The main reason for low efficiency in some commercial focal plane shutters is the excessive distance between shutter and focal plane. An extreme non-typical example of this is an aerial camera which, employing an f:2.5 lens, has a shutter with a $\frac{1}{8}$-in. slit; the shutter is 0.75″ from the focal plane. The resulting efficiency is 29.5 percent. In this case the $\frac{1}{8}$-in. slit is cutting across a cone of light 0.3-in. diameter, and at an effective exposure speed of 1/900 sec., the actual or motion stopping speed is 1/265 sec.

An interesting effect upon the efficiency of a focal plane shutter occurs when a glass pressure plate of thickness t is placed in the focal plane and the lens is refocused. According to the well-known formula, this necessitates a lens displacement of $(n-1/n)t$ away from the focal plane, where n is the index of refraction of the glass. Figure 16 illustrates this effect.

Clearly the diameter of the cone of light from the lens at the plane of the shutter is less when the glass intervenes between shutter and film, than when this space is all air. AA' are the relative positions of the shutter and focal plane in air, and BB' are the same positions when a focal plane glass plate is used.

$$d' = d-(n-1)t/n. \quad (22)$$

Substituting $n=1.5$ into (22),

$$d' = d-t/3,$$

and the new formula for efficiency becomes

$$E = W/[W+(d-t/3)/f]. \quad (23)$$

The major optical effect produced by focal plane shutters, when there is a component of relative motion at right angles to the optical axis between the camera and photographic subject, is image distortion. This distortion is so familiar to all, that were racing cars to be photographed without showing the tilted elliptical wheels, the illusion of motion would be lost. In fact, several

years ago, an automobile (the Graham) was so designed as to give, while standing still, just this illusion of speed. This particular distortion results from use of a news-type camera in which the focal-plane shutter travels down, exposing the objects in the bottom portion of the field of view before exposing the objects in the top portion of the field of view.

The distortion effects produced by focal plane shutters are of two types. The first type, mentioned above, occurs when image motion and shutter travel are at right angles to each other.

Consider a net of equal-time coordinates in the focal plane as shown in Fig. 17, and a line image lying on the horizontal axis.

Suppose the shutter slit and line image start together at the origin. This line is an image of a corresponding line on the ground and is moving upwards at the rate of one vertical division per unit of time. The shutter slit, which is perpendicular to the horizontal axis, moves to the right at the rate of one horizontal division per unit of time. The dotted line, therefore, indicates the final position of the image on the film. The characteristic feature of this type of distortion is the angle θ, which specifies the distortion completely.

$$\theta = \tan^{-1}(V_i/V_c), \tag{24}$$

where V_i = linear speed of image,
V_c = linear speed of curtain.

A simple method for calculating V_i results from the fact that $V_i \cong 0.5''$/sec. per foot of focal length at 300 m.p.h. at 10,000 feet altitude.

Thus, for a 40-in. lens at 30,000 feet, with airspeed of 300 m.p.h., and a linear curtain speed of 200 inches/sec.,

$$\theta = \tan^{-1}(0.555/200) = 0.16°. \tag{25}$$

The second type of distortion produced by focal plane shutters occurs when the direction of image motion is parallel to the direction of shutter slit motion. If the image and the shutter travel in the same direction, the image suffers an increase in length in the direction of motion; if image and shutter motion are opposite to each other, the image suffers a decrease in length. The equation below for relative distortion is derived in the appropriate reference, and will be stated here without proof.

$$\text{Relative distortion} = \Delta l/l.$$

$$\Delta l/l = \left\{\frac{88}{60}\frac{VF}{H\left[V_c \mp \left(\frac{F-d}{F}\right)\frac{88}{60}\frac{VF}{H}\right]}\right\} \cdot \left\{\frac{d/f+w}{l} + \frac{F-d}{F}\right\}, \tag{26}$$

where V = velocity of aircraft in m.p.h.,
F = focal length in inches,
H = altitude in feet,
V_c = velocity of curtain in inches/sec.,
d = distance from shutter to film,
f = f stop of lens,
w = width of shutter slit, and
l = length of image.

Upon making the substitutions

$$V_i = 88VF/60H, \quad \alpha = (F-d)/F, \quad c = d/f, \tag{27}$$

the equation for relative distortion becomes

$$\Delta l/l = [V_i/(V_c \mp \alpha V_i)] \cdot [\alpha + (c+w)/l]. \tag{28}$$

Since for any group of calculations both α and c will be constant, and V_i will, in general, be constant for an entire flight, formula (28) is preferable for computational purposes.

The upper sign in both (26) and (28) refers to the case in which shutter slit and image are moving in the same direction, the lower sign to the case when slit and image movement are opposite in direction.

One of the interesting features of this type of distortion is the fact that small images are distorted more, percentage-wise, than are large images.

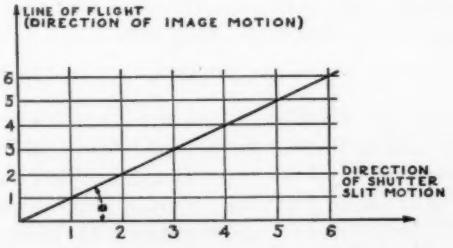

FIG. 17. Type 1 focal plane shutter distortion.

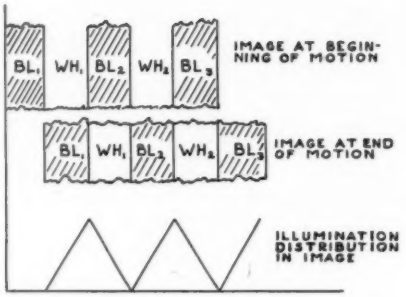

FIG. 18. Illumination distribution in blurred image of resolving power target.

IX. EFFECT OF SHUTTERS UPON RESOLVING POWER OF AERIAL CAMERAS

An important question to consider is the effect of shutters on the resolving power of an aerial camera in flight, or, to rephrase the problem, the effect of shutters on definition in the aerial photograph.

The aerial camera in flight is subject to several motions. In addition to the most obvious one, linear motion due to aircraft speed, the camera may be vibrating with both linear motion of and angular motion about its center of gravity. With no vibration present, the camera may be partaking of the several angular motions of the aircraft-pitch, yaw, and roll. All these effects induce motion of the image with respect to the film during the exposure, and consequent loss of definition.

The linear velocity of the image caused by forward aircraft speed is given by

$$V_i = 88VF/60H, \tag{27}$$

and the linear velocity of the image due to an angular velocity of the optical axis $\dot{\theta}$ is

$$V_i = F\dot{\theta}. \tag{29}$$

From Eqs. (27) and (29), it is seen that an angular velocity of the optic axis,

$$\dot{\theta} = 88V/60H, \tag{30}$$

yields the same image velocity as that due to forward motion of the aircraft. For an aircraft flying 300 m.p.h. at 30,000 feet, the critical value of $\dot{\theta}$ is about 0.83°/sec., a truly small angular velocity, and one easily realized or exceeded under normal flight conditions.

These effects, resulting in blur or loss of definition of the photographic image, are directly proportional to shutter speed, especially at the higher shutter speeds (over 1/500 sec.). The lower shutter speeds (say, 1/100 sec.) are approximately of the same order of frequency (6000 c.p.m.) as many of the disturbing vibrations found in aircraft, and direct proportionality does not hold true in this case. The one safe generalization which may be made is that high shutter speed reduces all image-motion effects and yields photographs of better definition than result from use of low shutter speeds. The working rule for the aerial photographer is employment of highest possible shutter speeds consistent with getting a properly exposed negative.

An apparent anomaly in the blurring resulting from high speed low altitude flight is the fact that the amount of motion as measured from the photograph is usually of the order of ½ that to be expected from the calculation of actual aircraft motion during the exposure. For example, an aircraft flying at 250 m.p.h. will move 3.65′ during an exposure interval of 1/100 second. It might be expected, therefore, that a resolving power target consisting of equal width black and white lines, of width 3.65′, and oriented perpendicular to the line of flight, would be completely smeared out in the resulting photograph. Actually, this target would be clearly resolved. The reason for this effect follows from consideration of Fig. 18, which shows that the illumination distribution in the image of a blurred resolving power target, where motion equals one line width, is such as to yield a reasolvable final image. One of the assumptions underlying the construction of the illumination distribution is that of a 100 percent efficient shutter, and infinite target contrast. The correction necessitated when the shutter efficiency curve is taken into account will modify the triangular illumination distribution on both toe and shoulder portions, but will not change the predicted and observed resolution. Clearly the total effect is also a function of target contrast and the development process.

A more complete analysis of this effect is underway, but has not yet been completed.

A possible source of vibration of the camera

and consequent deterioration of the image comes from the shutter itself. Never thoroughly explored, this possibility can no longer be wishfully ignored, and it is hoped that more information on this effect may be forthcoming soon.

A little known property of louvre shutters was first pointed out to the writer and other members of the Photographic Laboratory by Dr. James G. Baker, who predicted loss of resolving power resulting from diffraction effects. This effect, easily verified by visual observation on a bench test, is a maximum, and causes complete deterioration of the image in one direction, when the projected area of louvres is equal to half that of the total area of beam cross section. This deterioration, although certainly present, is not readily observed or identifiable in aerial photographs made with louvre shutters. Its presence at all is sufficient to rule heavily against the louvre shutter.

X. THE SHUTTERLESS STRIP CAMERA AND MOTION COMPENSATION

Perhaps the major invention in the field of serial photography in the last half-dozen years is the strip camera, and the corollary principle of image motion compensation.

The principle of the strip camera is simple. In the S-7 strip camera a 200-ft. roll of 9½-in. wide film is pulled past a narrow slit in the focal plane at a velocity exactly equal to that of the image. The resulting strip is a continuous photograph of the ground below.

Remarkable low altitude photographs with image definition greatly exceeding anything possible with conventional cameras and the highest speed shutters have been made with this camera, and certainly under these conditions (e.g., 500 m.p.h. airspeed at 100 feet) the conventional camera and shutter would make a poor showing. An even greater advantage afforder by the strip camera is its ability to get good low altitude photographs under weather and light conditions which would necessitate shutter speeds of about 1/50 sec. or slower. At 400 m.p.h. at 100-feet altitude a photograph made with a 6-inch lens at 1/50 sec. would suffer from image motion of about 0.7″, and would, in general, be unusable. Excellent strip photographs have been made under more severe conditions.

The general principle of forward image motion compensation, by moving the film in synchronization with the image, is being applied with conspicuous success to all AAF cameras.

Use of a moving film magazine in conjunction with a focal plane shutter which moves in line of flight will eliminate the second type of image distortion caused by focal plane shutters, and would, therefore, permit mapping with focal plane shutter cameras.

Two other methods of image motion compensation which work well, but which will not be discussed in detail here, are the use of a pair of revolving prisms mounted in front of the lens, and the swinging mount, developed by Drs. Baker and Chandler, respectively.

Following the general principle of doing everything to improve the photographic resolving power, the photographer will be happy to use the moving-film cameras, but as insurance, and to minimize errors due to lack of synchronization and image motions other than in the direction of flight, he will, or should, use as high a shutter speed as light conditions will permit.

XI. WARTIME PROGRESS IN SHUTTERS

The impetus furnished by wartime necessity resulted in the development of several new types of shutters, consideration of many more, and great improvement in several existing shutters.

A focal plane shutter having many slits, each of which moves a short distance, in contrast to to the standard single-slit focal plane shutter, was proposed and designed by Dr. Langer, then of Mt. Wilson Observatory. This focal-plane type shutter, consisting of three thin, appropriately slotted sheets, would have the great advantage of more or less simultaneous exposure of all points in the focal plane. Acting in this respect like a between-lens shutter, this shutter could be used for mapping. Its major disadvantages are

(a) it is extremely tricky to make,
(b) the very narrow slits required make for inefficiency,
(c) a peculiar type of distortion is present, resulting in doubling of the image in the regions of overlap of adjacent slits.

Having for long proved a fertile field for scientific fiction writers, the birefringent phenomena of physical optics were suggested as a possible tool to use in construction of a high speed shutter. This attempt was abandoned early in the war on the grounds of unpracticality and inefficiency. It is unfortunate, but nonetheless true, that high shutter efficiency is easily obtained in slow speed shutters (where efficiency is of little or no consequence), but is rarely obtained in high speed shutters when exposure is critical. Since the birefringent shutters proposed could not have an efficiency of at least 50 percent, the whole matter was then dropped. Investigations now under way at the Boston University Optical Research Laboratory may point the way to utilization of these interesting phenomena.

At least once or twice a year someone invents the multiple layer disk type between-lens shutter. These shutters depend for their high speed upon the coincidence at the diaphragm position of sectors cut out of disks rotating about the same vertical axis at relative speeds of, say, 3:4:5. These disks are accelerated gradually to high speed. One of the major disadvantages of this type shutter is that for the large opening long focal length lenses which could use a high speed shutter, the over-all size of the shutter is tremendous. The main reason for lack of interest in this type shutter, however, has been that high speeds are more easily obtainable with focal plane shutters.

In an attempt to increase the speed of the standard 24-in. K-17 and K-18 shutters, various materials were examined and evaluated as possible substitutes for the steel leaves. This search for new materials was motivated by the necessity of finding materials which were simultaneously (a) lighter and stronger than the steel leaves, permitting higher speeds because of reduced moment of inertia of the blade, and (b) of sufficient life because of increased strength as compared to steel.

As a result of the public hearings before the Temporary National Economic Committee of the 76th Congress, and the subsequently published testimony in connection with the monopoly and international cartel aspects of this committee's investigation, the attention of the writer was drawn to the extensive use of beryllium alloys by Germany. This testimony is to be found in volume 5 of the public hearings before the Temporary National Economic Committee, and in the final reports and recommendations of this committee. Additional information is to be found in the book *Patents for Hitler* by Gunther Riemann, published by Vanguard Press in 1942.

Beryllium is the fourth element in the Atomic Table and is the lightest metal. It is hard enough to scratch glass and, when alloyed with copper in small percentages, will confer extraordinary endurance properties to springs made of the alloy. When alloyed with aluminum in the proportions 30 percent beryllium, 70 percent aluminum, the alloy has a specific gravity of about 2.4 and a modulus of elasticity approximately $\frac{2}{3}$ that of steel.

To further the work on shutter leaf design, a shutter leaf tester was constructed by (then) Captain Lewis A. Scholz; this tester subjected a leaf to oscillations at the rate of 20,000 per minute.

The Materials Laboratory of the Engineering Division furnished enough of sheet beryllium-aluminum alloy to make a set of shutter leaves for the 24-in. K-17 shutter. The crudely made beryllium-aluminum alloy leaves lasted approximately four minutes on the tester described above; this is to be compared to the time of about 30 seconds for standard steel leaves. The alloy leaves were less than half the weight of the steel leaves. The top speed of the standard 24-in. K-17, or K-18 shutter is 1/110 second (actual time open). The speed obtained with the beryllium aluminum alloy leaves was 1/170 second.

After these extremely promising results the entire investigation was abandoned because no known source of beryllium-aluminum alloy was found among the United Nations. The samples obtained from the Materials Laboratory, Engineering Division, were made by Cooper-Wilford of Philadelphia, Pennsylvania on a purely experimental basis.

Postwar investigations have indicated that Be-Al alloy shutter leaves were not used by either Germany or Japan. The preliminary work done by the Photographic Laboratory seems to have stimulated several American manufacturers, and it is believed that some work is now pro-

ceeding leading to the utilization of such alloys in between-lens shutters. It is clear that such utilization will effect considerable shutter speed increases only if the shutter leaves have most of the effective moment of inertia of the system.

The description below, of the work done on the shutter of the 6-in. K-17 camera, indicates that for this shutter, use of Be-Al leaves would not yield a substantial speed increase.

In 1943, George Mitchell, of the Mitchell Camera Corporation, undertook the job of speeding up the shutter of the 6-inch focal length K-17 camera. This camera, utilizing the Metrogon lens, and taking a photograph nine inches square, had it had a shutter faster than the nominal 1/300 sec., would have been very useful for low altitude reconnaissance.

At the 1/300th-sec. speed setting the actual time open was about 1/230 sec. Mitchell's analysis led him to change but one part of the shutter—the main-drive cam; reducing the moment of inertia of this one piece, the actual time open was decreased to 1/480 sec.—more than doubling the previous top speed.

Two prototype high speed shutters modified by Mitchell were rushed overseas and used with extraordinary success for several difficult low altitude reconnaissance missions in the Italian campaign. A detailed account of the use of these cameras, together with other material on the employment of aerial cameras, will be found in a paper by the author in the July 1948 issue of the Journal of the Optical Society of America.[1] This improved shutter with some slight further modifications by the Graflex Corp., has now been standardized and is found in all 6-in. K-17C cameras which were made by the Graflex Corp. during the war.

Thus encouraged by the application of basic principles to shutter design, attention was turned to the focal plane shutter of the K-22 camera. This camera, hastily developed at the start of the war to enable utilization of large lenses for which between-lens shutters were impractical, had a focal plane shutter rated up to 1/800 second. In previous discussion on focal plane shutters, it was pointed out that the linear speed of the curtain is sufficient to describe the performance of the shutter, if the other geometrical constants are known. The following discussion will concern itself, therefore, only with curtain speed. The efficiency of the K-22 focal-plane shutter is low; this inefficiency is due primarily to the enforced use with this camera of a film magazine originally designed for the K-17 cameras, which use between-lens shutters. The focal plane of this magazine is 0.370″ above its seating surface. The ease by which focal plane shutter efficiency can be achieved in original design is enough to ensure high efficiency on all future design.

TABLE I. Curtain speeds: low tension setting, K-22 shutter.

	Initial speed	Final speed	Ave. speed	Acceleration
Standard shutter	60	90	75	50%
Additional wind-up only	83	107	95	36%
Lightened rollers only	81	117	99	44%
Lightened rollers and additional windup	100	125	113	25%

TABLE II. Curtain speeds, high tension setting, K-22 shutter

	Initial speed	Final speed	Average speed	Acceleration
Standard shutter	93	185	139	100%
Additional windup only	133	200	167	50%
Lightened rollers only	119	192	156	61%
Additional windup and lightened rollers	151	201	175	33%

As originally constituted, the slit of the K-22 shutter curtain had about 1½″ of travel before exposure was started. The addition of an extra 1½″ of pre-exposure travel increased the linear speed and at the same time reduced the acceleration characteristic. Cutting roller weight in half accounted for additional gain in speed and decrease in acceleration. The net effect of these changes may be summarized in the Tables I and II, which give curtain speed in inches/sec.

This very fruitful work was supplemented by the addition of a remarkably simple invention of (then Sgt.) Robert Jackson, whose invention consisted of a method of using a powerful booster spring to get the shutter up to high initial speed, and then cutting this booster spring out as the shutter slit started the exposure. The addition of ball bearing roller supports, plus this booster spring, yielded high tension setting performance

[1] Amrom H. Katz, J. Opt. Soc. Am. 38, 604–10 (1948).

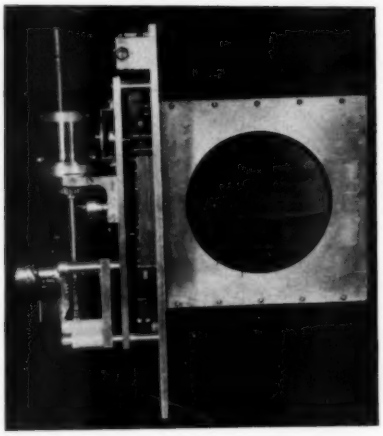

FIG. 19. Louvre shutter for 48" f:6.3 lens; plan view.

of 220"/sec. for initial speed and 275"/sec. for final speed, with average speed =247"/sec. and acceleration =25 percent. Thus average speed was increased from 139 to 247 inches/sec., and at the same time acceleration was cut from to 100 percent to 25 percent. These improvements mean that wider slits can be used, thus increasing efficiency and therefore actual (or motion-stopping) speeds; they are now part of the K-22A camera.

Advantage has been taken in the design of the K-34, 9×18-inch focal plane shutter, of the theory and practice developed in redesign of the K-22 shutter. The shutter of the K-34 travels at 250"/sec., with a maximum exposure variation of about 10–15 percent. This camera was designed and built by the Chicago Aerial Survey Company.

The problem of providing a suitable shutter for the f:6.3 9×18 Eastman Telephoto lens was enormous. The K-34 previously described had not been thought possible by the industry.

Mr. William Mungall, of the Wright Field Photographic Laboratory, with mathematical assistance by the writer, designed and built a novel louvre shutter of very high performance. The urgency of the problem, plus the difficulties in building a shutter, ruled out the usual empirical approach of building, testing, and rebuilding. A goal of 1/500-sec. actual time open was set for this shutter. Extensive calculation and formulation of an adequate theory of action of the shutter preceded the construction of the shutter; upon completion, the shutter performed as predicted with about 5 percent deviation from predicted characteristics.

This louvre shutter is considerably larger (4½-in. aperture) and twice as fast as the German Louvre shutter previously mentioned. An interesting sidelight on the 48-in., 9×18 camera is that the designer of the shutter and camera, acting as photographer, used the camera with outstanding results to record the 1946 Bikini atom bomb tests. Two photographs of this shutter are shown in Figs. 19 and 20, and a schematic wiring diagram is shown in Fig. 21. This diagram and the photographs of the shutter are included because they illustrate the complexity of modern high performance aerial camera shutters. Further discussion of this point will be found in subsequent paragraphs.

XII. GENERAL COMPARISON OF SHUTTER TYPES

Mapping cameras have heretofore used only between-lens shutters. Although, as pointed out in one of the previous sections, the use of a moving film magazine (image-motion compensation) in conjunction with a focal plane shutter will permit distortionless photography, it is unlikely that future mapping cameras will utilize focal plane shutters.

Standard mapping cameras taking photographs nine inches square employ a six-inch focal length lens. Such wide-angle photography is employed because of economy in flying the mapping mission and in the subsequent calculation and map assembly operations. The maximum diaphragm aperture for the 6-inch f:6.3 metrogon mapping is but 0.75 inch, posing no particular problem for between-lens shutter design.

If and when larger mapping cameras will be needed and developed, the same ratio of film size to focal length will be maintained. The maximum diaphragm opening for a 12-inch focal length mapping lens is about 1.5 inch, and presents no difficult problem.

A serious factor which limits the maximum utilizable shutter speed of mapping cameras is lens vignetting which arises from the wide-angle of coverage. Because the mapping lenses are relatively slow, the top utilizable shutter speed

for mapping cameras is of the order of 1/500 second. The combination of small-area shutter requirement and relatively low utilizable shutter speed both combine to rule out shutters other than the between-lens type for mapping cameras.

Present aerial reconnaissance requirements and anticipated future requirements indicate the need of long-focus large aperture lenses as large as or larger than the 48-inch f:6.3 lens previously discussed. The problem of providing a high efficiency, long-lived shutter for the large lenses referred to above, with shutter speeds variable between, say, 1/50th second and 1/1000th second, and with cycling rates up to one per second, has ruled out the between-lens shutter for daytime operation. Shutters for use in night photography are a separate problem, and will be so discussed.

For the designer, the problem of high speed large aperture between-lens shutters is extraordinarily difficult. As in the case of the louvre shutter discussed above, all parts must move with high speed. The action of latching devices, cams, retard mechanisms—all take place within a time interval of the same order as the shutter operating time. Efficiency in a between-lens shutter is attained only if the opening and closing portions of the shutter operating cycle are a small fraction of the total open time.

Focal plane shutters can be made efficient by the simple process of paying close heed to the formula for efficiency (cf. (13)).

Hence, efficiency is attained in a focal plane shutter by placing the shutter close to the focal plane, a matter of geometry; efficiency in a between-lens shutter necessitates high speed movement of shutter components.

The ratio of the total operating time or transit time to the effective exposure time of a focal plane shutter is given approximately by the ratio of length of shutter travel to shutter slit width. This shutter transit time is of the order of twenty or thirty times the effective exposure time for aerial camera shutters. The designer of a focal plane shutter has, therefore, the great advantage of working with relatively slow-moving mechanisms; shutter speed is achieved by an artifice, high speed scanning of the focal plane.

The large day reconnaissance cameras now under development will utilize focal plane shutters and a 9×18-inch format size. Such use of focal plane shutter cameras, with interchangeable lens comes ranging in focal length from 12 inches to 48 inches, afford two further important advantages over similar cameras equipped with between-lens shutters.

First, only one camera with one shutter need be stocked for perhaps four lenses, whereas were between-lens shutters used, each lens assembly would require a shutter. Second, the use of large lenses which weigh as much as 100 pounds has posed unique problems in mounting the lens and its components; this is especially true when temperature and pressure compensation are used to insure maintenance of lens focus under all environmental conditions. Both of these latter problems are more easily solved, if the lens cone is uncomplicated by insertion of a between-lens shutter.

Night photography has heretofore been accomplished with the K-19 type camera, utilizing a 12-inch f:2.5 lens. The between-lens shutter of this camera is about $3\frac{5}{8}$ inches in diameter and

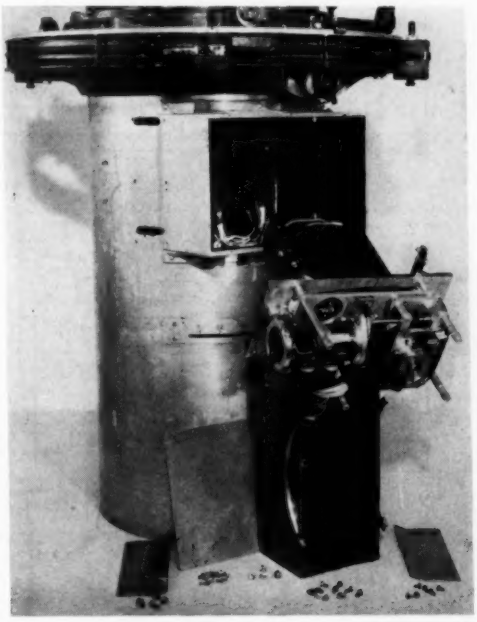

FIG. 20. Photograph of 48″ lens cone, showing installation of louvre shutter.

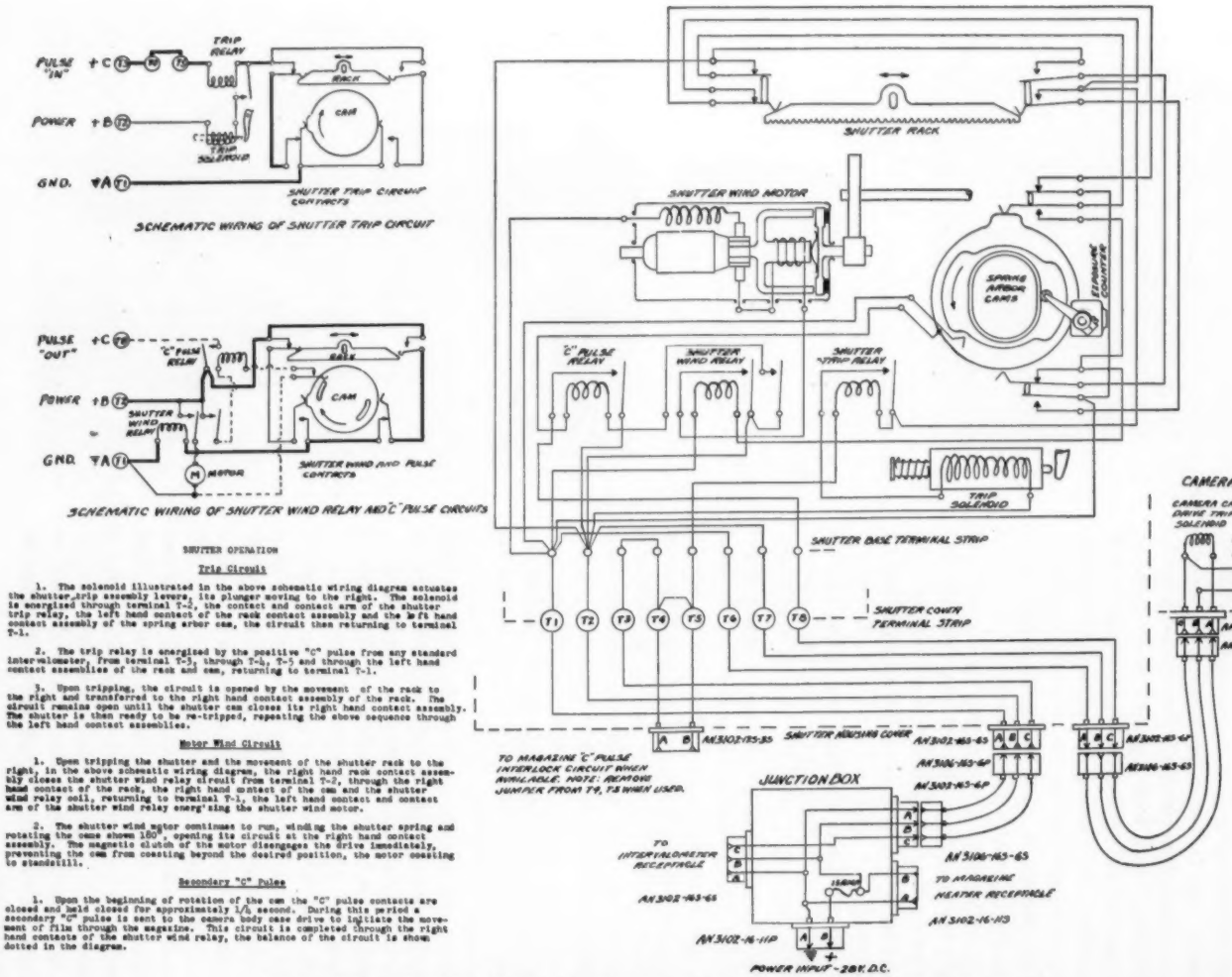

SHUTTER OPERATION

Trip Circuit

1. The solenoid illustrated in the above schematic wiring diagram actuates the shutter trip assembly levers, its plunger moving to the right. The solenoid is energized through terminal T-2, the contact and contact arm of the shutter trip relay, the left hand contact of the rack contact assembly and the left hand contact assembly of the spring arbor cam, the circuit then returning to terminal T-1.

2. The trip relay is energized by the positive "C" pulse from any standard intervalometer, from terminal T-3, through T-4, T-5 and through the left hand contact assemblies of the rack and cam, returning to terminal T-1.

3. Upon tripping, the circuit is opened by the movement of the rack to the right and transferred to the right hand contact assembly of the rack. The circuit remains open until the shutter cam closes its right hand contact assembly. The shutter is then ready to be re-tripped, repeating the above sequence through the left hand contact assemblies.

Motor Wind Circuit

1. Upon tripping the shutter and the movement of the shutter rack to the right, in the above schematic wiring diagram, the right hand rack contact assembly closes the shutter wind relay circuit from terminal T-2, through the right hand contact of the rack, the right hand contact of the cam and the shutter wind relay coil, returning to terminal T-1, the left hand contact and contact arm of the shutter wind relay energizing the shutter wind motor.

2. The shutter wind motor continues to run, winding the shutter spring and rotating the cams shown 180°, opening its circuit at the right hand contact assembly. The magnetic clutch of the motor disengages the drive immediately, preventing the cam from coasting beyond the desired position, the motor coasting to standstill.

Secondary "C" Pulse

1. Upon the beginning of rotation of the cam the "C" pulse contacts are closed and held closed for approximately 1/8 second. During this period a secondary "C" pulse is sent to the camera body case drive to initiate the movement of film through the magazine. This circuit is completed through the right hand contacts of the shutter wind relay, the balance of the circuit is shown dotted in the diagram.

FIG. 21. Schematic wiring diagram showing louvre shutter operation. (48" 9"×18" camera.)
(Designed by William Mungall, Photographic Laboratory, Wright Field, Ohio.)

is synchronized to the flash-bomb illuminant by a photo-cell trip unit. When used with an Edgerton-type flash unit, synchronization is simpler; the shutter, when wide open, triggers the flash unit through an auxiliary contact within the shutter. Because of the illumination characteristics of the flash-bomb, relatively long exposures of about 1/25 second are used, but the shutter must be fully open within 12 or 13 milliseconds after detonation for optimum efficiency. The combination of camera stabilization, antivibration mounting, and image motion compensation will yield greater definition in night photography; and use of longer peak illuminants and longer exposures will then permit photography from greater altitudes.

Because of the shutter synchronization and illumination problems in night photography, focal plane shutters are impractical; no such shutters are contemplated for future night cameras. Under development at this time is a 9×18-inch format night camera which will employ a 24-in. focal length f:3.5 lens. This lens requires a between-lens shutter approximately 5.25 inches in diameter; shutter speeds will not exceed 1/40 second.

When the advantages and potentialities of the moving film principle were first realized, some enthusiasts felt that there was no further need for high speed shutters. Subsequent realizations of the important requirements for oblique photography have modified this thinking and forced the emergence of a clearcut shutter doctrine, with respect to both tactical employment and developmental trends. This doctrine calls for exposure control via shutter speed control; hence the shutter will have to provide sufficient range for exposure control; it is estimated that a range in shutter speeds of about 30 to 1 will suffice for this aspect of the development trend. As noted earlier, most deleterious effects on definition—vibration, angular motion of camera axis, error in image motion synchronization—are reduced as shutter speed is increased; the aerial photographer will or should always use the highest shutter speed consistent with good exposure.

MEMORANDUM REPORT REFERENCES

1. EXP-M-59-680-46-1, *Characteristics of Between-Lens Shutters*, August 11, 1942.
2. EXP-M-59-680-46-2, *Methods for Testing Between-Lens and Focal-Plane Shutters*, August 11, 1942.
3. EXP-M-59-680-47-1, *Characteristics of Focal Plane Shutters*, August 11, 1942.
4. EXP-M-59-676-23-1, *Investigation of Possibilities of a Shutter Based on Birefrigence*, January 20, 1943.
5. ENG-M-59-680-47-3, *Use of the Strobotac for the Testing of Focal Plane Shutters*, February 10, 1943.
6. ENG-59-680-47-4, *Effect of a Glass Pressure Plate upon the Characteristics of a Focal Plane Shutter*, May 27, 1943.
7. ENG-59-680-47-5, *Shutter Tests of British F-52 and F-24 Cameras*, May 27, 1943.
8. ENG-59-680-16-4, *The Mitchell High Speed 6" K-17 Shutter*, August 30, 1943.
9. ENG-59-680-60-1, *Measurement of Slow Shutter Speeds by Use of Strobotac and Hurd Tester*, September 16, 1943.
10. ENG-59-680-60-2, *Shutter Characteristics of the K-22 Camera*, October 19, 1943.
11. ENG-59-680-60-3, *Proper Mounting of Focal-Plane Shutters for Oblique Aerial Photography*, January 7, 1944.
12. ENG-59-680-60-4, *Theory and Calculation of Distortion Produced by Focal Plane Shutters*, January 14, 1944.
13. ENG-59-680-60-5, *Use of Be-Al Alloy for Shutter Leaves in Aircraft Cameras*, January 29, 1944.
14. ENG-59-680-60-5a, *Errors in Photo Interpretation Due to Tip, Tilt, Variable Angle of Attack of Photo Aircraft, and Other Factors*, February 5, 1944.
15. TSEPL-4-675-170-1, *Optimum Film-Lens-Shutter, Combination for Proposed 70-mm Attack-Strike Camera*, June 28, 1945.
16. TSEPF-4-680-70-2, *New AAF Universal Shutter Tester*, October 12, 1945.
17. TSEPF-675-145-1, *Shutter Materials*, May 22, 1947.

Colorimetric Analysis of Dye Mixtures*

DAVID L. MACADAM
Kodak Research Laboratories, Eastman Kodak Company, Rochester, New York
(Received September 29, 1948)

Distributions of chromaticities have been computed for 171 pairs of typical dyes, involving five yellows, nine cyans, and nine magentas. Beer's law was assumed, and the computations were performed on automatic, punched-card computing and tabulating machines. A selected ordinate method was used. The concentrations of the dyes in each mixture were considered to be varied systematically, so that ninety chromaticities were computed for each pair of dyes. Since each dye was used in combinations with each of as many as eighteen other dyes, the results show the influence of various characteristics of spectrophotometric curves on chromaticity distribution, gamut, and luminous transmittance. Some computations were made to study the behaviors of neutral mixtures of triads of dyes when the concentrations of all components are changed by a common factor.

AN extensive series of colors[1] can be produced by using any colorant[2] in increasing concentration. A much greater variety of colors can be produced by mixing various concentrations of two suitably selected colorants. The complete range of dominant[1] and complementary wave-lengths[1] can be produced by mixtures of three suitable colorants, taken in pairs. When all three colorants are used together, each chromaticity[1] can be produced with luminous transmittances[1] ranging from very low values up to the maximum produced by one of the pairs. Some sets of colorants produce greater purities[1] than others, and some produce the various chromaticities at higher luminous transmittances than other sets.

The purpose of this investigation is (1) to determine the chromaticity range (gamut) and the maximum luminous transmittance of each chromaticity produced by typical sets of colorants (dyes in solution), (2) to compare the gamuts and transmittances of various sets, and (3) to associate the differences with the spectral-transmittance curves of the dyes, so that the advantages and disadvantages of any dye for color production can be judged from such curves.

Since the relation between the spectral transmittance of colorants and the colorimetric behavior of their mixtures is the subject of this paper, the simplest case has been studied. Beer's law has been used and the spectral transmittance of each combination has been computed as the product of the spectral transmittances of the components. Although the colorants are called "dyes" and are considered as if they were homogeneously dispersed, they may be of any nature, provided that the shape of the curve of $\log D_\lambda$ is invariant.[3] If the density produced by one colorant at some selected wave-length is taken as the measure of its *effective* concentration, the form of Beer's law may be used even though that law is not followed with respect to molar concentration. Variation in the shape of the curve of $\log D_\lambda$, whether caused by chemical reactions of any of the colorants, or to optical scattering, or limitation of maximum density by reflections from the surfaces of opaque samples, invalidates the use of Beer's law. Although these conditions would make the quantitative results of this

* Communication No. 1217 from the Kodak Research Laboratories.

[1] The nomenclature used in this article is that recommended by the committee on colorimetry of the Optical Society of America, in J. Opt. Soc. Am. **34**, 245–266 (1944). Familiarity with that nomenclature, and with the principles of color measurement and specification, and with the conventions recommended in 1931 by the International Commission on Illumination, is assumed. Those subjects are fully explained in the report cited, and also in J. Opt. Soc. Am. **34**, 633–648 (1944), in the *Handbook of Colorimetry* (Technology Press, Cambridge, Massachusetts, 1936, 1948), and in W. D. Wright, *The Measurement of Colour* (Adam Hilger, Ltd., London, 1944).

[2] The term *colorant* has been used to refer to substances which are responsible for selective absorption. They should not be called "color" because color is a visually perceived characteristic of light. The colorants encountered by the light on its way from the source to the eye are obviously not the sole determinants of the color. The source and the processes of human vision are just as important in determining the color.

[3] Optical density, D, is defined as the logarithm (to the base 10) of the reciprocal of transmittance. The subscript, λ, indicates values taken at specific wave-lengths. The expression $\log D_\lambda$ represents the logarithm to the base 10 of such values of density.

study inapplicable, the trends and general conclusions remain valid.

This investigation was undertaken because of its bearing on color photography, and on the choice of colorants for subtractive processes. The results are, however, applicable in many other fields where the special considerations of color photography are not involved.

Figures 1 to 5 show the spectral-transmittance curves of twenty-three dyes taken to be typical of the variety of dyes which will produce extensive gamuts of high brightness in three-component mixtures. Dyes used in some processes of color photography are represented fairly closely by some of these curves. The characteristics of some new dyes which are thought to be improvements on those used at present are represented, at least in the general features which are expected to be advantageous. Insofar as possible, the curves for different dyes have been made coincident, so that the differences in color-mixture behavior would be clearly consequences of the prominent features in which the curves differ. Such features include wave-length of the midpoint of each absorption edge, slope of each absorption edge, extreme red transmittance of cyans, and violet transmittances of cyans and magentas. A sufficient variety of these features, with enough system among the differences, has been provided so that the colorimetric behavior of mixtures of dyes not included can be estimated by interpolation, without extensive further computation.

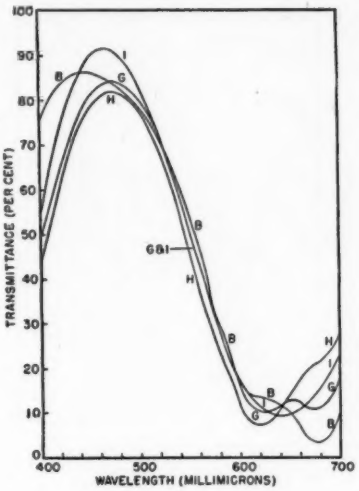

FIG. 2.

Four hundred and five sets of three dyes, one yellow, one magenta, and one cyan, can be selected from the twenty-three dyes represented in Figs. 1 to 5. The colorimetric behaviors of all these sets have been computed. The curves shown in Figs. 1 to 5 are for concentrations which produce nearly neutral three-dye combinations,

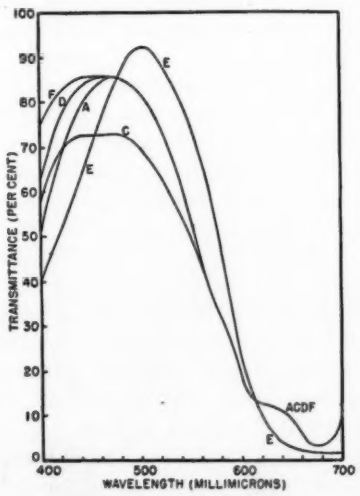

FIG. 1.

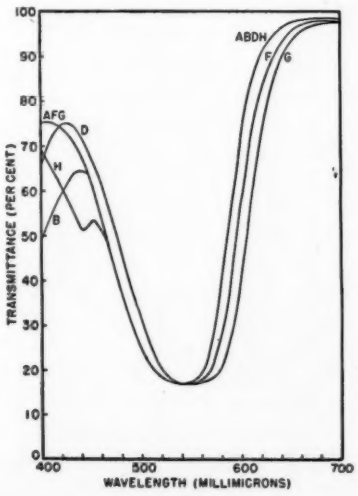

FIG. 3.

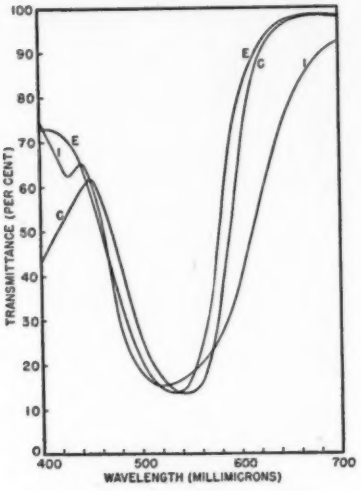

FIG. 4.

transmitting about ten percent of the incident light.

All the colorimetric computations were performed on the punched-card equipment at the Rochester Service Bureau of the International Business Machines Corporation, following a procedure devised by the author. The thirty-selected ordinates method[1] was used, and the ordinates were selected for the ICI standard source, *C*, "artificial daylight." Ninety cards, each punched

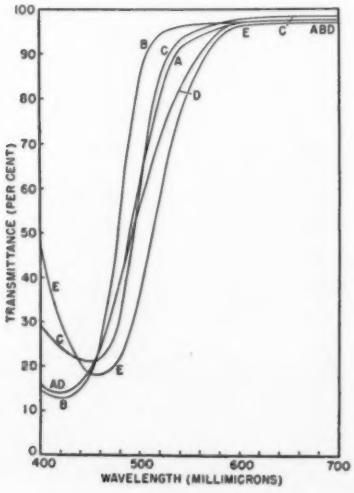

FIG. 5.

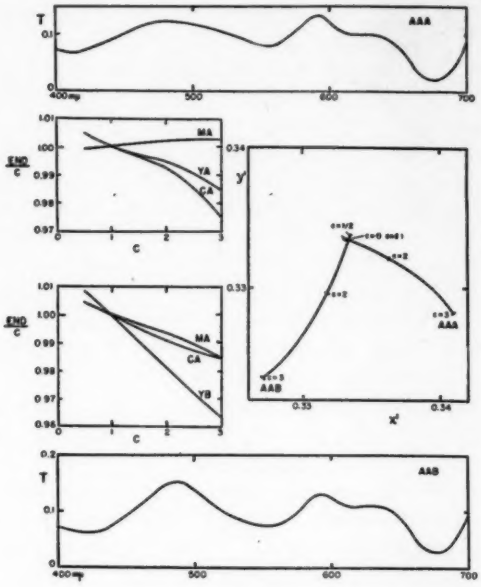

FIG. 6.

in three columns to indicate the value of one selected ordinate of the curve shown in Figs. 1 to 5, were prepared for each of the twenty-three dyes. Each card of these sets of ninety cards was identified by alphabetical identifications punched in two columns, the first *A*, *B*, or *C* identifying the dye as a cyan, magenta, or yellow, the second identifying the particular dye as indicated on Figs. 1 to 5. Each card was further identified by *X*, *Y*, or *Z* indicating which of the sets of selected ordinates it contained, and by numerical punches in two columns showing the specific ordinate of each set of thirty.

A set of cards constituting a table of numerical powers of decimals from 0.010 to 0.999 was prepared. In addition to one of the 990 possible values of transmittance for unit concentration, punched in the same columns as the "dye" cards prepared from Figs. 1 to 5, each "powers" card had twenty powers of that decimal punched in twenty other sets of three columns each. Those powers were: 0.01, 0.02, 0.05, 0.1, 0.2, 0.3, 0.4, 0.5, 0.6, 0.8, 1.2, 1.4, 1.6, 1.8, 2.0, 2.2, 2.4, 2.6, 2.8, and 3.0, and the numbers punched were therefore the transmittances for those concentrations of the dye.

After the dye cards were all prepared, they were sorted according to the values of the selected ordinates behind the corresponding powers cards. The powers cards were identified as a set by a special controlling punch, so that when the combined file was passed through a reproducing punch, all the information punched in the sixty columns specified above was automatically transcribed to each dye card that followed any one powers card. Thus, the selected transmittances of each dye for twenty other concentrations were determined and recorded at the rate of one hundred cards per minute, or two thousand selected ordinates per minute. This transcription, or gang-punching, procedure is by far the most efficient method available on the standard business computing machines, and was used in obtaining over ninety percent of the results in the present study.

After the dye cards were punched with the values of the selected ordinates for the unit and twenty other concentrations, they were resorted, according to dye and ordinate set. The sets of selected ordinates were then added and summary cards containing the totals and identifications of the dye and ordinate set were punched, in a single automatic operation. The selected ordinates for as many as eleven concentrations of any one dye were added simultaneously, at a rate of 80 cards, or 880 ordinates per minute. The summary cards were then sorted according to the dye identifications, the three totals of the selected ordinates for each of the concentrations were added, and the grand total was punched. With three further simple, automatic operations, the subtotals were multiplied by the reciprocal of the grand total to determine the chromaticity coordinates, x' and y', for each concentration of each dye. These are not the standard ICI chromaticity coordinates, because the adjustment factors for selected ordinates, corresponding to the ICI source, C, were omitted. The chromaticity diagram obtained by plotting x' and y' in rectangular coordinates is so similar to the standard diagram that all of the results of the present study are shown in that manner.

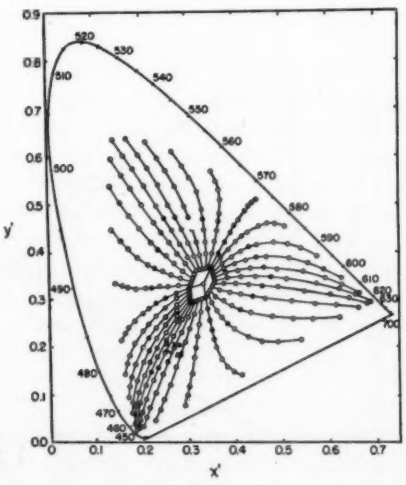

FIG. 7.

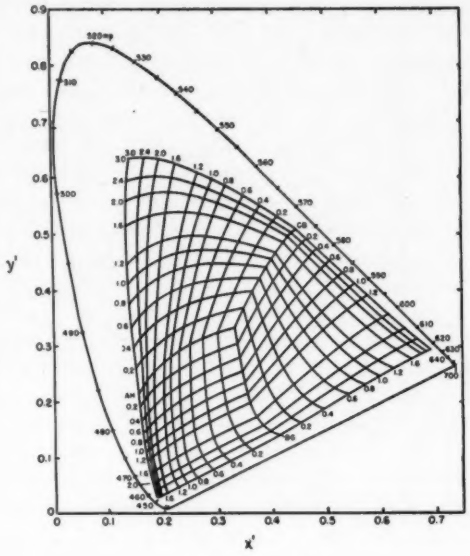

FIG. 8.

The corresponding ordinates for unit concentration of each of the three dyes in all of the 405 possible sets of three dyes were automatically multiplied together. The totals of the selected ordinates, and the chromaticity coordinates of each of the resulting, nearly neutral, combinations were computed automatically and tabulated. Modifications of the concentrations were estimated from the results, so as to obtain closer approximations to neutral combinations transmitting ten percent. The selected ordinates and chromaticities of the improved neutrals were computed similarly. A third approximation was

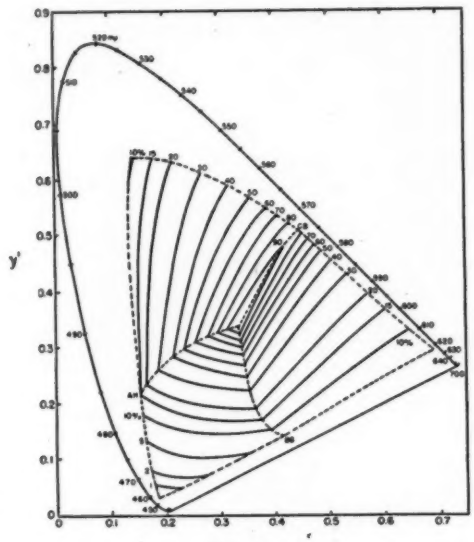

FIG. 9.

made in necessary cases. The selected ordinates of the resulting neutral mixtures were then raised to the 0.5, 2, and 3 powers by automatic transcription from the cards which constituted the table of powers. The resulting chromaticities and luminous transmittances were computed and tabulated. The results for two cases are shown in Fig. 6. Spectrophotometric curves, plotted from the computed ordinates for the unit-density neutral combinations, are shown at the top and bottom of the figure. The variation of chromaticity when all components are increased or decreased in the same proportions are shown to the right of center. Equivalent neutral density (abbreviated END in the diagram at the left of each figure) is a measure of the effectiveness of each dye component in producing a neutral mixture. It is the common logarithm of the reciprocal of the luminous transmittance of the achromatic combination which can be formed by combining the dye deposit with just-sufficient concentrations of the other two dyes of the set. Concentration, C, was measured by the algebraic exponent which was applied to the ordinates of the perfectly neutral unit density. The ratio of END to C indicates the loss or increase of chromatic- and density-producing efficiency of each dye when its concentration is changed. Such dependences are shown in the diagrams at the left of Fig. 6. It will be noted that the effectiveness of any particular dye depends upon the other two dyes with which it is used.

The most important information concerning the behavior of dyes in subtractive mixtures is obtained by a study of mixtures of pairs of dyes. The extent of the gamut of obtainable colors, and the maximum luminous transmittance with which each chromaticity can be produced, are indicated by mixtures of pairs of dyes. Addition of a third dye cannot increase the saturation of the hues produced by any pair of dyes, and it always darkens the two-dye combination to which it is added. The third dye does, of course, make possible the production of all the hues which were not producible by the original pair, but these increases of gamut are properly investigated by considering the combinations formed by pairing the third dye with each of the other two dyes, separately.

For the investigation of all the possible mixtures of pairs of the twenty-three dyes, the spectral transmittances (selected ordinates) of unit density of each dye were multiplied by the corresponding selected ordinates for five multiples (0.2, 0.4, 0.6, 0.8, 1.0) of the unit density of each of the dyes of the other two classes. Thus, each ordinate for each yellow dye was

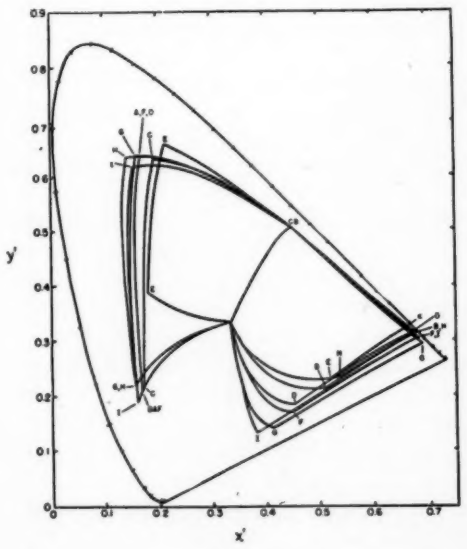

FIG. 10.

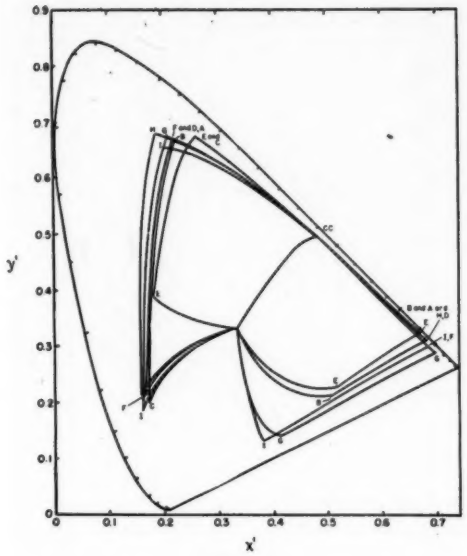

FIG. 11.

used as a common multiplier for ninety ordinates, all at the same wave-length. These consisted of one ordinate for each of five different concentrations of each of nine different cyan dyes and for five concentrations of each of nine different magenta dyes. The chromaticities of one set of the resulting combinations are shown by solid dots in Fig. 7. Each selected ordinate of each of these combinations was raised to nine different powers (0.2, 0.4, 0.6, 0.8, 1.2, 1.6, 2.0, 2.4, 3.0) by the rapid method of transcription previously described. This procedure corresponds to changing the concentration of both of the dyes in each mixture without changing the ratio of their concentrations. The resulting chromaticities are represented by the open circles in Fig. 7. It is an easy matter to select from these points, or to interpolate between points, so as to trace the loci of constant concentration of each of the component dyes. This has been done for all the possible pairs of dyes. One of the resulting diagrams is shown in Fig. 8. The luminous transmittance of each mixture is determined, of course, as part of the determination of chromaticity. The transmittance was written on the chromaticity diagram when the points were originally plotted. Contours representing constant luminous transmittance of mixtures of pairs of dyes were easily interpolated between the computed points. The results in one case are shown in Fig. 9. Forty-five diagrams of each of the two kinds just shown, supplemented by thirty-six diagrams of the lower left sectors (for the remainder of the eighty-one possible pairs of nine cyan and nine magenta dyes) were prepared from the automatically computed and tabulated results. Each of the complete diagrams, such as Fig. 8, represents 300 computed chromaticities, involving 2430 multiplications, transcription of 21,870 powers, and addition of 25,200 entries.

The dependence of the gamut of colors upon the spectral characteristics of the component dyes is shown in Figs. 10 to 14. The gamuts in each of these diagrams were traced from all the diagrams involving some one dye. In Fig. 10, the second yellow dye, CB, is common to all mixtures. The gamuts attainable with that dye, when combined with each of the nine cyan dyes, and with each of the nine magenta dyes, are shown in outline. Judged on this basis alone, the cyan dye, H, would appear to be best if high purities of bluish green were desired, but the cyan dye, E, would appear preferable if high purities of yellow greens were desired even at considerable sacrifice of bluish greens. Figure 11, in which the yellow dye, CB, has been replaced

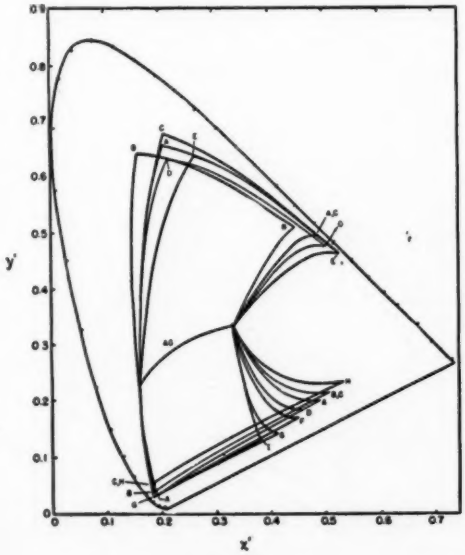

FIG. 12.

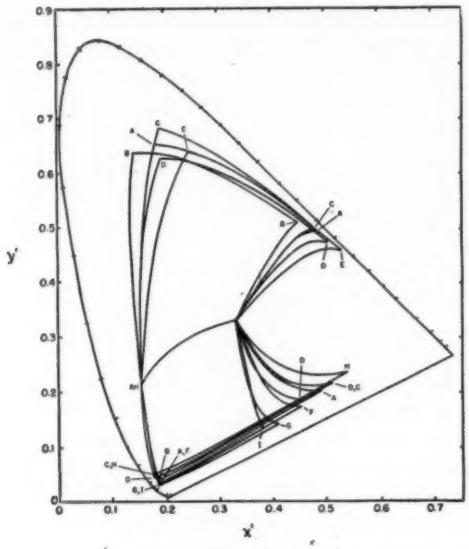

FIG. 13.

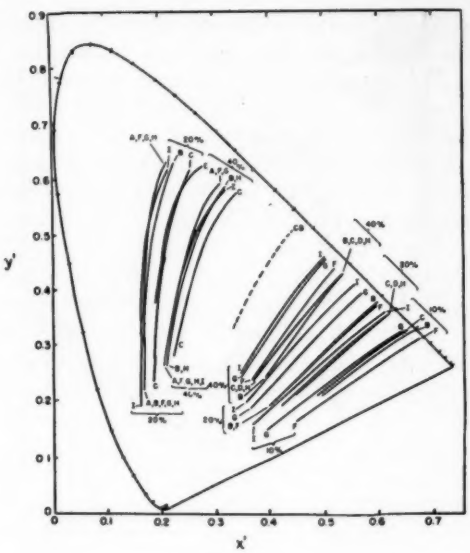

FIG. 15.

with another yellow dye, CC, shows substantially the same results, but now the cyan dye, C, is as good as E if yellow greens are the prime consideration. In both Figs. 10 and 11, the magenta dye, *G*, produced the highest purities of reds, with *F* and *I* tied for second preference. In Figs. 12 and 13, yellow and magenta dyes are compared on the basis of the gamuts obtained in mixtures with first one, AG, and then a second cyan dye, AH. These diagrams reveal the usual fact, which has some exceptions, that the relative merits of dyes do not depend upon the dyes with which they are combined for gamut tests. In Fig. 14 cyan and yellow dyes are compared on the basis of gamuts obtained in combination with the magenta dye, BF.

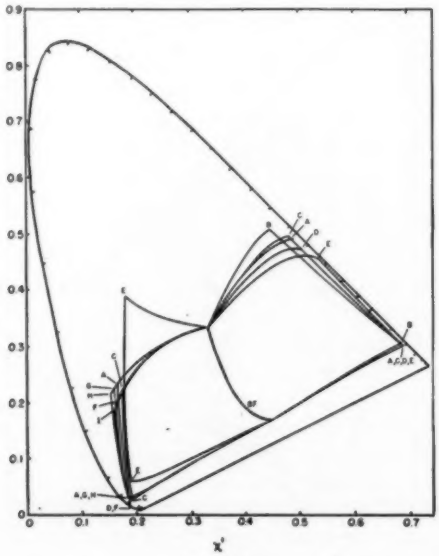

FIG. 14.

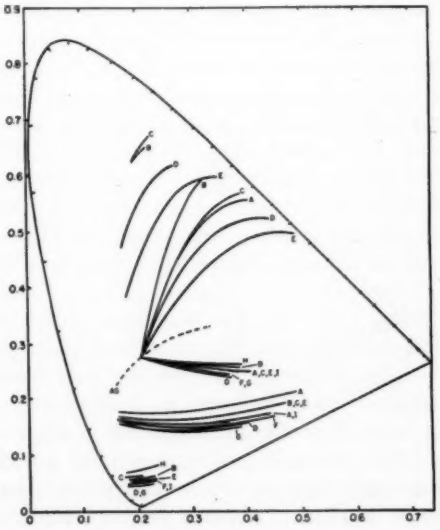

FIG. 16.

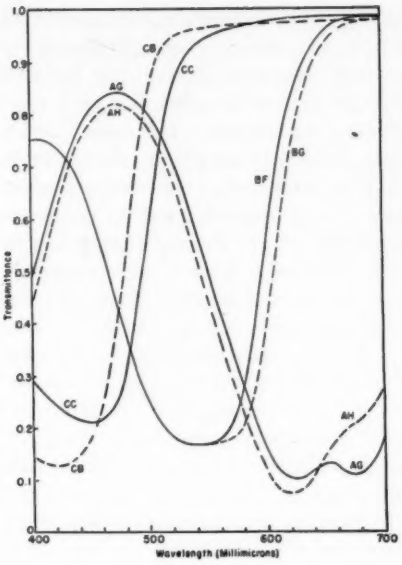

FIG. 17.

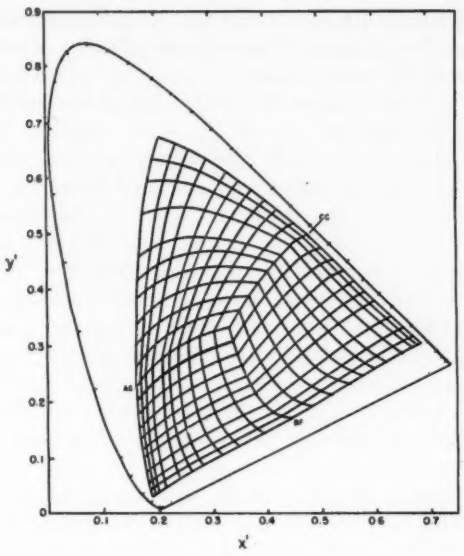

FIG. 19.

Figure 15 shows for luminous transmittances, 10, 20, and 40 percent, the limits of chromaticity of combinations of cyan and magenta dyes with the yellow dye, CB. The cyan dye, H, which gave the greatest gamut in the bluish-green region is among the best on the basis of transmittance also, but the cyan dye *E*, which was best for attaining high purity in the yellow greens, is poorest on the basis of transmittance.

The magenta dye, G, which produced the purest reds, is nearly as good as the best magenta dye on the basis of transmittance. It is remarkable, however, that the magenta dyes, F and I, which gave practically identical gamuts, give

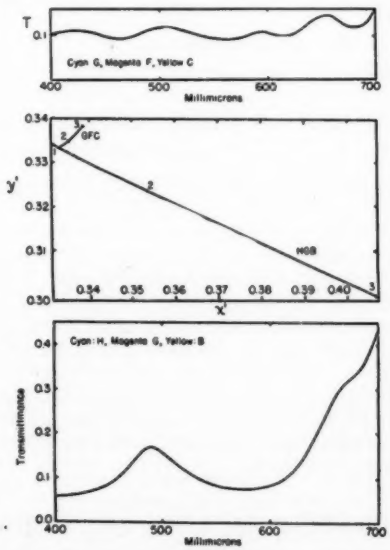

FIG. 18.

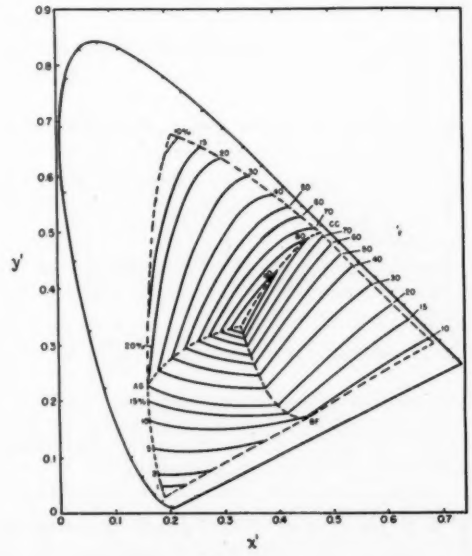

FIG. 20.

extremely different transmittance values, F yielding the highest transmittance of all magenta dyes, and I the lowest.

Figure 16 shows the limits of chromaticity for transmittances, 10 20, and 40 percent, for mixtures of each of the yellow and magenta dyes with one cyan dye, AG. The yellow dye, B, which gave the greatest gamut in the bluish green also gives the highest transmittance for all chromaticities obtained by mixtures with either of these cyan dyes. The magenta dyes, B and C, which gave the best violet gamuts, are among the poorest magenta dyes on the basis of transmittance, but the magenta dyes, D and G, which give the highest transmittance, were nearly as desirable as B and C on the basis of gamuts.

Similar comparisons can be made of the transmittance of mixtures of each of the yellow and cyan dyes with any one of the magenta dyes. As a result of all of these comparisons, an optimum set of dyes can be selected from the twenty-three considered. Such a set is shown by the solid curves in Fig. 17. The broken curves shown in Fig. 17 indicate a set which is slightly superior in gamut and transmittance to the set indicated by the solid curves, but the behavior of neutrals formed by the second set is very undesirable. Incidentally, the gamut and transmittance limits of this set are shown in Figs. 8 and 9. Figure 18 shows the spectrophotometric curves of the neutrals formed by these two sets of dyes. It also shows the variations from neutral when the concentrations of all components are changed by the same ratio. Neutrals which are as unstable as that indicated by H, G, B do not remain neutral when carried from the illumination for which they were designed (such as daylight) into some other, such as that from incandescent tungsten lamps.

The chromaticity gamut and loci of constant concentration of one component of each two-dye mixture of the optimum set are shown in Fig. 19. The corresponding limits of transmittances are shown in Fig. 20. Such chromaticity and transmittance limits can be attained by use of dyes chosen judiciously from dyes that are available today.

JOURNAL OF THE OPTICAL SOCIETY OF AMERICA VOLUME 39, NUMBER 1 JANUARY, 1949

Reflected Light and Ghosts in Optical Systems

ALLEN E. MURRAY
Scientific Bureau, Bausch and Lomb Optical Company, Rochester, New York
(Received July 16, 1948)

Each surface in an optical system reflects a small fraction of the incident flux, which thus is lost to the image; these surfaces singly and in combination form ghost images of the light source, in various locations in and about the system. The number of first-order ghosts is equal to the number of surfaces, and the number of second-order ghosts equals the number of pairs of surfaces. The total flux through the ghosts is shown to be $F_0\rho(1-t^{2n})/1-t^2$ for first-order ghosts, and

$$\rho^2 t^n \sum_2^n (i-1)t^{2(n-i)} = \frac{\rho^2 t^n}{1-t^2}\left[n-\frac{1-t^{2n}}{1-t^2}\right]$$

for the double reflection second-order ghosts, where n is the number of surfaces at which reflection can take place, t the transmittance, and ρ the reflectance at each surface. The left member has a simple interpretation.

In the general case of s interreflections, $1<s\leq n$, combinational theory indicates an expression:

$$\frac{n!}{(n-2)!2!}+2\frac{n!}{(n-3)!3!}+3\frac{n!}{(n-4)!4!}+\cdots+(s-1)\frac{n!}{(n-s)!s!}$$

for the number of ghosts, since (a) interreflection potentially can happen an unlimited number of times in any group, so that all multiplets of order less than s must be included, and (b) first reflection is prohibited at the first surface in all multiplets, because of the direction of light flow.

The relations are applied to a system of triplet condensers and projection lenses, coated and uncoated in all combinations. Even though the ghost flux is minimum in the condenser-unfilmed, objective-filmed objective, it offers no advantages over the all-filmed case, because of the lower transmission.

THE presence of reflected light in an optical system has long been recognized as the principal limiting factor in image contrast. Every image forming optical system inevitably degrades the contrast by the instrumentality of the flux scattered at the surfaces bounding the

elements, even though these surfaces be scrupulously cleaned. The natural lower limit of image flux is fixed by the reflectance of the element surfaces, their number, their radius, and the refractive power of the intervening components, it being assumed that the light scattered from the lens mount is completely negligible. Only the first factor is, after a fashion, at the disposal of the lens designer, since the primary considerations of geometrical image quality usually dictate the remaining lens parameters.

The use of transmission films has led to an amelioration of the flare, which has been perhaps the most important improvement effected by filming. The human eye, and to a large extent the photographic film, are comparatively insensitive to light levels, certainly within a scale of 2, but are by their nature delicately responsive to image contrast. An increase in brightness by a factor of 2 or 3 is less noticeable than an equivalent improvement in image contrast.

The calculation of transmittance increment with coating is a straightforward matter, requiring only a table of powers. The assessment of the decrease in flare light proves to be more involved. At no place in the available literature does there seem to be a thorough discussion in the general case of the number, strength, and distribution of the ghost images responsible for the reduction in contrast. Even so, numerous papers have been written on interreflections in optical systems,[1–4] and the main facts are widely appreciated.[5,6]

Thus, Tuckerman[1] is concerned with the interreflections in a pile of plates and the consequent transmitted and reflected flux after an infinite number of interreflections. This scholarly, well written article is not directly germane to our problem, however. Baker[3] derives the classic expression for the transmission of a pile of plates,

$$1-\rho/1+(n-1)\rho,$$

and thus by simple extension to the flare flux in the form

$$(1-\rho)/(1+(n-1)\rho)-(1-\rho)^n = (t)/(1+(n-1)\rho)-t^n,$$

where n is the number of surfaces, ρ the reflectance, and t the transmittance per surface. In these derivations an infinite number of interreflections has been assumed.

Benford[2] appears to be the first to realize that because of multiple interreflections, the order of differing filters is not commutative in combination.

Goldberg[5] clearly understood the physics of the ghost sources of flare light, and gave the correct formula for the number of second-order ghosts. He investigated the location, size, and numerical aperture of the ghost images from four lenses, including a Cooke triplet. The general effect of flare is brilliantly discussed in Mees,[6] but with a photographic emphasis.

There has seemed to be an irrational fear that the relations derived for a finite number of reflections would be needlessly cumbersome, or inaccurate, so a limiting process customarily has been invoked to simplify the expressions. Tuckerman showed that little error is introduced by the processes, which is evident also on simple grounds. If the reflectance of each of n surfaces is ρ, the flux reflected from the surfaces successively will be proportional to ρ^n. Thus if $\rho=0.04$, the Fresnel reflectance for crown glass, at the second surface only 0.16 percent of the incident flux is reflected, and at the third 0.006 percent, so that very little of the total flux can possibly be contributed by the higher order reflections.

At each surface of a lens system, a certain amount of flux will be reflected, to be reflected again and again until it is either absorbed or has found its way out of the lens either on the incident side of the system after an odd number of reflections, or the emergent side after an even number.

[1] L. B. Tuckerman, "On the intensity of light reflected from or transmitted through a pile of plates," J. Opt. Soc. Am. **37**, 818 (1947).

[2] Frank Benford, "Interface reflections between plane parallel surfaces," Gen. Elec. Rev. **38**, 277 (1935).

[3] T. Y. Baker, "Transmission of light through a pile of plates," Trans. Opt. Soc. **22**, 88 (1920–1921).

[4] C. Tuttle and H. E. White, "Factors which affect the contrast of a lens image in the motion picture camera," Trans. S.M.P.E. **31**, 591 (1927).

[5] E. Goldberg, *Der Aufbau des Photographischen Bildes* (Wilhelm Knapp, Saale, 1922), p. 24 *et seq.*

[6] C. E. K. Mees, *The Theory of the Photographic Process* (The Macmillan Company, New York, 1942), p. 788 *et seq.*

Note added in proof: In a private letter from Kodak Park, Mr. H. O. Hoadley reports another derivation of Eq. (5) in a more formal manner, and includes a reconciliation of it and the relationship of Tuttle and White.

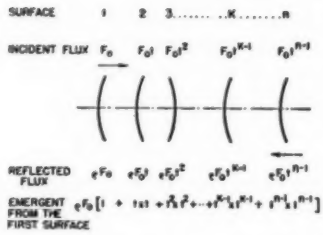
SURFACE 1 2 3 ..... K ..... n
INCIDENT FLUX F_0 F_0t F_0t^2 F_0t^{K-1} F_0t^{n-1}
REFLECTED FLUX ρF_0 ρF_0t ρF_0t^2 ρF_0t^{K-1} ρF_0t^{n-1}
EMERGENT FROM THE FIRST SURFACE $\rho F_0[1 + 1\cdot t + \rho^2 t^2 + \cdots + \rho^{K-1}t^{K-1} + \rho^{n-1}t^{n-1}]$

FIG. 1. First-order ghosts. The arrows indicate the direction of light flow.

FIRST-ORDER REFLECTIONS

Thus on the first or incident side of the system there is one ghost from each of the surfaces (see Fig. 1). Each of these primary ghosts has a strength given by the product of the surface reflectance and the flux at the surface. Assuming no losses by absorption, the flux at the kth surface, reckoning from the incident surface, will be F_0t^{k-1}. The flux returning from this surface will be $F_0\rho t^{k-1}$. This flux will have to pass through $k-1$ surfaces to emerge from the system, and will suffer an attenuation t^{k-1}, so the flux emergent from the kth surface ghost will be $F_0\rho t^{2(k-1)}$. Then the total ghost flux from all the first-order ghosts will be

$$F_0\rho[t^{2(n-1)}+\cdots+t^4+t^2+1]=F_0\rho\sum_1^n t^{2(k-1)}.$$

Now since

$$(1-x^{s+1})/(1-x)=1+x+x^2+\cdots+x^s \qquad (x^2<1), \quad (1)$$

the flux from all the first-order ghosts becomes

$$F_0\rho\sum_1^n t^{2(k-1)}=F_0\rho(1-t^{2n})/(1-t^2). \qquad (2)$$

The flare on this side is strong because of the single power of ρ. It would be important in reducing the potential contrast of projected pictures, for instance, by illuminating a glass slide from its front. It would also degrade the contrast in photographic practice in being reflected from the inside surface of a before-the-lens filter.

SECOND-ORDER REFLECTIONS

On the emergent side, the strongest ghosts are those arising from two reflections, the second-order ghosts (see Fig. 2). These are the ghosts which have received attention in the literature, for they are the ones which clearly have major effect on the image.

Obviously, each pair of surfaces is responsible for a ghost of the second order. Their number then is equally clearly the number of pairs that can be formed from the surfaces in the system:

$$n!/(n-2)!2!=\tfrac{1}{2}n(n-1),$$

which is the widely quoted formula for the number of second-order ghosts. The number of ghosts, and thus the flare flux, increases rapidly with the complexity of the system.

The flux through the second-order ghosts is derived in a manner similar to that used for the first order. The flux incident on the *last* surface of the system will have had $n-1$ surfaces to traverse before it arrives, and thus will be proportional to t^{n-1}; the surface will reflect a fraction ρ, so that starting through the system in the counter direction is a flux proportional to ρt^{n-1} from reflection at the last surface. Now this flux encounters first the penultimate surface, at which a flux proportional to ρ^2t^{n-1} is reflected toward the image. This will suffer a loss t on passing through the last surface, so that ρ^2t^n leaves. By the same token, the flux leaving the last surface after suffering first reflection at the last and second at the antepenultimate is clearly ρ^2t^{n+2}, since the penultimate surface has been traversed twice. In the same way a flux proportional to ρ^2t^{n+1} is incident on the fourth last surface, coming from the last, and will have three surfaces to traverse, so that the flux leaving the system after reflection at the last and third last surfaces is proportional to ρ^2t^{n+4}. Proceeding in the same way, considering the flux reflected first at the ultimate surface and at each of the preceding surfaces in turn, and summing to find the total flux from this sytem of ghosts, we find it to be proportional to

$$\rho^2t^n[1+t^2+t^4+\cdots+t^{2(n-2)}]=\rho^2t^n\sum_0^{n-2}t^{2i}$$
$$=\rho^2t^n\left[\frac{1-t^{2(n-1)}}{1-t^2}\right] \qquad (3)$$

by virtue of Eq. (1). This is the flux from the $n-1$ ghosts arising from reflection at the last surface and successively at the preceding surfaces.

The calculation of the flux from the $n-2$ ghosts whose first reflection occurs at the penultimate surface proceeds in the same manner. Here the flux ρt^{n-2} is reflected, since $n-2$ surfaces are traversed before it is reached. Reflection at the antepenultimate surfaces means 2 more surfaces to pass through before exit for a flux proportional to $\rho^2 t^n$. At the fourth last surface a flux ρt^{n-1} is incident. This must traverse three surfaces in leaving the lens to give $\rho^2 t^{n+2}$ as the flux leaving under these circumstances. The total flux from these ghosts is

$$\rho^2 t^4[1+t^2+t^4+\cdots+t^{2(n-3)}]=\rho^2 t^n \sum_0^{n-3} t^{2i}$$

$$=\rho^2 t^n\left[\frac{1-t^{2(n-2)}}{1-t^2}\right].$$

Generally, the flux from the system of ghosts arising from first reflection at the $n-p$th surface, where p is reckoned from the last surface and $1\leq p\leq n-1$, and subsequent reflection at each of the preceding surfaces is:

first reflection at last surface	$\rho^2 t^n[1+t^2+t^4+\cdots+t^{2(n-p-1)}]$
first reflection at penultimate surface	$\rho^2 t^n$
first reflection at penultimate surface	$\rho^2 t^n$
first reflection at third penultimate surface	$\rho^2 t^n$
first reflection at second penultimate surface	$\rho^2 t^n$
total	$\rho^2 t^n \sum_0^{n-(p+1)} t^{2i}=\rho^2 t^n\left[\frac{1-t^{2(n-p)}}{1-t^2}\right]$. (4)

The total flux from all the $\frac{1}{2}n(n-1)$ ghosts is given by the sum of these expressions up to $p=n-1$:

$$\rho^2 t^n \sum_{p=1}^{n-1} \sum_{i=0}^{n-(p+1)} t^{2i}=\rho^2 t^n \sum_1^{n-1} \frac{1-t^{2(n-p)}}{1-t^2}$$

$$=\frac{\rho^2 t^n}{1-t^2}\left[(n-1)-\sum_1^{n-1} t^{2(n-p)}\right],$$

or

$$\rho^2 t^n/(1-t^2)[n-(1-t^{2n})/(1-t^2)] \qquad (5)$$

in place of the more complicated relationship quoted by Tuttle and White[4] and Mees (reference 6, note in proof).

An equivalent, and very interesting and revealing alternative form of this expression can be found by summing all the expressions on the left-hand side of Eqs. (3) and (4); this will give, after omitting the common factor $\rho^2 t^n$,

$$1+t^2+t^4+\cdots+t^{2(n-3)}+t^{2(n-2)}$$
$$1+t^2+t^4+\cdots+t^{2(n-3)}$$
$$\cdots\cdots\cdots\cdots\cdots\cdots\cdots\cdots\cdots\cdots$$
$$1+t^2$$
$$1$$

$$(n-1)+(n-2)t^2+(n-3)t^4+\cdots 2t^{2(n-3)}+t^{2(n-2)}$$

which is obviously expressible in the general form

$$\sum_2^n (i-1)t^{2(n-i)}. \qquad (6)$$

Thus the proportionate flux in the second-order ghost images is given by either of the two equivalent relations

$$\rho^2 t^n \sum_2^n (i-1)t^{2(n-i)}=\frac{\rho^2 t^n}{1-t^2}\left[n-\frac{1-t^{2n}}{1-t^2}\right]. \qquad (7)$$

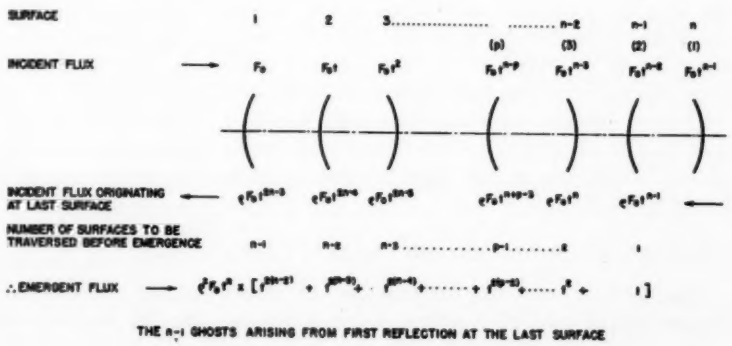
SURFACE
INCIDENT FLUX
INCIDENT FLUX ORIGINATING AT LAST SURFACE
NUMBER OF SURFACES TO BE TRAVERSED BEFORE EMERGENCE
∴EMERGENT FLUX
THE n−1 GHOSTS ARISING FROM FIRST REFLECTION AT THE LAST SURFACE

FIG. 2. Second-order ghosts. The $n-1$ ghosts whose initial reflection occurs at the last surface. The arrows indicate the direction of flow of the flux.

The expression on the left has a simple and very interesting physical interpretation. To make the introductory argument concrete, take the case of a triplet in which $n-6$. Then

$$\rho^2 t^6 \sum_{2}^{6} (i-1)t^{2(6-i)} = \rho^2 t^6[t^8+2t^6+3t^4+4t^2+5].$$

If the surfaces are numbered consecutively 1 through 6, the arguments will be made clearer. There are palpably five pairs of consecutive surfaces, 6–5, 5–4, 4–3, 3–2, and 2–1, and thus five ghosts arising from reflections at immediately adjacent surfaces. It is easy to see that the flux in these ghosts has had six surfaces to traverse, so it will be proportional to $\rho^2 t^6 \times 5$. There will be two ghosts arising from reflections in the ultimate-second (6–2) and penultimate-first (5–1) pairs of surfaces. This light will have traversed 5 and 4 surfaces, respectively, to first reflection, 3 between reflections, and 4 and 5 to leave the lens for a total of 12 surfaces, and a term $\rho^2 t^6 \times 2t^6$. The other terms can be accounted for in the same manner. There is obviously but one ghost arising from reflection at the last and first surfaces. This flux will have traversed five surfaces to first reflection, four between reflections, and five out of the lens for fourteen surfaces and the term $\rho^2 t^6 \times t^8$.

The generalization of this argument is clear. There will be $n-1$ ghosts from reflections at consecutive surfaces, in which at the $n-p$th surface there will be $n-p+p$ surface traversals to give the term $(n-1)\rho^2 t^n$. There will likewise be 2 ghosts arising from reflection at the ultimate and second, and penultimate and first surfaces. The flux in these ghosts will have traversed $n-1$ and $n-2$ surfaces to first reflection, $n-3$ between reflections, and $n-2$ and $n-1$ out of the lens for a total of $3n-6$ surfaces and a term $\rho^2 t^n \times 2t^{2(n-3)}$. Finally, there will be only one ghost arising from reflection at the last and first surfaces, in which the light has had $(n-1)+(n-2)+(n-1)=3n-4$ traversals in its course to-and-fro in the lens to give a term $\rho^2 t^n \times t^{2(n-2)}$.

NUMBER OF GHOSTS IN THE GENERAL CASE

The general law for the number of ghost images of the sth order, where $1<s\leq n$ can be stated as follows: The number of ghost images arising from s interreflections in a lens system of n surfaces is equal to the number of pairs which can be formed from the n surfaces, plus twice the number of triplets, plus three times the number of quadruplets, etc. The expression for this number is:

$$\frac{n!}{(n-2)!2!}+2\frac{n!}{(n-3)!3!}+3\frac{n!}{(n-4)!4!}+\cdots+(s-1)\frac{n!}{(n-s)!s!}.$$

It is clear that no new ghosts are added for $s>n$, so that the number of higher order ghosts is given by the same expression properly repeated.

The presence of the factor $s-1$ seems at first odd, but is reasonable on the basis of the unique position occupied by early surfaces in the reflection sequence. In any multiplet of order s, there are essentially only $s-1$ different ways in which interreflection can occur because the initial reflection cannot take place at the first surface.

This law is only of academic interest in view of the speed with which ρ^n converges to zero in repeated reflections. Further pursuit of the general laws from this standpoint would seem a sterile mathematical exercise.

EXAMPLE OF CONTRAST CALCULATION

Equations (7) give an upper bound to the ghost flux in the image space, since it is assumed that all the reflected flux finds its way to the image, which is an obviously false assumption in the presence of absorption at the walls. In fact, much of the ghost flux will be dissipated over the whole of the image space, since some of the ghosts at least will be in or near the last free aperture of the lens. From the ghost locations close to the lens, it is evident that the maximum illumination occurs near the axis of the image, except where by mischance an image lies close to the focal plane, when the ghost will lie on the principal ray through the source.

The relationships for the most important ghosts, those of the second order, lend themselves to the investigation of flare light. Using the

TABLE I. Ghost flux in combination filmed and unfilmed triplet systems.

		I	
		Filmed	Unfilmed
II	Filmed	16.8	14
	Unfilmed	204	170

standard values,

$$\rho=0.04, \quad t=0.96,$$
$$\rho=0.01, \quad t=0.99,$$

for unfilmed and filmed systems, respectively, and taking the case of a system of 6 surfaces, Eq. (7) gives for the ghost flux in the filmed and unfilmed systems 0.14 percent and 1.7 percent of the incident flux, respectively. By straightforward calculation it is easy to show that the transmittance gain on filming this system is 20 percent. Now if we set up four compound systems of six lenses each, in which each half of the system is filmed and unfilmed in turn, and include the two cases of all filmed and all unfilmed, we can calculate the ghost flux in each arrangement and in turn the ideal contrast for the important case of a projection system. Dropping the common factor F_0, the incident flux, and labeling the front half of the system I and the rear half II, and neglecting the ghost flux from I, the flux incident on II will be 1.20 and 1.00, with I filmed and unfilmed, respectively. This will give rise to ghost fluxes 0.0014×1.20, and 0.0014×1.00, if II is filmed, and 0.017×1.20 and 0.017×1.00, if not. These calculations can be displayed to best advantage in the following scheme (Table I), after multiplying by 10^4 to remove decimal fractions.

TABLE II. Reciprocal ghost flux, transmittance, and contrast relative to unfilmed optical systems.

I / II	Filmed filmed	Unfilmed unfilmed	Filmed unfilmed	Unfilmed filmed
1/ghost flux	990%	100%	83%	1210%
Relative transmittance	145%	100%	120%	120%
Contrast	1430%	100%	100%	1450%

Now if the all unfilmed system is taken as standard and the contrast defined as the maximum possible highlight-shadow ratio, the contrast can be evaluated by multiplying the reciprocal of the ghost flux by the transmittance referred to the proper basis. This has been done in Table II.

These figures have been qualitatively verified in our plant, as have similar calculations on other projection systems. A complete quantitative substantiation is not to be expected by virtue of the unrealistic assumptions and the exquisite character of the photometric techniques required.

It is a bit surprising that there should be so wide a difference in the ghost fluxes in the I filmed–II unfilmed, I unfilmed–II filmed, as against the all filmed and unfilmed cases, respectively. It is reasonable, however, that the maximum ghost flux should occur under conditions of maximum flux and reflectance, and the minimum where the flux and reflectance are smallest. The all filmed case occupies an intermediate position, for here the flux is high but the reflectance low. These differences are cancelled when the contrast of the whole system is computed. Naturally, the contrast in the image is fixed only by the objective, and in our case it is only the last half of the system which is effective.

Sensitivity of a Rapid Test for High Speed Parabolic Mirrors*

D. H. Rank, Paul Yoder, Jr., and Joseph Vrabel
Spectroscopy Laboratory, Physics Department, Pennsylvania State College, State College, Pennsylvania

(Received October 11, 1948)

A rapid test which has previously been used in testing the perfection of Schmidt cameras during construction has been used in the testing of a large, high speed parabola during figuring. Calculations are made which quantitatively show the state of perfection of figure obtainable by means of this test. Conditions are derived to show under what circumstances the test shows the maximum degree of correction.

RECENTLY we have constructed a parabolic of 16-in. aperture and 24-in. focal length for use on a long-wave vacuum infra-red spectrometer. The conventional method of testing the figure of such a mirror, making use of autocollimation and the Foucault test, would be extremely difficult and time consuming.

A parabola of the aperture and speed mentioned above departs from a sphere by an amount much too great to be corrected by polishing. It is necessary to obtain the major portion of the aspheric correction by figuring in the fine grinding stage. In order to make a test of the figure by the conventional method, it would be necessary to produce a reasonably good polish on the mirror after each fine grinding correction. In addition, it is difficult, time consuming, and awkward to make the necessary adjustments for the auto-collimation test when relatively short focal lengths and high aperture ratios are used.

H. A. Lower[1] has described a rapid simple test which he has used for the testing of the figure of a high aperture Schmidt camera. This test consists of setting up a slit at the focus of the camera and viewing the virtual image produced from a relatively large distance. The virtual image of the slit has the appearance of being localized on the correcting plate and is a straight line when good correction has been achieved.

It is easy to see that, to a first approximation, the test mentioned above yields proof of removal of spherical aberration when the localized virtual image appears to be a straight line and remains a sharp, straight line as the eye traverses the aperture. It is also apparent that this test can be used at least for preliminary correction of a parabolic mirror with very considerable saving in testing and trial polishing time. Obviously the "lower" test by its very nature must be made with the eye at a finite distance from the mirror. Observation at a finite distance will, of course, leave a small amount of residual spherical aberration when the localized virtual image has been figured into a straight line.

Quantitatively it is possible to calculate the perfection of the "Lower" test for a parabola by tracing selected rays by means of the law of reflection and the geometry of the system.

As a first example, we shall calculate the shape of the localized virtual image for a sphere under a definite set of practical conditions.

The geometrical problem is indicated in Fig. 1. The slit S is located at the paraxial focus of the sphere. The z axis is the axis of the optical sys-

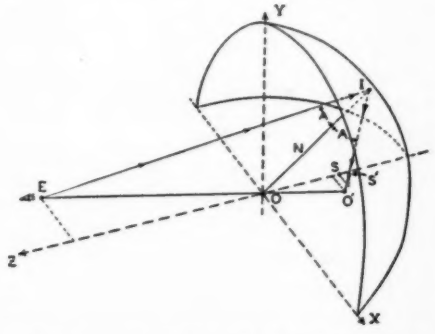

FIG. 1. Schematic diagram showing the course of skew rays reflected by a concave spherical mirror. X, Y, Z are rectangular coordinate axes. E, point of origin of ray, I, point of incidence on spherical mirror, O and N are the center of curvature and normal to the sphere. S is the position of a point on the slit, S' the intersection of the reflected ray with the plane containing the slit (Z=constant). A is the angle of incidence and angle of reflection of the ray.

* This research was carried out on Contract N6onr-269, Task V, of the Office of Naval Research.

[1] H. A. Lower, Amateur Telescope Making (Advanced). (Munn and Company, Inc., 1937), pp. 412.

tem. The eye will always be in the XZ plane when viewing the localized image. Since the rays emanating from the mirror are not strictly parallel (finite length slit), the mirror will appear to be illuminated only at those points on its surface where it sends rays through the pupil of the eye.

We shall first make our calculation with the eye located 25 focal lengths from the center of curvature of the mirror. (The choice of this distance is not completely arbitrary since it is well known that the aberrations of optical systems are nearly the same when the object distance is 25 focal lengths and the aberrations produced by the object are at infinity.) In addition, one still has reasonable sensitivity at this distance. The present calculation will be made with the eye located halfway between the center and the rim of the mirror in the $-x$ direction. At first thought, it might seem natural to trace the rays from the slit to the eye by way of the mirror. However, it can be seen that this would introduce unnecessary complexity into the problem since the optical system is not free of distortion, which aberration would require an adjustment of both X and Y coordinates of the point of incidence to pass the ray through the exit pupil (eye). If the path of the ray is traced from the eye to the slit, the desired result can be obtained in a much more simple fashion.

By reference to Fig. 1, the solution of the geometrical problem is obvious. The assumption is made that the incident ray lies in a plane parallel to the XY plane. The coordinates of E, I, the point of incidence, and O, which is on the normal N at the center of curvature, are all known, which allows all the sides and angles of the triangle EOI to be calculated. From the law of reflection, the angle of incidence, A, is equal to the angle of reflection. It is now possible to determine the side EO' in the triangle IEO'. Once EO' is known, the coordinates of O' can be calculated and the equation of the reflected ray obtained. Simultaneous solution of the equation of the reflected ray with the equation of the plane containing the slit (Z = constant) yields the coordinates of S'. In a similar manner, several points are calculated for different I's, only the Y coordinate of the I being changed. The resultant S''s are plotted in Fig. 2.

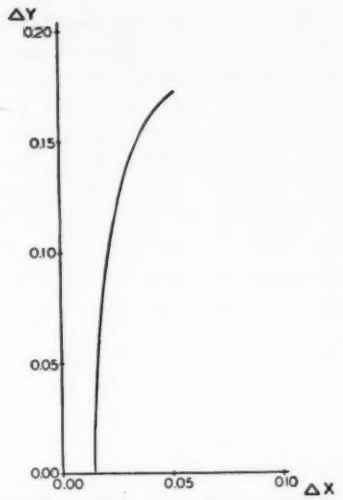

FIG. 2. Trace produced on plane containing the slit (Z = 24) when points of incidence, I, lie in a plane parallel to the YZ plane containing E. Coordinates of E are—4, 0, 600. Radius of curvature of mirror 48 inches.

The significant feature of Fig. 2 is that no point on this curve represents illumination of the mirror since the actual illuminated slit itself is on the y axis., i.e., no rays passing through the points of incidence (I's) in a plane parallel to the YZ plane will enter the eye. However, it is simple to find the X coordinates of the points of incidence which will pass the rays through the

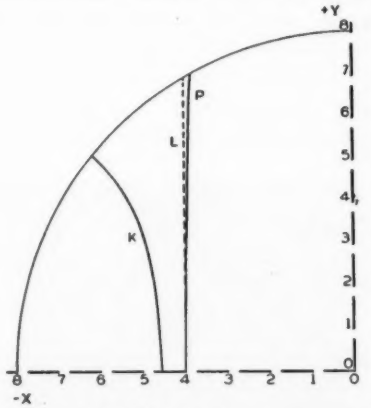

FIG. 3. Curves calculated showing appearance of mirror 16 inch diameter (Spherical 48-inch radius of curvature, parabolic 24-inch focus) when illuminated slit is 24 inches from mirror. The coordinates giving the location of the eye are—4, 0, 600. K locus of illumination produced by sphere. P locus of illumination produced by parabola. L illumination produced when mirror is figured to the "Lower" test.

pupil E. The method consists simply in choosing a new X for the point of incidence and recomputing the coordinates of S'. When $\Delta X = 0$ the incident ray passes through E and S and the coordinates of the point of incidence represent a point of illumination of the mirror. The curve, K, in Fig. 3 represents the illumination of a spherical mirror radius of curvature 48″, diameter 16″. Slit is 24 inches from mirror, and the coordinates of the eye point E are -4, 0, 648.

Making use of the same general procedure of calculation as outlined above for the sphere, the trace of illumination of a parabola of 24-in. focus was calculated. Except for the fact that it is necessary to obtain the coordinates of the point O (intersection of the normal with the z axis) by means of the calculus, the method of computation is identical with that used for the sphere. The curve P, Fig. 3, represents the trace of illumination produced by a parabolic mirror focus 24.00″ as seen by the eye located at -4, 0, 648. Curve L is the straight line which corresponds to the "Lower" test.

It can be seen by reference to Fig. 3 that the "Lower" test yields slightly better than 90 percent correction of the spherical aberration when used at 25 focal lengths from the mirror. A calculation was made for the eye point at 100 focal lengths from the parabola, and the result was that the "Lower" test then yields 97.5 percent correction of spherical aberration.

SENSITIVITY OF TEST

We can now arrive at the sensitivity and optimum physical conditions of applying the "Lower" test by performing a few mental experiments. Let us suspend a plumb line so that it will accurately bisect the "Lower" trace throughout its length. It is well known that the sensitivity of the eye to setting a filar line on the center of a moderately narrow illuminated image is approximately 12 seconds of arc. The calculations as shown by curve P, Fig. 3, show that the parabola is displaced from the "Lower" line by 52 seconds at the rim of the mirror for an eye distance of 25 focal lengths. This displacement is approximately 4 times the minimum detectable amount. Since it has been shown that the departure of the parabola from the "Lower" line is nearly inversely proportional to the eye distance, it is easy to see that the optimum eye distance for the unaided eye would be 50 focal lengths. In this case, the spherical aberration correction would be 95 percent. The test can be somewhat improved by using a telescope of 5 to 6 power with the objective stopped down to 0.5 cm instead of the unaided eye. In any event, the correction obtained by the "Lower" test is good enough so that if better correction is desired, it can be obtained by polishing and the employment of the conventional auto-collimation Foucault test.

Haidinger Fringes in a Basal Section of Calcite

BRUCE H. BILLINGS
Research Laboratories, Baird Associates, Inc., Cambridge, Massachusetts
(Received September 22, 1948)

Haidinger fringes were obtained with a partly silvered basal section of calcite. Two sets of fringes were observed: one associated with the ordinary ray, and one with the extraordinary ray. With a linear polarizer the two series are separated on the pattern diameters parallel to the polarizer axes. The oppositely polarized fringes periodically coincide and give rise to beats or a Moiré. An analysis is made to show that this coincidence occurs when the ratio of the fringe numbers of the coinciding fringes is the ratio of the squares of the two principal refractive indices.

THE Haidinger fringes in silvered mica were examined recently by A. H. Pfund[1] and interpreted by B. H. Billings.[2] Although the general case was treated in the second-mentioned paper, no further experimental work was done. Since the laboratory possessed several hundred basal sections of calcite, it seemed practical to examine the Haidinger fringes in this case as a further test of the calculations.

THEORETICAL

The general equation describing the Haidinger fringes in a plate which is isotropic or anisotropic but symmetrical about its normal can be written

$$\Gamma = (2nd/\lambda_a n_a)\cos r = Kn\cos r, \qquad (1)$$

where Γ is the retardation between the transmitted and twice-reflected ray, d is the plate thickness, λ_a is the wave-length in the immersion medium, n is the index of the plate, n_a is the index of the immersion medium, and r is the angle of refraction of the light in the slab.

For uniaxial crystal plates cut normal to the optic axis the index n will assume two values—n_o, the ordinary index for light whose electric vector is vibrating at right angles to the plane of incidence, and

$$n_e' = [n_e n_o/(n_e^2\cos^2 r + n_o^2\sin^2 r)^{\frac{1}{2}}] \qquad (2)$$

for light whose electric vector is vibrating in the plane of incidence. The two sets of fringes will be given by the expressions

$$\Gamma_o = Kn_o\cos r_o \qquad (3)$$

and

$$\Gamma_e = Kn_e n_o\cos r_e/[(n_e^2\cos^2 r_e + n_o^2\sin^2 r_e)^{\frac{1}{2}}], \qquad (4)$$

where the subscripts o refer to the ordinary rays and the subscripts e refer to the extraordinary rays, and where Γ_e or Γ_o must be a whole number of wave-lengths to have a bright fringe. Since these equations involve r as the only variable, they represent a series of circles. The two patterns will be independent and in each case a single linear polarizer will block a large part of two opposite quadrants of the circles.

The exact arrangement of the two sets of circles can be seen by a closer examination of Eqs. (3) and (4). Along the optic axis where $r=0$ the two indices are the same and the retardation through the crystal is the same for both polarizations. The first ring for one polarization will have a smaller diameter than the first ring for the opposite polarization. For a given retardation the relationship between the radii of different rings will be given by the

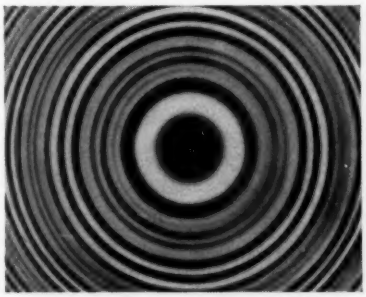

FIG. 1. Haidinger interference fringes in a basal section of silvered calcite 0.090″ thick. Photograph taken with unpolarized light at 546 mu.

[1] A. H. Pfund, J. Opt. Soc. Am. **32**, 383 (1942).
[2] Bruce H. Billings, J. Opt. Soc. Am. **35**, 570 (1945).

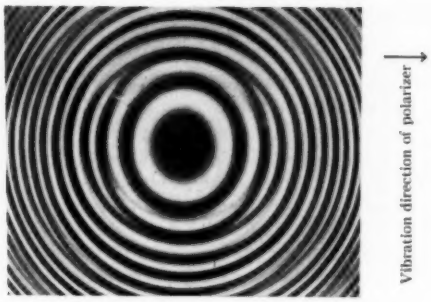

FIG. 2. Haidinger interference fringes in a basal section of calcite 0.090" thick. Photographs taken with linear polarized light at 546 mu.

equation

$$\cos r_o = n_e \cos r_e / [(n_e^2 \cos^2 r_e + n_o^2 \sin^2 r_e)^{\frac{1}{2}}]. \quad (5)$$

Since the retardation in the plate observed below is of the order of eight thousand waves, the smallest ring diameter is approximately 0.02 radian and $\sin r_o$ may be replaced by r_o. Equation (5) then becomes

$$r_o^2 = (n_o^2/n_e^2) r_e^2 / [1 + [(n_o^2/n_e^2) - 1] r_e^2]. \quad (6)$$

This can be further approximated to give

$$r_o^2 = (n_o^2/n_e^2) r_e^2. \quad (7)$$

For calcite $n_o = 1.6583$ and $n_e = 1.4864$. Thus the equation can be rewritten

$$r_o^2 \sim (5/4) r_e^2. \quad (8)$$

This factor connecting the ring radii is so large that one would expect a moiré or scalar interference pattern from the coincidence of fringes of opposite polarization.

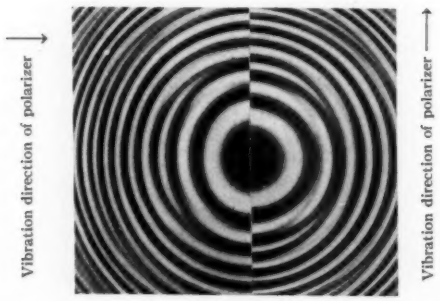

FIG. 3. Superposition of ordinary and extraordinary fringes from two Haidinger fringe photographs with polarized light.

Such a pattern was observed in the case of biaxial crystals and has also been studied for overlapping polarization interference patterns.[3] With the calculated ratio of the ring radii which give equal retardation it is possible to calculate which rings will coincide to give the moiré pattern. Since the index along the optic axis is the same for both polarizations, the retardation will be the same for both polarizations. Accordingly, if the fringes of opposite polarization are numbered starting from the center as fringe zero, fringes with the same number will correspond to equal retardations. Let "a" stand for the ring number associated with the ordinary ray which coincides with the ring number "b" associated with the extraordinary ray. At coincidence

$$r_{oa}^2 = r_{eb}^2. \quad (9)$$

Equation (7), which shows the relation between radii of ordinary and extraordinary rings of equal retardation, may be rewritten

$$r_{ob}^2 = (n_o^2/r_e^2) r_{eb}^2. \quad (10)$$

This equation can be combined with Eq. (9) and put into Eq. (3) to give

$$\begin{aligned} \Gamma_{ob}^2 &= K^2 - K^2 r_{ob}^2, \\ \Gamma_{oa}^2 &= K^2 - (n_e^2/n_o^2) K^2 r_{ob}^2. \end{aligned} \quad (11)$$

Since the ring number is approximately the retardation difference between the normal and the angle r,

$$\Gamma_{ox}^2 = (K - x)^2 \simeq K^2 - 2Kx. \quad (12)$$

If this is put in the two Eqs. (11), one finally gets

$$2b = K r_{ob}^2, \quad 2a = (n_e^2/n_o^2) K r_{ob}^2. \quad (13)$$

These can be divided to give

$$a/b = n_e^2/n_o^2 \sim \tfrac{4}{5}. \quad (14)$$

The ring numbers which coincide can then be written

$$r_{o,\,4i} = r_{e,\,5i}, \quad (15)$$

where i is an integer.

From this it is apparent that the fringe numbers which coincide are modulo 4 for the ordinary ray and modulo 5 for the extraordinary ray.

[3] Bruce H. Billings, J. Opt. Soc. Am. **34**, 267 (1944).

EXPERIMENTAL

Since Haidinger fringes are theoretically seen only in plane parallel slabs, it was necessary to select a piece of calcite which was not wedged. A preliminary survey was made by looking at a distant light source through the plates and determining which did not shift the source angularly. On the basis of this test a plate of calcite was selected which showed essentially no wedge.

An almost opaque coat of silver was deposited by evaporation on opposite sides of the crystal plate.

Although at first glance the plate was not sufficiently plane parallel to give Haidinger's fringes, a complete pattern was finally obtained by using a technique developed by Raman and Rajagopalan.[4,5] They showed that the effect of irregularities could be removed by using a small section of the plate and that this section will be large enough to observe a fringe of radius r if the size of the aperture is

$$a > 2d \tan r, \qquad (16)$$

where d is the thickness of the plate. Thus the complete fringe system can be seen if the radius of the aperture is greater than twice the thickness of the plate. If the irregularities of the plate are such that the fringes are blurred even with the reduced circular aperture, they can be seen by using a rectangular slit lying perpendicular to the direction of maximum irregularity. Even though this aperture may be so narrow that diffraction makes it impossible to see the fringes perpendicular to the slit, the pattern may be quite sharp in a direction parallel to the slit.

The small area in the crystal was exposed through a hole in a piece of tin foil. Light from an H4 mercury lamp was focused on this hole. The photographs were taken on lantern slide plates. A Wratten 77 filter was placed in the system so that the fringes would be formed only by the 546-mu line. The camera had a focal length of 135 mm and was focused at infinity. Photographs were taken of the crystal alone and of the crystal plus a linear polarizer.

Figure 1 shows the fringes obtained with unpolarized light. The beats between the two patterns are clearly shown. In Fig. 2 are the fringes obtained when a linear polarizer is placed in the beam. This effectively unscrambles the two sets of fringes—one appearing on the pattern diameter parallel to the plane of polarization and the other on the diameter at 90° to this. Figure 3 is a composite made by slicing Fig. 2 in two directions so that the ordinary fringes can be compared directly with the extraordinary fringes. From this figure it is clear that the ordinary fringes numbered modulo 4 are coindident with the extraordinary fringes numbered modulo 5.

It is a pleasure to acknowledge the help of Mr. George Economou in the preparation of this paper.

[4] C. V. Raman and V. S. Rajagopalan, J. Opt. Soc. Am. 29, 413 (1939).
[5] C. V. Raman and V. S. Rajagopalan, Phil. Mag. 29, 508 (1940).

JOURNAL OF THE OPTICAL SOCIETY OF AMERICA VOLUME 39, NUMBER 1 JANUARY, 1949

The Optical and Electrical Properties of Zinc Silicate Phosphors

ELEMÉR NAGY
Research Laboratories of the United Incandescent and Electrical Company, Ltd., Ujpest 4, near Budapest, Hungary
(Received October 14, 1948)

The spectra of zinc silicates with varying concentrations of manganese were measured at several temperatures. It was found that these emission spectra could be separated into bands conforming to Gauss error curves and that the location of these bands is almost unaffected by temperature and composition changes. It is shown that the width of these bands increases linearly with temperature and that the bands become wider as the activator concentration departs from the optimum. The dielectric losses of these phosphors were also measured as a function of the temperature and the very close connection between luminescence and dielectric losses first reported by Szigeti and Nagy for a zinc silicate sample was found valid for any zinc silicate. The electrical and luminescent constants all show maxima for the best fluorescing substances. These data make it very doubtful that activation is confined to divalent manganese. Consequently, a close analogy between the emission spectra of these silicates and the absorption spectra of permanganate and manganate compounds is worth studying.

OWING to the scarcity of reliable and noncontradictory data on the details of the fluorescence process as published during the first years of this decade, it was felt desirable to start a new series of measurements, with a greater accuracy than before and adopting new angles of attack, if possible. Zinc silicate activated with manganese was the fluorescent material selected for the investigation. Its emission spectrum and electrical conductivity were measured as functions of the temperature for various manganese concentrations. This material, artificial willemite, had already been the subject of thorough and successful studies, e.g., by Fonda,[1] Randall,[2] and Kröger.[3] The partial repetition of these investigations seemed worth while only under the condition that a greater accuracy of measurement could be achieved so that finer details might be found.

Any measuring apparatus with poor spectral resolution is naturally out of the question. A spectrophotometer of any type which depends on the eye as its indicator cannot be of the intended accuracy, and the merits of spectrophotographic work are lost in the necessary evaluating process. In the course of these experiments a new semi-objective method was used, the detailed description of which is published in a paper by Szigeti and Nagy.[4] Briefly the fluorescent emission and the light of a standard incandescent lamp were sent together through the spectrograph, after having been modulated by a rotating sector. The rotating sector, the light sources, and the slit were so arranged that to every pulse of fluorescent light there follows a pulse of incandescent light of the same duration and vice versa. This alternating beam of light strikes a multiplier photo-tube; the resulting a.c. (from the difference of the intensities of both sources in a given narrow frequency interval) is amplified and observed on a C.R. oscilloscope. By adjusting the aperture of a lens before the standard incandescent lamp, this a.c. current is made to disappear. The resulting accuracy of this arrangement is better than 1 percent of the maximum photoelectric response, and in some places, predominantly in the red, is much better, nearer to 0.1 percent.

TABLE I. Concentration of activator in phosphors.

Sample	Percent of manganese
A	0.005
B	0.23
C	0.74
D	1.16
E	2.9
F	5.9

[1] Gorton R. Fonda, J. Phys. Chem. **43**, 561 (1939).
[2] J. T. Randall, Proc. Roy. Soc. **170**, 272 (1939).
[3] F. A. Kroeger, *Luminescence of Solids Containing Manganese* (Elsevier Publishing Company, New York and Amsterdam, 1940).

BAND STRUCTURE OF ZINC SILICATES

The composition of the zinc silicates was invariably 60 parts ZnO and 40 parts SiO_2 by weight, and to these constituents were added various quantities of manganese in the form of

[4] G. Szigeti and E. Nagy, Publications of the University for Technical Sciences, Budapest. 1, No. 3 (1948).

TABLE II. Fluorescence of zinc silicates at various temperatures. For each sample the maximum at room temperature is taken as 100.0, all the other data are in its units.

	Sample *A*			
	Temperature			
Energy	20°	130°	217°	293°
2.52	29.8			
.51	30.6			
.50	31.3			
.49	39.2	33.9		
.48	45.6	39.5		38.4
.47	40.8	48.5		39.4
.46	47.9	53.0		36.5
.45	53.7	61.0	63.5	41.3
.44	65.5	65.9	63.4	46.2
.43	67.3	73.0	68.0	50.5
.42	75.6	79.2	73.0	51.3
.41	82.0	83.9	74.7	52.3
.40	88.3	86.0	79.9	55.6
.39	92.5	91.1	85.4	57.7
.38	97.2	97.4	82.8	59.1
.37	99.7	98.4	85.4	61.2
.36	99.8	100.0	85.9	61.6
.35	97.8	99.7	91.2	63.1
.34	96.5	98.6	91.0	62.8
.33	93.7	96.5	90.7	62.5
.32	87.3	92.4	88.0	61.7
.31	86.5	90.0	85.5	60.6
.30	86.4	84.5	83.5	60.9
.23	49.8	59.4	62.4	45.9
.22	42.8	57.6	61.5	40.8
.21	41.0	52.2	58.9	38.3
.20	33.2	51.0	55.4	35.3
.19	34.2	49.7	51.0	31.3
.18	26.9	48.8	46.9	28.4
.17	24.0	45.9	44.2	26.1
.16				24.9

TABLE II (*cont.*)

	Sample *B*					
	Temperature					
Energy	−160°	23°	111°	191°	273°	330°
2.50	25.0	33.9		29.3		
49	38.4	41.8	36.8	34.7		
48	45.0	46.1	41.1	37.6		
47	35.0	50.2	44.5	40.9		
46	43.7	54.4	48.2	44.1	36.7	
45	53.0	61.2	52.7	47.5	38.4	31.7
44	65.2	65.0	57.8	49.9	43.3	32.6
43	73.4	72.7	62.6	55.5	46.0	35.7
42	87.0	75.5	69.4	59.2	48.8	36.7
41	96.0	82.5	73.8	63.2	52.4	38.2
40	105.5	86.9	78.2	66.8	55.6	39.8
39	112.2	90.8	81.2	68.9	56.8	40.7
38	118.5	95.2	84.0	71.6	57.8	41.8
37	119.0	99.8	86.0	73.0	58.0	42.9
36	118.0	100.1	86.2	73.7	58.5	42.5
35	111.5	99.0	85.0	72.6	58.0	41.8
34	106.2	97.8	83.7	70.3	56.9	42.5
33	107.0	93.0	81.8	67.9	55.0	41.3
32	97.3	88.5	77.9	66.8	53.3	40.7
31	95.9	88.1	73.7	63.6	51.6	38.9
30	95.7	83.2	71.4	60.0	48.7	37.4
2.23	40.8	52.8	44.2	37.4	37.2	29.8
22	38.0	43.4	40.2	35.9	33.5	27.3
21	36.8	39.4	38.7	32.6	30.7	27.0
20	32.0	34.5	30.3	29.4	28.7	24.6
19	28.3	32.8	27.4	27.9	28.0	23.4
18	29.0	32.4	25.3	25.3	26.4	22.6
17	30.4	29.7	25.9	24.6	24.8	21.4
2.11		19.6	21.7	18.4	21.3	25.9
10		18.2	13.8	17.5	18.8	21.4
09	14.1	15.0	14.1	15.2	18.5	18.0
08		13.4	12.2	15.6	16.5	14.5
07	14.6	12.8	9.6	11.7	14.4	12.0
06		12.0	9.5	9.9		11.7
05		9.0	8.0	7.6		8.9

nitrate as shown in Table I. This mixture was repeatedly ground and fired at 1250°C. The emission spectra of all the samples examined at different temperatures are compiled in Table II. The spectrum, plotted in photon numbers *versus* energy or wave number, closely resembles a Gaussian error function. This form of the emission spectrum had already been reported in several cases. Henderson[5] and M. P. Lord and co-worker's[6] analysis shows that for ZnS and the tungstates the Gaussian function indeed describes the emission spectrum, and for zinc silicates and zinc beryllium silicates Szigeti,[7] K. H. Butler,[8] and Szigeti and Nagy[4] found the same result. The last-named authors suggested a simple explanation for this form of the emission spectrum, and discussed the conditions of validity for this expression.

The emission spectra were analyzed into their component bands by first plotting the measured points against the energy, then by assuming the validity of the form

$$y_0 = a_0 \exp[-b_0(h\nu - h\nu_0)^2],$$

taking its logarithm

$$\log y_0 = \log a_0 - b_0(h\nu - h\nu_0)^2$$

and with a suitably chosen maximum ($h\nu_0$) plotting $\log y_0$ against $(h\nu - h\nu_0)^2$. This representation has to give straight lines. If the graph is curved, the procedure is repeated with a slight displacing of the maximum. The straight parts of the graph, if the measured points do not fall below it, give the slope "b_0." Then the Gaussian is calculated and these values sub-

[5] S. T. Henderson, Proc. Roy. Soc. **173**, 323 (1939).
[6] M. P. Lord, A. L. G. Rees, and M. E. Wise, Proc. Phys. Soc. **59**, 473 (1947).
[7] Gy. Szigeti, Elektrotechnika, **39**, No. 4 and 5 (1947) in Hungarian.
[8] Keith H. Butler, J. Electrochem. Soc. **93**, 143 (1948).

TABLE II (*cont.*)

Energy	Sample *C* Temperature −180°	22°	125°	197°	269°	330°
2.50			24.6			
49		33.4	30.1	28.7		
48	11.2	34.2	34.7	31.7		
47	17.3	40.0	36.4	34.0		11.4
46	25.2	42.7	37.9	36.0	22.8	
45	34.3	48.7	42.0	37.7	25.7	12.8
44	44.9	53.7	49.8	38.5	27.7	
43	59.9	56.0	54,5	41.9	29.0	14.5
42	74.8	65.5	57.5	48.7	30.5	
41	90.9	73.0	62.7	51.0	32.3	17.0
40	108.4	82.6	66.3	53.2	34.1	
39	119.6	89.6	69.8	55.3	36.1	18.8
38	127.4	95.8	72.0	57.8	37.5	
37	128.8	99.0	75.0	58.8	38.4	20.8
36	127.1	96.0	76.0	62.2	39.5	
35	117.6	97.6	75.0	60.0	39.7	21.4
34	111.0	94.8	74.2	59.8	38.9	
33	100.7		71.8	56.0	38.1	21.2
32	90.0	86.0	70.2	55.2	37.4	
31	80.9	84.0	67.0	54.5	36.4	20.4
30	70.5	81.0	62.5	56.0	34.6	
29		75.4	66.0	54.6		20.0
23	36.7	42.5	36.0	32.3	29.7	18.7
22	36.3	40.5	36.3	30.4	30.0	
21	30.3	38.5	34.8	26.7	28.6	16.3
20	29.0	34.6	33.3	24.6	26.3	
19	26.4	29.7	31.0	22.4	25.2	14.8
18	23.9	28.3	29.5	22.2	23.7	
17	23.7	28.8	28.1	21.5	22.4	13.2
16	22.1	29.5	25.8	19.4	20.7	
2.11	10.9	20.1	17.5	13.4	13.7	9.7
10		18.2	15.4	10.4	12.3	
09		16.6	15.2	8.6	11.4	5.9
08		14.5	10.9	7.1	10.8	
07		11.0		6.8	9.3	4.4
06				5.5	8.9	
05		8.8		4.5	7.9	
04						
03					5.7	

TABLE II (*cont.*)

Energy	Sample *D* Temperature −180°	−60°	23°	75°	148°	207°	252°	317°
2.50	12.6	16.2	14.1	12.8	11.9	11.8	11.8	6.5
49	21.9	17.4	16.1	16.4	15.3	13.8	14.5	7.4
48	25.8	25.9	20.2	20.2	18.0	16.2	15.6	8.2
47	25.1	25.6	23.6	24.5	20.3	19.0	17.5	9.3
46	26.3	28.3	27.7	29.2	23.9	22.2	19.4	10.3
45	28.4	32.3	31.8	35.6	27.6	25.0	21.5	11.6
44	34.9	44.1	37.4	41.0	32.0	27.8	23.5	12.2
43	43.1	49.8	45.8	47.6	36.4	32.4	25.0	13.2
42	47.2	57.5	54.1	54.0	40.0	35.0	26.7	13.9
41	64.1	70.2	60.9	61.3	44.6	37.3	28.7	14.7
2.40	81.9	82.8	69.6	69.1	48.3	39.8	30.2	15.5
39	98.8	95.0	77.7	74.0	51.7	41.3	31.6	16.4
38	113.2	104.4	85.7	80.2	54.6	42.8	33.0	16.5
37	126.0	112.3	92.2	84.0	57.0	44.3	33.8	17.2
36	132.4	117.0	97.0	87.2	58.8	45.0	34.2	17.4
35	136.0	118.8	99.8	88.1	60.1	45.0	34.0	17.5
34	134.5	116.2	99.6	88.1	59.8	45.2	33.9	17.6
33	126.4	112.3	98.7	88.0	60.3	44.7	33.7	17.4
32	125.0	107.0	96.2	86.1	59.6	43.7	33.0	16.8
31	125.0	106.3	93.2	82.8	57.8	42.7	32.3	16.8
2.30	108.2	100.5	88.6	79.4	57.0	41.4	31.8	16.5
29	112.2	101.2	83.8		54.0	41.6	30.5	15.9
23		55.8	49.3	51.3	37.0	29.5	22.6	13.2
22		49.5	42.7	46.1	33.8	24.7	20.3	11.0
21	50.3	47.6	38.9	38.2	31.0	22.5	18.2	10.0
20		43.1	33.0	35.5	27.6	20.0	17.1	9.2
19	41.0	38.5	28.3	33.1	24.8	17.8	14.2	8.8
18		34.4	25.7	30.2	22.4	16.4	14.2	7.9
17	34.2	30.2	22.3	23.8	20.9	15.2	12.8	7.5
2.10		10.7	12.3	12.1	10.4	7.1	6.7	4.5
09	27.8	10.8	10.3	11.4	9.0	6.4	5.4	4.1
08		10.6	7.3	9.7	8.0	5.3	4.6	3.8
07	25.2	10.0	6.6	7.4	7.5	4.3	4.3	3.5
06		10.6	5.4	7.6	6.1		3.8	3.5
05	20.2	9.0	5.5	6.5			3.9	3.0
04		9.3	4.5	5.3				
03		6.6		4.2				

tracted from the measured ones, the difference plotted again and analyzed as before. Special care must be taken when two maxima are rather near, by repeating the process until complete agreement is reached. In the case of willemites, however, this procedure is not at all cumbersome, because almost half of the main band is free from any other band, so the repetition of the analysis was very seldom necessary.

The main band lies in the neighborhood of 2.35 ev. Its position is almost unaffected by temperature changes, but shows a slight but nevertheless clearly recognizable shift towards longer wave-lengths on increasing the amount of manganese.[9,1]

[9] H. W. Leverenz and F. Seitz, J. App. Phys. 10, 479 (1939).

The first subsidiary band lies at 2.17 ev. It could be found at any concentration of manganese and at any temperature. The behavior of this band is strictly parallel to that of the main band. For example, the shift of the main band to 2.32 ev in sample "*F*" is accompanied by the shift of this band to 2.13 ev. In Fig. 1 is plotted the spectrum of one of the brightest powders, sample "*D*," at room temperature, and in Fig. 2, the spectrum of sample "*F*" at liquid air temperature. Another band lies at 2.26 ev. Due to the almost complete coincidence of this band with the green mercury line, these present investigations could not elucidate the accurate laws for this band. Nevertheless, the measured points at 2.31–2.29 and, on the other side, between 2.23–2.18, lie invariably higher in most cases, more than would correspond to the

sum of the 2.35 and 2.17 ev bands, and this difference always increases towards the supposed band center.

A fourth band is to be found at 2.48 ev. It is again difficult to analyze this band and its constants thoroughly, for this band is extremely sensitive to higher temperatures. At room temperature its area is merely 2–3 percent of the main band, but the ratio increases at liquid air temperature to 6–10 percent. This band seems to be gradually suppressed by larger amounts of manganese.

The last band to be found in zinc silicates is situated at 2.04–2.05 ev. Addition of beryllium as in zinc beryllium silicates enormously enhances the emission in this band by simultaneous suppression of the emission in all the other bands. It is to be stressed, however, that the incorporation of beryllium in the lattice is by no means the necessary condition for the appearance of this band, for the same effect, although with a remarkably lesser efficiency, can be achieved by adding larger quantities of manganese, as was found here for sample "*F*" and by Kröger.[3] At the temperature of liquid air, as is to be seen in Fig. 2, this band is clearly separated from the others.

The constants of these bands are compiled in Tables III–V.

The origin of this complicated system of bands has previously been very obscure, so that many

TABLE II (*cont.*)

	Sample *E* Temperature				
Energy	−180°	24°	98°	146°	203°
2.54		12.5			
53		16.0			
52		19.7	20.8		
51		24.9	22.9		
50		26.5	23.3	18.8	
49		27.7	23.6	20.0	11.7
48		30.5	26.2	23.3	15.6
47		31.9	31.8	24.1	15.6
46		37.2	34.5	26.1	17.9
45		42.7	38.5	28.8	19.7
44		48.0	40.7	32.3	21.6
43		52.8	44.3	35.2	23.3
42		62.4	48.6	38.0	25.0
41	82.8	66.8	53.5	41.5	26.7
40	89.8	73.6	57.1	43.5	28.6
39	96.4	79.5	60.0	46.6	30.0
38	106.1	84.5	64.0	49.5	32.2
37	111.1	90.2	65.3	50.5	33.5
36	114.0	95.0	67.8	53.1	33.8
35	122.2	97.0	68.2	54.8	34.4
34	119.0	99.9	72.0	55.5	34.5
33	123.0	101.0	71.5	54.6	35.3
32	121.0	100.2	71.8	54.8	34.7
31	112.0	98.0	70.0	54.0	34.7
30	104.0	94.9	69.0	51.6	33.5
2.23	70.6	62.9	48.5	40.7	27.3
22	67.5	59.9	47.1	37.3	26.0
21	66.0	56.4	45.5	37.2	24.9
20	63.0	53.5	43.6	34.7	24.0
19	62.9	50.9	42.0	33.9	23.8
18	61.1	49.8	39.3	32.8	22.8
17	52.2	49.7	38.0	31.2	21.8
16	57.5		36.0	29.9	
2.11	43.6	35.7	27.4	21.3	17.1
10	45.0	35.2	25.5	19.2	15.8
09	43.2	35.6	23.8	17.8	14.4
08	39.2	32.3	21.1	16.1	13.3
07	38.0	29.5	20.8	14.6	12.2
06	30.8	26.0	18.4	12.6	10.8
05	36.5	27.9	18.3	10.9	11.4
04			15.3	9.8	9.3
03	21.8	21.5	13.1	7.9	8.1
02			10.9	6.8	6.9
01		12.8	8.4	5.4	5.7

TABLE II (*cont.*)

	Sample *F* Temperature			
Energy	−180°	23°	42°	68°
2.50		15.8	17.9	
49		18.5	21.2	24.4
48		21.8	24.8	27.2
47		28.3	30.3	30.8
46		32.8	34.4	35.1
45		38.4	39.4	38.6
44		44.5	44.3	42.0
43		50.8	48.9	45.7
42	54.6	57.0	53.0	49.0
41	63.7	63.1	58.0	54.4
40	73.5	68.1	64.5	58.0
39	84.4	75.2	68.0	60.7
38	97.8	80.4	72.8	63.2
37	106.6	85.5	78.4	65.9
36	115.0	90.7	82.2	67.9
35	121.8	95.2	84.5	70.4
34	127.7	98.3	87.2	72.0
33	131.3	99.8	90.3	73.6
32	131.6	100.5	86.7	73.8
31	131.0	99.5	86.5	73.5
30	128.3	97.5	85.4	72.9
2.23	86.1	70.5	66.2	59.0
22	79.0	67.9	64.4	56.2
21	76.3	64.8	57.0	53.6
20	74.4	60.8	55.7	51.0
19	71.3	58.2	54.0	47.3
18	69.4	55.7	49.3	44.8
17	69.8	54.2	48.5	42.2
2.11	56.4	43.7		40.6
10	52.7	43.4	37.0	32.9
09	47.6	37.4	34.6	27.7
08	41.8	35.4	33.9	27.2
07	38.2	34.4	30.8	21.3
06	35.8	32.2	28.8	
05	43.2	30.0	28.0	
04	40.9		24.8	
03	34.8		20.7	
02	24.9			
01	21.8			

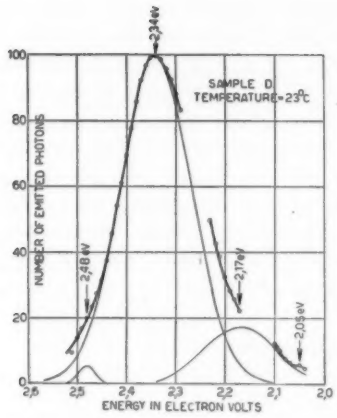

FIG. 1. Spectral distribution at 23°C of sample *D*, zinc silicate containing 1.16 percent manganese.

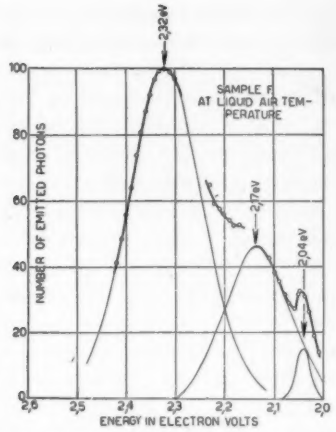

FIG. 2. Spectral distribution at liquid air temperature of sample *F*, containing 5.9 percent manganese.

authors disregarded even its existence. Szigeti, Nagy, and Makai[10] have shown, however, that the 2.35-, 2.26-, and 2.17-ev bands are all to be found as peaks in the absorption spectrum of the monovalent permanganate ion, and the band at 2.48 ev very probably belongs to the same compound. The 2.05-ev band likewise corresponds closely to the single bell-shaped absorption band of the divalent manganate ion. If we assume that the centers of luminescence are these ions themselves, then the recurrence of these bands in the zinc and zinc beryllium silicates and in a series of similar manganese activated materials is readily understandable. A further proof of the existence of these bands is given in the already quoted work of Butler[8] who found the same bands, with the exception of the 2.48 ev band, situated almost exactly at the same position. Butler, who restricted his studies to a single temperature, has inferred that the change in composition does not affect the broadening or sharpening of these bands, the widths being, according to him, always the same. This conclusion is hardly tenable, for it was found here beyond doubt, that the band width is the narrowest (the band the sharpest) at just that concentration of manganese, at which the quantum efficiency is a maximum, appr. 0.5–1.5 percent Mn, samples "*C*" and "*D*." At lower and higher concentrations the band flattens out again, and this broadening becomes more prominent, as the concentration of manganese departs from the optimum concentration.

[10] Gy. Szigeit, E. Nagy, and E. Makai, J. Chem. Phys. **15**, 881 (1947).

TABLE III. Constants of the main band.

Sample	Temperature	Max. ratio	Band width β in ev	Area ratio	Band max. at
A	20	100.0	0.1242	100.0	2.36
	130	100.0	0.1400	112.8	2.35
	217	91.2	0.1518	111.5	2.34
	293	63.1	0.1800	91.2	2.34
B	−180	119.0	0.0904	94.0	2.37
	23	100.0	0.1142	100.0	2.36
	111	86.2	0.1290	97.3	2.36
	191	73.1	0.1364	87.4	2.36
	273	58.3	0.1491	76.1	2.36
	330	42.5	0.1676	62.3	2.36
C	−180	129.0	0.0690	97.3	2.37
	22	100.0	0.0917	100.0	2.36
	125	75.3	0.1200	98.6	2.36
	197	59.1	0.1300	83.8	2.36
	269	39.4	0.1423	61.3	2.35
	330	20.7	0.1470	33.2	2.35
D	−180	136.0	0.0700		2.35
	20	100.0	0.1013	100.0	2.34
	75	89.5	0.1147	101.1	2.34
	148	60.2	0.1260	74.8	2.34
	207	45.2	0.1314	58.7	2.35
	252	34.0	0.1475	49.5	2.35
	317	17.5	0.1530	26.5	2.35
E	−180	123.4	0.1070	103.1	2.34
	24	100.0	0.1280	100.0	2.33
	98	72.0	0.1460	82.2	2.33
	146	55.2	0.1486	64.1	2.33
	204	35.2	0.1580	43.4	2.33
F	−180	132.3	0.1063	106.5	2.32
	23	100.0	0.1320	100.0	2.32
	42	87.2	0.1440	94.9	2.32
	68	73.2	0.1600	88.6	2.32

The position of these bands seems to be almost independent of temperature, although some variations in the position of the maxima of the order of 0.01 ev could be observed in some cases.

The most interesting peculiarity of this band complex is undoubtedly its temperature dependence. In this connection, only the main band and the band at 2.17 ev could be analyzed completely. First of all, it is remarkable that the ratio of the total number of emitted quanta in both bands is almost constant for a sample over a wide range. This observation, together with their uniform shift with manganese concentration, seems to suggest a very intimate connection between these bands, such as exists between the components of a doublet.

The temperature dependence of the band width, as shown in Fig. 3, is also worth studying. Szigeti and Nagy[4] have given for a zinc silicate specimen the following expression:

$$\beta = c_1 + c_2 T^{3/2},$$

where c_1 and c_2 are constants, T denotes the absolute temperature, β the band width in ev, to be calculated from the equation of the error function:

$$y = e \cdot \exp[-(h\nu - h\nu_0)^2/\beta].$$

The validity of this equation is confirmed in these experiments, especially since the widths at low temperatures are in many cases considerably greater than would correspond to a linear extrapolation of the band widths from above room temperature. Within the limits of experimental accuracy, however, in samples "*B–F*" this function may be equally well described in rather long intervals by a linear formula: $\beta = \kappa_1 + \kappa_2 T_1$, the the slope of which corresponds to $\kappa_2 = 1.5\text{–}1.6k$.

The analogy between the behavior of the 2.35- and 2.17-ev bands is also striking in that their curves run almost parallel for each sample. It is also worth mentioning that for the best fluorescing substances, samples "*C*" and "*D*," these band widths are of the same order of magnitude, even when the sub-band is flatter.

The other samples are characterized by increasing width of the main band, and increasing sharpness (decreasing width) of the sub-band. The difference between the widths of the main band and the sub-band seems to increase as the concentration of manganese deviates from the optimum.

TABLE IV. Band at 2.17 ev.

Sample	Temperature	Max. ratio	Band width	Area ratio	Band max. at
A	20	18.3	0.0425	6.2	2.17
	130	25.4	0.0612	11.1	
	217	15.2	0.0766	8.0	
	293	does not exist			
B	−180	25.0	0.0427	14.3	2.17
	23	22.9	0.0486	9.8	
	111	16.8	0.0684	9.0	
	191	18.8	0.0815	11.2	
	273	21.9	0.0895	13.2	
	330	20.7	0.1000	12.0	
C	−180	17.9	0.0696	18.1	2.17
	22	27.2	0.1067	31.5	
	125	28.2	0.1146	27.3	
	197	23.0	0.1204	20.9	
	269	36.6	0.1344	34.1	
	330	41.5	0.1338	37.2	
D	20	17.4	0.1053	18.3	2.17
	75	16.7	0.1295	18.8	
	148	18.0	0.1418	20.3	
	207	17.6	0.1355	18.2	
	252	14.2	0.1630	15.7	
	317	15.6	0.1581	16.1	
E	−180	41.5	0.0892	34.6	2.15
	24	32.7	0.0776	19.8	2.14
	98	26.4	0.0832	15.0	2.14
	146	27.9	0.0877	16.5	2.14
	204	29.4	0.0913	17.0	2.14
F	−180	46.3	0.0967	42.1	2.135
	23	33.2	0.0866	21.8	2.13
	42	25.2	0.0967	17.1	2.13
	68	19.0	0.1068	12.9	2.13

TABLE V. Band at 2.05 ev.

Sample	Temperature	Max. ratio	Band width	Area ratio	Band max. at
E	−180	17.5	0.0644	10.5	2.05
	24	18.5	0.0544	7.8	2.05
	98	12.9	0.0600	5.3	2.05
	146	7.6	0.0610	3.1	2.05
	204	14.6	0.0656	6.0	2.05
F	−180	13.5	0.0455	5.8	2.04
	23	14.0	0.060	5.7	2.05
	42	15.3	0.0754	8.0	2.05
	68		exists		

DIELECTRIC LOSSES OF ZINC SILICATES

As already reported by Szigeti and Nagy,[11] the temperature dependence of the fluorescence and that of the dielectric losses shows a very close connection for zinc silicates. It was found that when the number of emitted quanta remain

[11] Gy. Szigeti and E. Nagy, Nature 160, 641 (1947).

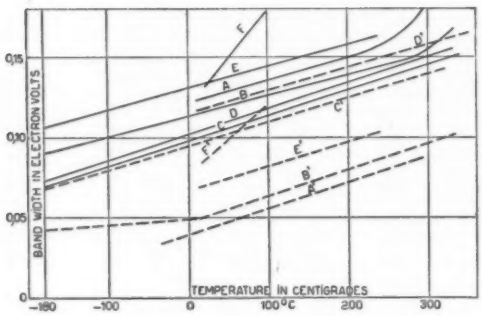

FIG. 3. Temperature dependence of band width.

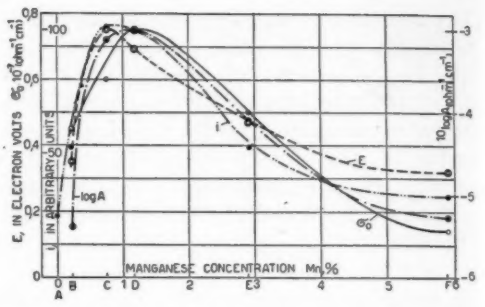

FIG. 4. Variation with manganese concentration of (1) activation energy E, (2) conductivity (σ_0), and (3) the factor A.

constant at low temperatures for a given excitation, the conductivity, σ_0, is also constant. A like correlation holds for higher temperatures also, for above a given temperature the conductivity begins to increase exponentially,

$$\sigma = \sigma_0 + A \exp(-E'/2kT),$$

and the luminescence decreases rapidly according to a law:

$$n_T = n_0/[1+\alpha \exp(-E''/2kT)].$$

This relation between luminescence and conductivity has been wholly verified for zinc silicates of varying manganese concentrations. The activation energies found for the conductivity were the same as for the decrease of luminescence, and the constant α was found to be independent of temperature. Inasmuch as some theoretical explanations have already been given,[4,11] only the variation of these quantities with the amount of manganese will be discussed in this article.

It must be regarded of crucial importance, that all these quantities, σ_0, E, A, as functions of the manganese concentration, show maxima for the best fluorescing substances as shown in Table VI. Moreover, the conductivity σ_0 is, within the limits of experimental accuracy, proportional to the total amount of emitted light at low temperatures. Although the relative errors are the greatest in determining σ_0, ca. 10 percent, it is evident beyond doubt that the samples with the optimum quantum efficiency have the greatest conductivity σ_0 and that the samples with greater or lesser amounts of manganese have invariably only a fraction of this value. The activation energy E and the factor A show maxima also for the best fluorescing substances, as shown in Fig. 4.

TABLE VI. Dielectric and fluorescent constants of the zinc silicates with varying manganese concentrations.

Specimen	Emitted light	$10^8 \cdot \sigma_0$	A ohm^{-1}cm^{-1}	E in ev	α
A	2.2				
B	4.4	4.5	$4.0 \cdot 10^{-6}$	0.35	0.14
C	10.0	6.0	$7.7 \cdot 10^{-4}$	0.75	0.18
D	9.8	7.5	$9.7 \cdot 10^{-4}$	0.69	0.15
E	4.5	5.0	$8.0 \cdot 10^{-5}$	0.47	0.28
F	2.8	1.5	$5.5 \cdot 10^{-6}$	0.32	0.12

These experimental data seem to indicate that the addition of divalent manganese does not increase the number of fluorescent centers. Their number shows a definite maximum for a given concentration, and just in this case the least damping, too. Incorporation of greater quantities of manganese, by gradually increasing the damping, shifts the emission maximum towards longer wave-lengths. It can be inferred from these data that the cause of temperature quenching is in some way closely related to the character of the luminescent centers themselves.

As stated above, the conductivity σ_0 was found proportional to the emitted visible light, i. Because the intensity of the exciting radiation was far below saturation, and the u.v. excitation was proportional to the emitted light, it is clear that only a small percentage of the luminescent centers takes part in the emission process at any moment. Even in the case of slightly luminescing compositions, there would be enough centers present to furnish the same emission in the green.

Therefore, it seems to be the more plausible supposition that the actual number of centers is more or less unknown, and that the sum of the quantum efficiencies of a great number of fluorescent transitions, or more clearly the ratio of the probability of a fluorescent and non-fluorescent absorption, decreases as we go further away from the optimum. But as the proportionality of σ_0 with i indicates, this would signify a mechanism closely analogous to the partial transference of an electron, with its conducting and luminescing potentialities, from the surroundings to the luminescent center.

These experimental findings seem to rule out conclusively the ability of the bulk of the added divalent manganese to form fluorescent centers. The manganese seems to be only necessary to the formation of negative manganate or permanganate ions, the spectra of which in solution have been found to be identical with the emission spectrum of these fluorescent materials.

ACKNOWLEDGMENT

The author wishes to express here his great indebtedness to E. Makai and G. Szigeti for their cooperative planning of these experiments and for their constant discussion of the results, to Professor P. Gombás for his continuous interest and exchange of ideas, and to the Directors of the United Incandescent and Electrical Company, Ltd., for rendering every facility for his experiments and for their permission to publish the results. He also wishes to acknowledge and thank Dr. Gorton R. Fonda of the Research Laboratory of the General Electric Company, Schenectady, New York, for editing the manuscript and for correcting the proofs in order to facilitate publication.

JOURNAL OF THE OPTICAL SOCIETY OF AMERICA VOLUME 39, NUMBER 1 JANUARY, 1949

Orientation of Methylene Blue Molecules Adsorbed on Solids

SCOTT ANDERSON
The Anderson Physical Laboratory, Champaign, Illinois
(Received February 4, 1948)

The author has investigated the state of orientation of methylene blue molecules absorbed on rubbed glasses. Reflection spectra made with polarized visible radiation demonstrate conclusively that the long axis of the molecules is perpendicular to the direction in which the glass was originally rubbed. Absorption spectra with polarized infra-red radiation show, in addition, that the molecules are adsorbed on the glass with the plane of their benzene ring parallel to the glass.

IT has been known for many years[1] that certain dye molecules assume definite orientations when adsorbed from solution onto solids previously polished in one direction only. For example, if a clean sheet of glass which has been rubbed in one direction only is placed in a methanol solution of methylene blue and withdrawn solely, the resultant plate, when dried, will be virtually transparent when viewed through a Nicol prism with the electric vector vibrating parallel to the rubbed direction, and will be dark purple when the vector is vibrating perpendicular to the direction of original rubbing.

The state of orientation of dyes adsorbed on solids has been the subject of some research,[2] but much has been left to conjecture. Sheppard and co-workers[2] have made adsorption isotherm studies on silver halides. Using these data and the geometric dimensions of the molecules as well as known particle size of the silver halide, they have correlated the number of dye molecules with the number of ions on the halide surface per square centimeter and have arrived at conclusions concerning the position of the dye mole-

[1] H. Zocher, Naturwiss. **13**, 1015 (1925).

[2] Lucien Demon, Ann. de physique **1**, 101 (1946); S. E. Sheppard, R. H. Lambert, and R. D. Walker, J. Chem. Phys. **7**, 265 (1939); H. Zocher and K. Coper, Zeits. f. physik. Chemie **132**, 295 (1928).

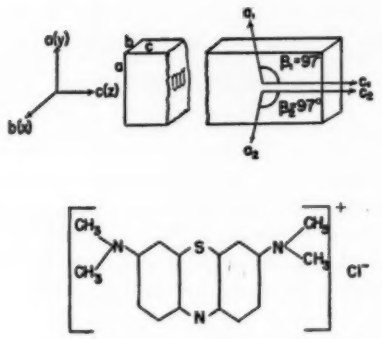

FIG. 1. Twinning in methylene blue chloride. The b axes of the individual molecules are up and down 90° with respect to the plane of the lath shaped crystal. Dimensions of unit monoclinic cell: $a=9.5$Å, $b=31.3$A, $c=6.9$A, $\alpha=90$, $\beta=97$, $\gamma=90$, The molecule sketched in the break is to indicate that its length is perpendicular to the $\langle ac\rangle_{Av}$ face. The x, y, and z in parentheses show the position of the x, y, and z semimajor axes of the electron cloud hypothesized by Lewis and Calvin.

cules on the halides. In most cases studied by them they have decided that the molecules were "on edge."

By using optically worked surfaces one can measure the absorption spectra in the visible and infra-red regions of the spectrum and, in many cases, determine uniquely and directly the orientation of the molecules on the solids. This we have done. The present publication proposes to show that in the case of oriented methylene blue molecules on rubbed solids, the molecules lie flat on the solid with the plane of their benzene rings parallel to the solid surface and with their long axis perpendicular to the direction of the original rubbing. The first half of the discussion is a correlation between the x-ray investigation of crystalline methylene blue and visible absorption spectra of the crystals and oriented films. From this it can be concluded definitely that the molecules are oriented on the rubbed glass with the conjugated double bond chain perpendicular to the direction of rubbing and that the intermolecular binding of the molecules on the glass is the same as in the crystals. The remainder of the report describes investigations with polarized infra-red radiation. These data indicated that the molecules lie flat on the glass and other polished and rubbed solids.

REVIEW OF X-RAY EXAMINATION OF METHYLENE BLUE CRYSTALS

Taylor[3] has investigated crystals of methylene blue chloride, iodide, and bromide. We are concerned with the chloride only. For this form of the dye stuff he was unable to tell uniquely the position of the sixteen water molecules in each unit cell of the crystals, but many other constants could be determined. The crystals are lath shaped (see Fig. 1) with the length of the molecules (direction of the conjugated double bond chain) making an angle of 90° with the (010) face ($\langle ac\rangle_{Av}$ in Fig. 1) of the crystal. The plane of the benzene ring is parallel to the (001) face and the crystals are twinned, i.e., in each (001) cross section the individual molecules are rotated almost 180° about their length with respect to the molecules adjacent to it, with the axes a_1 and a_2 of the individuals making an angle of 97° with the two c axes. The data for each monoclinic cell are all given in Fig. 1. The crystals of methylene blue are pleochroic. Unfortunately, those single crystals that we were able to make absorbed so strongly along all axes that their absorption spectra could not be determined directly. Nevertheless, the $\langle bc\rangle_{Av}$ and $\langle ab\rangle_{Av}$ faces reflect a green-gold color with great intensity, while the $\langle ac\rangle_{Av}$ face reflects a weak violet light. Obviously, the index of refraction varies between the crystal axes.

REFLECTION SPECTRA FROM CRYSTALS AND ORIENTED PLATES IN THE VISIBLE

The reflection data in the visible region of the spectrum from the various faces of methylene blue single crystals and films of oriented molecules show that the length of the molecules in the latter is parallel to the surface of the polished solid. In addition, the data with polarized infra-red light will show that the plane of the benzene rings of the molecules is also parallel to the solid surface.

The method of preparing the oriented sheets is quite simple (reference 2, Demon). A piece of polished window glass is cleaned carefully with Bon Ami and permitted to dry. The glass is then wiped clean with a cloth, using moderate pressure and always stroking the glass in the same direction. The cleaned rubbed glass is then immersed

[3] W. H. Taylor, Zeits. f. Krist. 91, 450 (1935).

in a methanol solution of methylene blue chloride (between 2 and 4 percent concentration) and withdrawn at a uniform slow rate. When the alcohol evaporates the molecules are left with a definite orientation upon the glass. This orientation is easily detected by viewing through a Nicol prism. By transmitted light the plate is practically transparent when the electric vector is parallel to the direction of original rubbing and a dark purple when the Nicol is rotated through 90°. By reflection the plate appears a bright green-gold (the same color exhibited by the (001) and (100) faces of the crystals) when the electric vector is perpendicular to the direction of the original rubbing (as well as by natural light) and reflects very little when the Nicol is rotated through 90°. The bright green-gold reflection in and of itself does not necessarily indicate orientation. Rather, as will be shown later, this results from the fact that the conjugated double bond chain of the molecules is parallel to the surface of the glass. Thus when this one condition is satisfied the plate will reflect the green-gold color whether or not the length direction of the molecules are parallel to one another or not. Under certain circumstances (orientation on mica, for example) a mosaic pattern is seen by viewing through a Nicol prism, i.e., regions of bright green-gold reflection surrounded by regions of weak purple. This results from the fact that adjoining regions have varying orientations. However, by reflected natural light the plate will appear uniformly green-gold.

Orientation may be obtained on polished crystals as well as on amorphous solids such as glass. For example, for work in the infra-red region of the spectrum we oriented molecules on polished rock salt and calcium fluoride. Methylene blue will orient on mica freshly cleaved under water without rubbing or polishing of any sort,

FIG. 2. Randomly oriented methylene blue crystals on unrubbed plate. (a) Illustrates the color when viewed by reflection at near normal incidence (natural light); (b) Crystals viewed at an angle of incidence near 90° with respect to the normal to the plate. Sides and ends of crystals situated properly to reflect the light send back a bright green-gold color so that the complete surface appears to be brightly colored.

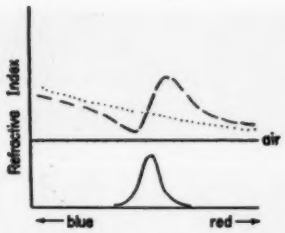

FIG. 3. Plot of index of refraction of highly absorbing medium. Continuous line indicates position of absorption band. Broken line plots course of index of refraction for electric vector vibrating in the plane of greatest absorption. Dotted line indicates curve for a transparent body or for a vector vibrating in a plane perpendicular to the plane of greatest absorption.

but the direction of orientation varies from region to region across the mica sheet, depending upon the fracture (reference 2, Demon). Zocher and Coper[2] report over fifty dye stuffs that can be oriented to some extent in this manner. Some dyes can be oriented by letting crystals form on an unrubbed glass and then polishing the dye surface by rubbing in one direction only. The list of such dyes is much smaller than the other, but methylene blue is on both lists. In the case of methylene blue oriented in this way the electric vector more strongly absorbed is parallel to the direction in which the crystals were rubbed. The optical properties of the oriented film are the same, regardless of method of orientation.

In general, the dye will aggregate in small crystals randomly oriented, when methylene blue is adsorbed from methanol solution onto a piece of glass not previously rubbed in a preferential direction or onto freshly cleaved rock salt. By examining the surface with a microscope one can see that the lath-shaped crystals are lying on the glass with their (010) plane parallel to the plane of the surface. Thus the individual molecules have their length and the plane of their benzene ring perpendicular to the glass surface. The glass with the crystals on it has the appearance of being slightly dirty when viewed by reflection at normal incidence. On the other hand, one gets a bright green-gold reflection if one tilts the plate so as to view it at an angle of incidence near 90° with the light incident from the same side as viewing (see Fig. 2). The experiment is very striking if one has the sun behind him and holds the plate so that the sun strikes

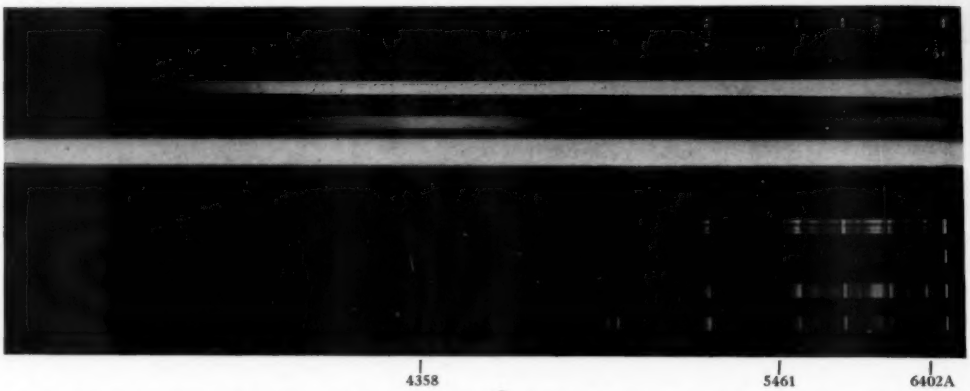

FIG. 4. Reflection spectra employing Hg-Ne discharge tube into which some air had leaked. Spectra made with a Hilger E2 (glass parts), Eastman 50 plate. All exposures given are based on No. 1 as unity. 1. Reflection spectrum from clean glass plate—natural light (exposure −1). 2. Reflection from oriented methylene blue film. Electric vector perpendicular to direction in which glass was originally rubbed (exposure −1). 3. Reflection from oriented methylene blue film. Electric vector parallel to direction in which glass was originally rubbed (exposure −1). 4. Reflection from edge ((100) face) of methylene blue single crystal. Electric vector perpendicular to length of crystal (parallel to *b* direction of individual molecules) (exposure −20). 5. Reflection from edge ((100) face) of methylene blue single crystal. Electric vector parallel to length of crystal (perpendicular to length of individual molecules). This is so faint that only one line shows on this plate (exposure −20). 6. Transmission spectrum of plate with oriented methylene blue film on it. Continuum from incandescent tungsten ribbon. 7. Continuum used for Spectrum 6. 8. Reflection from (010) face of methylene blue single crystal. Electric vector parallel to length of crystal and perpendicular to plane of individual molecules (exposure −20). 9. Reflection from (010) face of methylene blue single crystal. Electric vector perpendicular to length of crystal and parallel to plane of individual molecules (exposure −20).

it by passing over his shoulder. As one turns the plate, the weak purple reflection seen at normal incidence suddenly changes to a brilliant green-gold as the plane of the plate surface approaches the angle of 0° with respect to the line of sight. Such a plate does not polarize light by absorption. If the surface with the dye crystals is rubbed lightly, the surface acquires a green-gold color by reflection at normal incidence. Moreover, it will now polarize light by absorption—absorbing the vector vibrating parallel to the direction in which the plate was rubbed.

The absorption spectrum of the oriented layers of methylene blue is shifted towards the blue with respect to that exhibited by solutions of the same dye.[3] This is in agreement with the work of other authors.[4] This shift has no direct connection to the shift observed as a result of dimer formation in concentrated solutions studied by Rabinovitch and Epstein. Rather, it is the shift observed in going from a solution to the solid state. The absorption in dilute solutions has a maximum at 6565A, while in concentrated solutions, where dimers form, the maximum absorption occurs at 6000A. Experiments described in this section show that the absorption maximum for the oriented film occurs at 5000A and is the same as would be observed through the crystals along either the *a* or *c* axis.

Absorption spectra studies of crystals of methylene blue were prevented by the high extinction coefficient to all visible radiation in all directions through them. In the case of strongly absorbing materials, however, much of the same information can be obtained from reflection data by use of dispersion theory. Fresnel's laws of reflection state that the reflectivity at a boundary is a function of the change in index of refraction experienced when crossing that boundary. Dispersion theory shows that as an absorption band of a medium is approached from the red side on a wave-length scale the index of refraction increases. The index of refraction decreases abruptly when passing through the absorption band. The reflection is greater on that side of the absorption band where the index of refraction deviates most from that of the surrounding medium.[5] Thus for a strongly absorbing sub-

[3] Eugene Rabinovitch and Leo F. Epstein, J. Am. Chem. Soc. 63, 69 (1941).

[4] L. Michaelis and S. Granick, J. Am. Chem. Soc. 67, 1212 (1945).

[5] C. Schaefer, Zeits. f. Physik 75, 687 (1932).

stance in air, if the general course of the index of refraction of the material is greater than unity, the most intense reflection will occur just to the red side of the intense absorption band. This situation is illustrated in Fig. 3. In this figure, the full line indicates the position of an absorption band of high extinction. The dashed line shows the plot of the index of refraction as a function of wave-length. Therefore, for this hypothetical substance in air, a strong reflection takes place just to the red side of the absorption band and a very weak one on the blue side of the band.

Lewis and Calvin[6] have pointed out that most dye molecules have three characteristic absorption bands due to electronic transitions. They consider the electronic cloud of the binding electrons to enclose the conjugated double bond chain of the molecules in an ellipsoid. An absorption band corresponds to an electronic vibration along each semimajor axis of the electron cloud. They designate these bands as x, y, and z bands. Specifically, in the case of methylene blue, the x band corresponds to a vibration of the electron cloud in a direction parallel to the length of the molecule. Thus for polarized light vibrating in a direction parallel to the x direction (length of the methylene blue molecule in Fig. 1) the ray would be strongly absorbed at the characteristic frequency whether incident on the (001) or (100) face. At the same wave-length, then, the radiation polarized with the electric vector perpendicular to x, the molecule would behave as a transparent body. Consequently, in our Fig. 3, if the absorption band corresponds to the x band, the dashed curve plots the course of the index of refraction for a vector polarized parallel to x. The dotted line corresponds (very roughly) to the index of refraction for a vector vibrating in a plane turned through 90°. The actual position of the absorption band will depend upon the enrivonment of the molecule and the intermolecular binding. Therefore, by determining the reflection spectra with polarized light from the various faces of a single crystal of methylene blue wherein we know the position of the individual molecules, we were able to locate the orientation of the x band. Then by comparison with reflection spectra made with the oriented films on glass we were able to determine the position of the length of the molecules on the glass and show that the intermolecular binding was the same in the oriented films and in the crystals.

The author has determined the reflection spectrum from the various faces of the single crystals of methylene blue chloride and from oriented layers of the dye on glass using polarized light. It was his original hope to be able to use a source of continuous radiation and to calculate the index of refraction of the crystal along the various axes through it. Because of the low intensity of the spectra the results were only qualitative. Since the qualitative results are shown better by a line spectrum, those data are reproduced here. The source used was a Hg-Ne discharge lamp into which some air had leaked. The crystal had the following dimensions: $c=1.5$ mm, $a=0.1$ mm, and $b=0.01$ mm. The spectra were made using a Hilger E2 glass spectrograph. The crystal was mounted on a black cardboard square with Scotch Tape so that the crystal projected out away from a corner of the cardboard. The discharge channel was focused on the crystal and an image of the crystal focused on the spectrograph slit after passing through a piece of Polaroid. Good reflection spectra were obtained from the (010) and (100) faces of the crystal and from the oriented film. These and other pertinent spectra are reproduced in Fig. 4.

By comparing spectra 2 and 4 it is obvious that the reflection spectrum is the same from the oriented film when the electric vector is per-

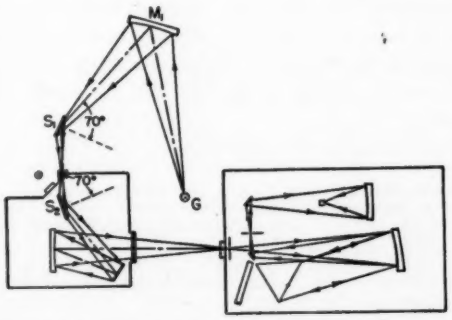

FIG. 5. Schematic drawing of infra-red spectrometer with polarizing attachment. Radiation polarized perpendicular to plane of diagram.

[6] G. N. Lewis and M. Calvin, Chem. Rev. 25, 273 (1939).

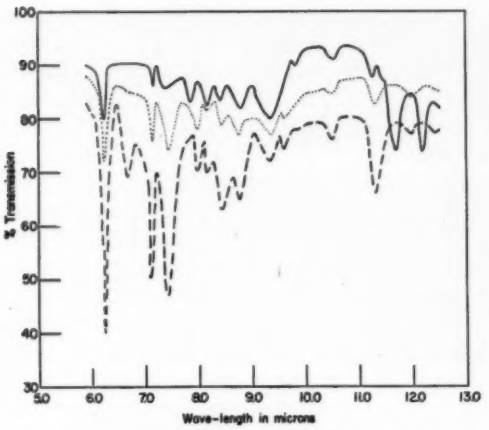

FIG. 6. Infra-red absorption spectra of methylene blue on freshly cleaved rock salt. Full line—randomly oriented crystals, long axis of individual molecules perpendicular to the surface of the salt plate and parallel to beam of radiation. Dotted line—absorption spectrum of molecules oriented by rubbing. Infra-red polarized with electric vector vibrating perpendicular to length of molecules. Broken line—absorption spectrum of molecules oriented by rubbing. Infra-red radiation polarized with electric vector vibrating parallel to length of molecules.

pendicular to the direction of rubbing as it is from the crystal when the electric vector is along the conjugated double bond chain of the molecules. Although it is not evident from this plate—spectrum 5 is too faint, the reflection spectrum from the oriented film (when the electric vector is parallel to the direction of rubbing the glass) is identical with that from the edge of the crystal (when the vector is perpendicular to the length of the individual molecules). Consequently, in the oriented film the *b* direction of the molecules is perpendicular to the direction of rubbing. It is to be noticed that the intense reflection in both cases is just to the red side of the absorption band of the oriented plate (spectrum 6). This gives strong indication that the intermolecular binding in the two states of aggregation is the same.

TABLE I.

Wave-length in μ	Assignment
6.23	in-plane vibration of phenyl ring[a]
7.13	
7.41	CH_3[b]
12.16	H perpendicular to plane of ring[c]
11.66	

[a] See reference 10.
[b] See reference 9.
[c] See reference 8.

Spectra 3 and 5 merely indicated that the *x* band is not excited by an electric vector vibrating at right angles to the *x* direction. From spectra 8 and 9 we can see that the radiation incident on the ends of the individual molecules does not excite the *x* band to any great extent. Moreover, the index of refraction for a vector vibrating in the *a* direction of the crystal (parallel to the *y* band) has a higher index of refraction than for one vibrating along the *c* direction (parallel to the *z* band). From this we can conclude that the *z* band lies farther into the ultraviolet than the *y* band, as is expected.

Reflection spectra from the ends of the crystal were not secured with sufficient clarity to justify their publication. Nevertheless, from visual observation (through the spectrograph) one can see that the reflection from the (001) face are the same as spectra 4 and 5 from the (100) face. The spectrum with the electric vector parallel to the *b* direction corresponds to 4, and when the polaroid is rotated 90° the spectrum corresponds to 5. Thus these spectra cannot be used to tell us whether the molecules are "on edge" or lying flat on the glass. Data with polarized infra-red radiation help us to conclude that they are lying flat.

CONSTRUCTION OF POLARIZER FOR FOR INFRA-RED SPECTROMETER

Following a suggestion of Pfund[7] a polarizing attachment was made for our Perkin-Elmer Model 12B infra-red spectrometer. Pfund showed that depolarization of light reflected from selenium mirrors did not exceed 0.01 over an incident angle range of 59° to 77°. Therefore, by using converging light and two reflections from selenium mirrors, infra-red light could be polarized as well as a Nicol prism polarizes light in the visible.

Our adaptation of his suggestion is shown in Fig. 5. A globar is placed at *G* with a spherical mirror (Al surface) at M_1. This mirror focuses the light halfway between the two selenium mirrors S_1 and S_2. The second of these is in the optical path of the original instrument, and from

[7] A. H. Pfund, J. Opt. Soc. Am. 37, 558 (1947).

that point on the optical path is identical with that of the standard spectrometer. The radiation is polarized with the electric vector vibrating parallel to the surface of the selenium mirrors. Specimens to be investigated are mounted before the slit of the spectrometer and rotated about the optical axis of the instrument to get the spectra in various orientations with respect to the plane of vibration of the electric vector. The degree of polarization obtained with this attachment is better than ninety-eight percent.

RESULTS

Freshly cleaved rock salt plates were immersed in 4 percent methanol solution of methylene blue and withdrawn. When the methanol evaporated, the plates were covered with small crystals of the dye. Microscopic examination showed that the crystals were randomly oriented with their (010) planes parallel to the plate surface. Thus the *b* direction of the molecules and the plane of their benzene ring were perpendicular to the plate surface (see Fig. 2). The absorption spectrum between 12.5μ and 5.8μ as determined with polarized radiation is shown in Fig. 6.

The plate was then rubbed briskly with a tooth brush in one direction only to orient the molecules. By reflected natural light the plate exhibited a uniform bright green-gold surface. Orientation is not as complete with this method as rubbing the surface first. Nevertheless, reasonably good orientation was obtained. Spectra with two positions of the electric vector with respect to the *b* direction of the molecules (determined by viewing in the visible with a Nicol prism) were determined.

Methylene blue has been oriented very well upon polished and rubbed CaF_2. The degree of orientation is superior to that displayed by these spectra. Since the extinction of CaF_2 is so great at wave-lengths greater than 10μ, the most interesting region of these spectra is missed. Therefore, we have not reproduced the spectra here.

DISCUSSION OF INFRA-RED SPECTRA

The previously described experiments on reflections in the visible spectrum showed that the length (*b* axis) of the molecules was parallel to the surface in oriented films. We now propose to show that the above-presented data with polarized infra-red radiation indicate that the plane of the benzene rings of the molecules also is parallel to the surface of the glass in oriented films. This will be done by showing, first of all, in crystals where we know the molecular orientation from x-ray data that the two bands at 12.16μ and 11.66μ are "out of the plane" vibrations and then that their absence in the other two curves of Fig. 6 shows that the molecules lie flat on the glass when they are oriented.

It is not possible to assign all the bands unambiguously although certain lines are definite. Our proposed assignment of some of the bands is given in Table I.

When the beam of radiation is incident on the ends of the molecules with the randomly oriented crystals, one would expect to excite strongly only those vibrations which are out of the plane of the molecule. Moreover, one would expect those vibrations to be at wave numbers less than 1000 cm^{-1}. In fact, Miller and Crawford[8] have reported an out-of-plane vibration at 851 cm^{-1}. This is degenerate and may have splitting. Thus, the two bands at 822 cm^{-1} and 857 cm^{-1} are assigned to out-of-the-plane vibrations with considerable certainty.

The bands at 7.41μ and 7.13μ are most likely methyl vibrations[9] with the major motion of the hydrogens along the length of the molecule. The first is a symmetric deformation of the methyl group and the second is the degenerate deformation. For the first, the change in the dipole moment is along the methyl-R bond. These conclusions are in agreement with the observations made with the Nicol prism in the visible. The band at 6.66μ is an in-plane vibration along the direction of greatest dipole moment change. It may be associated with the stretching of either the C=S or C=N linkages. The band of 6.23μ is the well-known in-plane vibration of the benzene ring.[10] This latter we would expect to absorb

[8] Hydrogen out-of-plane vibrations in benzene are less than 1000 cm^{-1}. In particular, there is a degenerate vibration (10*a*, *b*) at 951 cm^{-1} in benzene and this may have degeneracy splitting. See F. A. Miller and B. L. Crawford, J. Chem. Phys. **14**, 282 (1946).

[9] See for example, George Herzberg, *Infrared and Raman Spectra* (D. Van Nostrand Company, Inc., New York, 1945), pp. 338 and 360–361.

[10] This is a vibration designated by 8*A*, *B* by Kenneth S. Pitzer and Donald W. Scott, J. Am. Chem. Soc. **65**, 803 (esp. p. 815) (1943).

most intensely when the electric vector is vibrating in the plane of the ring. All this is consistent with our conclusions from the experiments performed in the visible. Nevertheless, they do not enable us to decide between an adsorption "on edge" or parallel to the surface. Even though the molecules were on edge, the in-plane vibrations at 6.23μ and 6.66μ as well as the methyl vibrations at 7.41μ and 7.13μ would still be most strongly excited with the electric vector along the b axis. On the other hand, the complete absence of the two out-of-the-plane vibrations at 12.16μ and 11.66μ in the spectra of the oriented molecules of Fig. 6 show that the oriented molecules must be on the surface with their benzene ring planes parallel to it. Otherwise, these bands would have appeared quite intense in the dotted curve of Fig. 6.

CONCLUSIONS

From the foregoing experiments with polarized light in the visible and infra-red, it appears that when methylene blue molecules are oriented on a polished and rubbed surface, the molecules have the plane of their benzene rings parallel to the surface and their length is perpendicular to the direction of original rubbing of the glass. Their length is parallel to the direction of rubbing when the dye is first adsorbed on the surface as randomly oriented crystals and then oriented by rubbing. In addition, the intermolecular binding appears to be the same among the adsorbed molecules as in the crystalline form.

ACKNOWLEDGMENTS

The spectra shown in Fig. 4 were made with a Hilger E2 (glass parts) spectrograph at the University of Illinois, and I am indebted to Professor G. M. Almy for permission to use it. In addition, I desire to express my gratitude to Professor F. A. Miller, Department of Physical Chemistry, University of Illinois, for aid in making the infra-red assignments shown in Table I. This work was done under the sponsorship of the Glass Division Research Laboratories of the Pittsburgh Plate Glass Company, and I am grateful to Mr. S. Frank Cox for permission to publish these findings.

Inter-Society Color Council—Seventeenth Annual Meeting

The 17th annual meeting of the Inter-Society Color Council will be held on Wednesday, March 9, 1949, at the Hotel Statler, New York City. The meeting will consist of a Discussion Session at which committee chairmen will report on the following problems:

2—Color Names (Revision of), Deane B. Judd, Chairman

6—Color Terms, Sidney M. Newhall, Chairman

7—Color Specifications, Walter C. Granville, Chairman

12—Studies of Illuminating and Viewing Conditions in the Colorimetry of Reflecting Materials, D. B. Judd, Chairman

14—A Study of Transparent Standards Using Single-Number Specification, Robert H. Osborn, Chairman

A Business Session will conclude the afternoon meeting. Anyone interested is invited to attend. Hotel reservations should be made directly to the hotel at least ten days prior to the meeting, indicating attendance at the ISCC meeting.

Meetings of the Optical Society of America are scheduled for the same hotel, March 10–12. Since it is usual for one or more O.S.A. sessions to be devoted to color, ISCC members who are interested may wish to plan to remain for these meetings.

High Members of the Principal Series in Caesium

J. RAND MCNALLY, JR.,* JULIUS P. MOLNAR,** WILLIAM J. HITCHCOCK,*** AND NORMAN F. OLIVER†
Massachusetts Institute of Technology, Cambridge, Massachusetts

(Received August 30, 1948)

The results of an investigation initiated several years ago are presented in summary form. The more intense doublet member of the principal series of caesium in absorption is recorded to the sixty-second quantum state, whereas the weaker doublet member is recorded to the fourteenth quantum state only. An empirical formula fitting the longer series to about ± 0.03 cm^{-1} is given. The calculated series limit of 31406.32 cm^{-1} corresponds to an ionization potential of 3.8929 volts for the caesium atom.

PHOTOGRAPHS of the principal series of caesium in absorption, taken in the MIT Spectroscopy Laboratory prior to World War II, have been found to show higher series members than previously reported. Bacher and Goudsmit[1] list the $n^2P_{1\frac{1}{2}}^{\circ}$ series to the $n=36$th quantum state. Kratz and Mack[2] have reported observing resolved doublets to $n=15p$ and the $1\frac{1}{2}$ series of levels to 66, although no detailed data have been published by them. In this note we list the higher series doublet members from $n=11$ to $n=14$ and the more intense member to the 62nd quantum state. The intensity ratio of the doublet lines for the higher series members is not in agreement with the simple theory which predicts a ratio of 2:1 (see Fig. 1). This difficulty of observing complete doublets involving high quantum states in absorption has been discussed by Fermi.[3]

The absorption tube used in this experiment consisted of an iron pipe approximately two inches in diameter and about one meter long with quartz windows Glyptalled on the ends. The tube was wrapped with asbestos and heater wire and the current adjusted to give fairly strong absorption of lines in the visible, the breadths of which were used as an indication of the vapor density. An entirely satisfactory continuum was obtained from a water-cooled, General Electric, type H-6 mercury lamp.

The absorption system was evacuated and caesium metal, produced by heating an intimate

FIG. 1. Reproduction of sections of wave-length film illustrating intensity anomaly in the eighth member of the caesium principal series doublets (at 3313A). Compare with the neighboring 3302A sodium principal series doublet.

* Now with Stable Isotopes Group, Carbide and Carbon Chemicals Corporation, Oak Ridge, Tennessee.
** Now with Bell Telephone Laboratories, Murray Hill, New Jersey.
*** Now with Baird Associates, Cambridge, Massachusetts.
† Now at 48 Almy Street, Fall River, Massachusetts.

[1] R. T. Bacher and S. Goudsmit, *Atomic Energy States* (McGraw-Hill Book Company, Inc., New York, 1932).
[2] H. R. Kratz and J. E. Mack, Rev. Mod. Phys. **14**, 104 (1942).
[3] E. Fermi, Zeits. f. Physik **59**, 680 (1929).

mixture of caesium chloride and calcium metal, was distilled into the main absorption tube which had been previously baked out. The pressure of foreign gases was maintained sufficiently low to eliminate line shifts attributable to foreign gases.[4] A large number of sharp lines in the arc spectrum of iron were used as comparison standards, the spectra being measured on the Harrison automatic comparator.[5]

TABLE I. High members of the principal series in cesium, $6^2S_{\frac{1}{2}}-n^2P_{1\frac{1}{2}}^{\circ}$.

n	λ	σ_K	σ	$\Delta\sigma$
11	3397.998	29420.69	29420.70	−0.01
12	3347.533	29864.19	29864.20	−0.01
13	3313.156	30174.05	30174.03	0.02
14	3288.634	30399.03	30399.02	0.01
15	3270.504	30567.55	30567.54	0.01
16	3256.708	30697.03	30697.05	−0.02
17	3245.949	30798.78	30798.71	0.07
18	3237.411	30880.00	30879.98	0.02
19	3230.508	30945.98	30945.97	0.01
20	3224.847	31000.29	31000.28	0.01
21	3220.150	31045.52	31045.51	0.01
22	3216.205	31083.60	31083.59	0.01
23	3212.859	31115.96	31115.94	0.02
24	3210.000	31143.68	31143.66	0.02
25	3207.536	31167.60	31167.60	0.00
26	3205.37	31188.6	31188.40	0.2
27	3203.529	31206.59	31206.60	−0.01
28	3201.885	31222.61	31222.61	0.00
29	3200.424	31236.86	31236.77	0.09
30	3199.148	31249.32	31249.35	−0.03
31	3197.995	31260.59	31260.58	0.01
32	—	—	31270.65	—
33	3196.038	31279.73	31279.71	0.02
34	3195.206	31287.87	31287.89	−0.02
35	3194.452	31295.27	31295.31	−0.04
36	3193.761	31302.03	31302.05	−0.02
37	3193.135	31308.16	31308.19	−0.03
38	3192.559	31313.81	31313.81	0.00
39	3192.034	31318.96	31318.96	0.00
40	3191.548	31323.73	31323.68	0.05
41	3191.109	31328.04	31328.04	0.00
42	3190.699	31332.05	31332.01	0.04
43	3190.323	31335.76	31335.78	−0.02
44	3189.969	31339.23	31339.22	0.01
45	3189.648	31342.39	31342.42	−0.03
46	3189.348	31345.34	31345.40	−0.06
47	3189.067	31348.10	31348.17	−0.07
48	3188.787	31350.85	31350.76	0.09
49	3188.543	31353.25	31353.18	0.07
50	3188.321	31355.43	31355.44	−0.01
51	3188.110	31357.51	31357.56	−0.05
52	3187.908	31359.50	31359.55	−0.05
53	3187.705	31361.49	31361.43	0.06
54	3187.55	31363.0	31363.19	−0.2
55	3187.35	31365.0	31364.85	0.1
56	3187.16	31366.8	31366.42	0.4
57	3187.03	31368.1	31367.90	0.2
58	3186.91	31369.3	31369.29	0.0
59	3186.77	31370.7	31370.62	0.1
60	3186.65	31371.8	31371.87	−0.1
61	3186.52	31373.2	31373.06	0.1
62	3186.41	31374.2	31374.19	0.0

TABLE II. High members of the principal series in caesium: $6^2S_{\frac{1}{2}}-n^2P_{\frac{1}{2}}^{\circ}$.

n	λ
11	3400.004
12	3348.734
13	3314.082
14	3289.318

The higher members of the $6^2S_{\frac{1}{2}}-n^2P_{1\frac{1}{2}}^{\circ}$ series are given in Table I, which lists the total quantum number, n; the observed wave-length in air in angstroms, λ; the vacuum wave number in cm^{-1} from Kayser,[6] σ_K; the wave number as calculated from the equation below, σ; and the wave number difference, $\Delta\sigma$. Table II gives similar information, in part, for the less intense member of the doublet. Additional absorption lines observed were: $K-3446.717$A; $Na-3302.990$A; and $Na-3302.383$A, the latter disagreeing with the *MIT Wavelength Tables*[7] average value by 0.049A.

The series from $n=11$ to $n=62$ satisfies, to a good approximation, the formula

$$\sigma = 31406.32 - \frac{109{,}737.30}{\{n-\mu+(b/(n-\mu)^2)\}^2},$$

where σ is the calculated wave number, n is the total quantum number, $\mu=3.55900$, and $b=0.38_1$. The series limit of 31406.32 cm^{-1} corresponds to an ionization potential of 3.8929 volts. This series limit differs from the value of 31404.6 cm^{-1} obtained by Bevan.[8]

[4] H. Margeneau and W. W. Watson, Rev. Mod. Phys. **8**, 22 (1936); N. Tsi-Zé and C. Shang-Yi, J. Opt. Soc. Am. **51**, 568 (1937).

[5] G. R. Harrison, J. Opt. Soc. Am. **25**, 169 (1935); Rev. Sci. Inst. **9**, 15 (1938); G. R. Harrison and J. P. Molnar, J. Opt. Soc. Am. **30**, 343 (1940).

[6] H. Kayser, *Tabelle der Schwingungszahlen* (S. Hirzel, Leipzig, 1925).

[7] G. R. Harrison, *MIT Wavelength Tables* (John Wiley and Sons, Inc., New York, 1939).

[8] P. V. Bevan, Proc. Roy. Soc. **A86**, 320 (1912).

JOURNAL OF THE OPTICAL SOCIETY OF AMERICA VOLUME 39, NUMBER 1 JANUARY, 1949

Aberrations in Ellipsoidal Mirrors Used in Infra-Red Spectrometers

J. RUD NIELSEN
Department of Physics, University of Oklahoma, Norman, Oklahoma

(Received September 21, 1948)

Since long slits are used in infra-red spectrometers, the image of the exit slit formed by the ellipsoidal mirror will suffer aberrations which lower the sensitivity and tend to increase the time of response. General formulas are derived for these aberrations, and a typical aberration pattern is computed. It is shown how the formulas may be applied to choose the most favorable eccentricity of the ellipsoidal mirror. The relation between the general formulas and a formula given by Randall and Firestone is discussed.

INTRODUCTION

AN ellipsoidal mirror is used in most infra-red spectrometers to focus the light passing through the exit slit upon the receiver of a thermocouple or bolometer. The mirror is placed so that its far focal point coincides with the midpoint of the exit slit. All the light that passes through the slit at this point and hits the mirror will then be focused at the near focal point. Light passing through the slit at some distance from the middle, however, will not be focused at a point. Since the low intensity of infra-red sources makes necessary the use of fairly long slits, the image of the exit slit formed by the ellipsoidal mirror will always be imperfect. The aberrations are all the more serious, since in order to have high sensitivity and rapid response the receiver should be as small as possible.

In the course of designing an infra-red spectrometer, the writer was faced with a number of questions calling for a knowledge of these aberrations, e.g., what is the most favorable eccentricity of the ellipsoidal mirror? What part of the mirror should preferably be used? With a given mirror and slit what should be the size and shape of the receiver? Although such questions must have presented themselves to every designer of an infra-red spectrometer, the writer was unable to find any treatment of aberrations in ellipsoidal mirrors in the literature. The present investigation was therefore undertaken. After its completion, the formula of Randall and Firestone[1] was called to the writer's attention. A brief discussion of the relation of this formula to the more general formulas developed here has therefore been added.

DERIVATION OF GENERAL FORMULAS

The surface of the ellipsoidal mirror forms part of an ellipsoid of revolution, the symmetry axis of which passes through the center of the mirror. Taking the center of this ellipsoid as the origin and the symmetry axis as the z axis of a Cartesian coordinate system (see Fig. 1), the equation for the ellipsoid may be written in the form

$$z^2/a^2+(x^2+y^2)/a^2(1-e^2)=1, \qquad (1)$$

where a is half the major axis and e the eccentricity. The foci F and F' have the coordinates $(o,o,-ea)$ and (o,o,ea), respectively.

Assuming that the exit slit lies in a plane perpendicular to the z axis passing through the far focus F and that the receiver lies in a parallel plane through the near focus F', we determine where a ray of light coming from a point ξ, η, $-ea$ of the exit slit cuts through the receiver plane after being reflected at the point x, y, z of the mirror.

The equations for the incident ray are

$$(X-x)/(x-\xi)=(Y-y)/(y-\eta)=(Z-z)/(z+ea), \qquad (2)$$

and its directional cosines are

$$\lambda=(x-\xi)/A, \quad \mu=(y-\eta)/A, \quad \nu=(z+ea)/A,$$

where

$$A=[(x-\xi)^2+(y-\eta)^2+(z+ea)^2]^{\frac{1}{2}}. \qquad (3)$$

The directional cosines of the normal to the ellipsoid at the point x, y, z, counted positive in an out-ward direction, are found by a well-known procedure of analytic geometry to be

$$\alpha=x/B, \quad \beta=y/B, \quad \gamma=(1-e^2)z/B,$$

[1] H. M. Randall and F. A. Firestone, Rev. Sci. Inst. 9, 404 (1938).

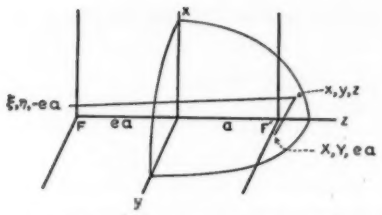

FIG. 1. Definition of coordinates. F and F' are the foci of the ellipsoidal mirror. A ray of light passing through the point ξ, η, $-ea$, of the exit slit is reflected by the ellipsoidal mirror at x, y, z and cuts through the receiver plane at X, Y, ea.

where

$$B=[x^2+y^2+(1-e^2)^2z^2]^{\frac{1}{2}}. \qquad (4)$$

Let $\mathbf{n}$ denote a unit vector in the direction of the outside normal to the ellipsoid, and let $\mathbf{s}$ and $\mathbf{s}'$ denote unit vectors in the directions of the incident and the reflected rays, respectively. Then, as may be seen from Fig. 2,

$$\mathbf{s}'=\mathbf{s}-2\mathbf{n}(\mathbf{s}\cdot\mathbf{n}). \qquad (5)$$

Hence, the directional cosines for the reflected ray are

$$\begin{aligned}\lambda'&=\lambda-2\alpha(\lambda\alpha+\mu\beta+\nu\gamma),\\ \mu'&=\mu-2\beta(\lambda\alpha+\mu\beta+\nu\gamma),\\ \nu'&=\nu-2\gamma(\lambda\alpha+\mu\beta+\nu\gamma),\end{aligned} \qquad (6)$$

and the equations for the reflected ray are

$$(X-x)/\lambda'=(Y-y)/\mu'=(Z-z)/\nu'. \qquad (7)$$

The x and y coordinates of the point where the reflected ray cuts through the receiver plane are then found by substituting $Z=ea$ into (7) and solving for X and Y. One first obtains

$$X=x+(ea-z)\lambda'/\nu', \quad Y=y+(ea-z)\mu'/\nu'. \qquad (8)$$

Substitution of (3) and (4) into (6) and of the resulting expressions into (8) gives, after considerable reduction,

$$\begin{aligned}X=-\{&[((1-e^2)^2a^2-e^2x^2+e^2y^2)z\\ &+(2-e^2)eax^2-e^3ay^2-(1-e^2)^2ea^3]\xi\\ &+2exy(a-ez)\eta\}/C,\\ Y=-\{&2exy(a-ez)\xi+[((1-e^2)^2a^2+e^2x^2\\ &-e^2y^2)z-e^3ax^2+(2-e^2)eay^2\\ &-(1-e^2)^2ea^3]\eta\}/C,\end{aligned} \qquad (9)$$

where

$$\begin{aligned}C=&(1-e^2)^2ea^3-(2-e^2)ea(x^2+y^2)\\ &+[(1-e^2)^2a^2-e^2(x^2+y^2)-2(1-e^2)(x\xi+y\eta)]z,\end{aligned}$$

and

$$z=[a^2-(x^2+y^2)/(1-e^2)]^{\frac{1}{2}}.$$

The expression for Y could have been obtained by making the substitutions $x=y$, $y=-x$, $z=z$, $\xi=\eta$ and $\eta=-\xi$ in the expression for X. In general, the formulas (9) cannot be simplified. However, some of the terms may be dropped for certain values of the variables.

APPLICATION OF FORMULAS

1. Typical Aberration Pattern ($\eta=0$)

If the midpoint of the exit slit is on the axis of the ellipsoidal mirror, as will normally be the case, and if the slit is not too wide, η may be taken equal to zero. To investigate the nature of the typical aberration pattern, we consider the case that the focal ratio is 7:1 and the far focal point 40 cm from the mirror, i.e., $e=0.75$ and $a=22.86$ cm. Taking $\xi=2$ cm, we compute the values of X and Y for a set of selected points x, y, z on the ellipsoidal mirror. The results are listed in Table I. The upper figure of each pair is X and the lower figure is Y. The center of the ellipsoidal mirror images the point $\xi=2$ cm, $\eta=0$, of the exit slit at $X=-0.286$ cm, $Y=0$. Thus, the aberrations, as here defined, are in this case $\Delta X=X+0.286$, $\Delta Y=Y$.

In the upper left part of Fig. 3 are shown the points x, y chosen on the ellipsoidal mirror. The corresponding values of the aberrations ΔX, ΔY are plotted in Fig. 3 on scale enlarged a hundredfold. To indicate the correspondence between points on the mirror and in the aberration diagram, the points $(\Delta X, \Delta Y)$ that belong to a given value of x are joined by straight lines, and this value of x is shown at the Δx axis. The point on this axis corresponds to $y=0$, and the points

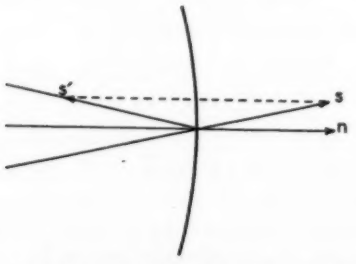

FIG. 2. Relation between the unit vectors in the directions of the incident and reflected rays.

farther from this axis to progressively larger values of y. It will be noticed that ΔX and, to a smaller extent, ΔY are larger numerically for a given positive value of x than for an equal negative value. For points $(0, y)$ on the mirror, $\Delta Y = 0$, and ΔX is comparatively small. These points in the aberration diagram are indicated by small circles. Thus, the most useful part of the mirror is a strip perpendicular to the exit slit and passing through the midpoint of the mirror. For points $(x, 0)$ lying on a line parallel to the slit ΔY also vanishes, but ΔX increases rapidly with increasing x. The greatest aberrations occur when both x and y are large, i.e., when the reflection occurs near the lines $y = \pm x$ on the mirror.

TABLE I. Computed values of X and Y for selected values of x and y ($a = 22.86$ cm, $e = 0.75$, $\xi = 2$ cm, $\eta = 0$).

	$y=0$	1	2	3	4 cm
	$X = -0.432$ cm	−0.436	−0.450		
$x=4$ cm	$Y = 0.000$ cm	−0.024	−0.052		
3	−0.363	−0.365	−0.375	−0.393	
	0.000	−0.016	−0.034	−0.055	
2	−0.319	−0.321	−0.330	−0.343	−0.364
	0.000	−0.010	−0.020	−0.034	−0.050
1	−0.295	−0.297	−0.303	−0.316	−0.333
	0.000	−0.004	−0.009	−0.016	−0.024
0	−0.286	−0.288	−0.294	−0.305	−0.321
	0.000	0.000	0.000	0.000	0.000
−1	−0.289	−0.291	−0.297	−0.309	−0.326
	0.000	+0.004	+0.009	+0.015	+0.023
−2	−0.307	−0.308	−0.316	−0.328	−0.347
	0.000	+0.009	+0.019	+0.032	+0.048
−3	−0.340	−0.342	−0.351	−0.366	
	0.000	+0.015	+0.031	+0.051	
−4	−0.394	−0.397	−0.409		
	0.000	+0.022	+0.047		

2. Choice of Eccentricity of Mirror

The increase in the aberrations with increasing eccentricity is shown in Fig. 4, in which the aberration patterns for ellipsoidal mirrors of focal ratios 5:1, 7:1 and 9:1, i.e., of eccentricities $\frac{2}{3}$, $\frac{3}{4}$, and $\frac{4}{5}$, are drawn to the same scale. To make the drawings clearer, fewer points are indicated than in Fig. 3.

The sensitivity of a thermocouple increases, and its time of response decreases, as the area of the receiver surface is reduced. Thus, in order to concentrate the radiation passing through the exit slit of an infra-red spectrometer upon the smallest possible receiver, it is desirable to use an ellipsoidal mirror of high eccentricity, or high ratio between the focal distances. However, as the eccentricity is increased, the aberrations caused by the finite length of the slit become larger, and when a certain eccentricity is reached the resulting spreading of the radiation will prevent any further reduction in the receiver area on which the radiation can be concentrated.

The exact determination of the optimum focal ratio, and the best receiver size, for given dimensions of prism and exit slit and for given focal

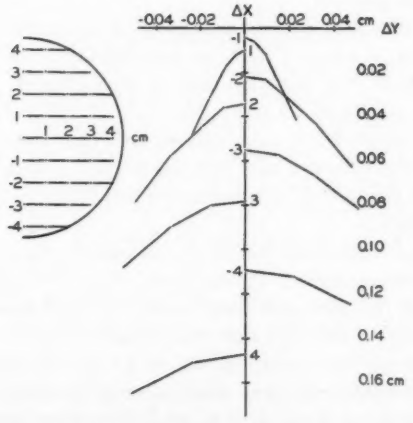

FIG. 3. Typical aberration pattern. Focal ratio 7:1, $\xi = 2$ cm, $\eta = 0$. The points of reflection x, y on the ellipsoidal mirror are shown in the upper left part. The aberrations ΔX, ΔY are plotted on a hundred-fold enlarged scale. Points belonging to a given value of x are joined by straight lines.

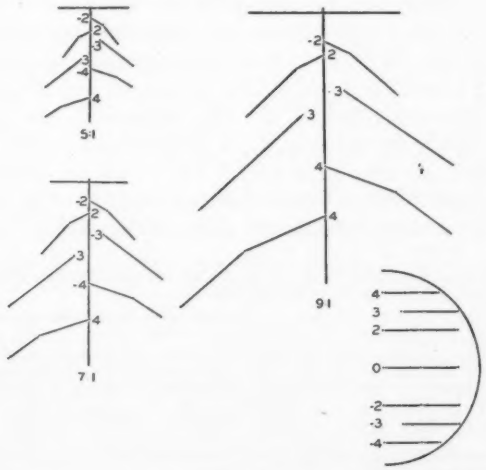

FIG. 4. Aberrations in ellipsoidal mirrors of different focal ratios.

length of the collimating parabolic mirror, would require laborious computations. However, as will be indicated by an example, it is not difficult to make a sufficiently accurate estimate.

In an infra-red spectrometer[2] having prisms with faces 10 by 15 cm in Wadsworth-Littrow mounting and a collimating paraboloid of one meter focal length it was desired to use slits of length 4 cm and an ellipsoidal mirror 40 cm behind the slit. By tracing rays through the optical system, it was found that the radiation passing through the exit slit would cover nearly uniformly a rectangular area of the mirror of height 6.6 cm and width 5.2 cm.

Calculations were made to determine the relative merits of ellipsoidal mirrors of focal ratios 5:1, 7:1, and 9:1 for receivers of width 0.2 mm and 0.3 mm. The results are summarized in Table II. The eccentricities corresponding to the focal ratios considered are listed in the second column. The third column gives the receiver lengths needed if it is required that the radiation coming from the ends of the exit slit and reflected at the points (3.3, 0) or (−3.3, 0) on the mirror is to reach the receiver. If there were no aberrations the receiver length l would be inversely proportional to the focal ratio. However, since the aberration ΔX increases with increasing focal ratio, l will first decrease and then increase as the focal ratio is made larger. It will be seen from Table II that l is somewhat greater for a 9:1 than for a 7:1 ellipsoidal mirror.

In the fourth column are listed the maximum slit lengths $2\xi_{0.2}$ which can be used with a receiver of length l and width 0.2 mm without any of the radiation reflected by the ellipsoidal mirror missing the receiver. $\xi_{0.2}$ was computed by substituting the values $x=3.3$ cm, $y=2.6$ cm, $\eta=0$, $Y=0.01$ cm, $a=22.86$ cm and $e=\frac{2}{3}$, $\frac{3}{4}$, or $\frac{4}{5}$, in the second formula (9) and solving for ξ. In column 5 are listed the greatest slit lengths $2\xi_{0.3}$ which can be used with a receiver of width 0.3 mm without loss of radiation caused by aberrations.

TABLE II. Receiver lengths, maximum slit lengths, and radiation losses.

Focal ratio	Eccentricity	l	$2\xi_{0.2}$	$2\xi_{0.3}$	$L_{0.2}$	$L_{0.3}$
5:1	2/3	9.9 mm	1.33 cm	2.00 cm	8.9%	2.7%
7:1	3/4	8.6	0.80	1.20	18.1	9.4
9:1	4/5	8.8	0.50	0.75	25.7	17.6

[2] J. Rud Nielsen, F. W. Crawford and D. C. Smith, J. Opt. Soc. Am. **37**, 296 (1947).

The last two columns of Table II give the losses $L_{0.2}$ and $L_{0.3}$ of radiation caused by the aberrations when the entire slit of length 4 cm is used. These losses were determined in the following manner. Taking $\xi=2$, $\eta=0$, the aberration ΔY was calculated for a number of selected points (x,y) within the illuminated area of the ellipsoidal mirror. By interpolation between the data thus obtained, curves were drawn through the points (x,y) for which ΔY is just equal to half the width of the receiver. The radiation coming from the top end of the exit slit and being reflected at points on the mirror lying inside these curves will reach the receiver, whereas the radiation reflected farther out will miss the receiver. Figure 5a shows these curves, C and C', for mirrors of focal ratios 5:1, 7:1, and 9:1, respectively, and for a receiver of width 0.2 mm. Fig. 5*b* shows the corresponding curves for a receiver of width 0.3 mm.

The sum of the corner areas lying outside the curves C or C' was measured by means of a planimeter and divided by the total area of the illuminated rectangle. The ratio thus obtained represents the relative loss caused by aberrations of the radiation passing through the top point of the exit slit.

For each focal ratio, and for each receiver width, a value ξ' lying approximately half way between $\xi_{0.2}$ (or $\xi_{0.3}$) and 2 was chosen, new curves C and C' were drawn, and the relative loss caused by aberrations of the radiation passing through the exit slit at the distance ξ' from the midpoint was determined in the manner described.

The radiation losses so obtained were now plotted against ξ. It was found that for receiver width 0.2 mm and focal ratio 5:1, and also for receiver width 0.3 mm and focal ratio 7:1, the three points corresponding to $\xi=\xi_{0.2}$, ξ', and 2, respectively, lie very nearly on a straight line. These lines were drawn, and the other sets of three points were joined by arcs of circles. Since the curvature of these was small in all cases, they may be assumed to provide a good approximation. The area under each of these curves was

measured by means of a planimeter and divided by 2. The results are the relative losses of radiation resulting from aberrations when the full slit, from $\xi=-2$ cm to $\xi=2$ cm, is used. In Table II these losses are expressed in percent.

To these losses must be added the loss of radiation cut off by the thermocouple housing. This loss could be eliminated by tilting the ellipsoidal mirror to such an extent that the reflected radiation is focused at a small area lying outside the cone of radiation coming from the exit slit. However, when this is done all points of the exit slit lie at considerable distance from the focus of the ellipsoidal mirror, and the aberrations are large. It is therefore not advisable, in general, to tilt the mirror, especially when it has a large focal ratio. The loss can be reduced, however, by making the thermocouple housing very narrow. For a housing of given width, this loss is smaller the greater the focal ratio.

In the spectrometers actually built it was found impractical to make the width of the thermocouple receiver less than 0.3 mm. On the other hand, the far focal distance was made 42 cm rather than 40 cm. The focal ratio was chosen to be 7:1, making the loss of radiation caused by aberrations slightly less than 9 percent. The thermocouple housing was made so narrow that the amount of radiation cut off by the housing was roughly equal to that lost as a result of the aberrations.

RANDALL-FIRESTONE FORMULA

Because of the aberrations the image formed by an ellipsoidal mirror of a long narrow slit having its midpoint at the far focal point will have the form of an X with the acute angles filled with light. The value of the acute angles, or the width of the slit image at a given distance from the midpoint, is determined by $2Y/X$. According to (9)

$$2Y/X=4exy(a-ez)/[(1-e^2)^2a^2z -e^2(x^2-y^2)z+(2-e^2)eax^2 -e^3ay^2-(1-e^2)^2ea^3]. \quad (10)$$

Assuming that the entire area of the ellipsoidal mirror is filled with light we may determine the point on the circular edge of the mirror for which $2Y/X$ is a maximum. If the polar coordinates $x=r\cos\varphi$, $y=r\sin\varphi$, are introduced,

$$z=(1-e^2)^{-\frac{1}{2}}((1-e^2)a^2-r^2)^{\frac{1}{2}}$$

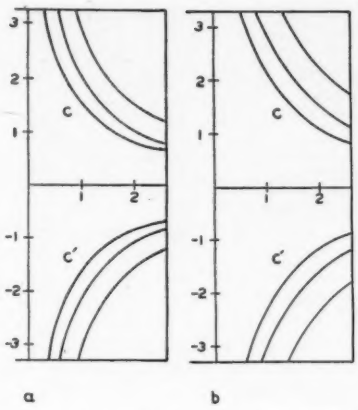

FIG. 5a. Curves through points of reflection on ellipsoidal mirrors of focal ratio 5:1, 7:1, and 9:1, so chosen that a ray coming from the top of the exit slit will on reflection hit the edge of a receiver of width 0.2 mm. ($\xi=2$ cm, $a=22.86$ cm.) Only half of the illuminated area of the mirror is shown.

FIG. 5b. Curves through points of reflection on ellipsoidal mirrors of focal ratio 5:1, 7:1, and 9:1, so chosen that a ray coming from the top of the exit slit will on reflection hit the edge of a receiver of width 0.3 mm ($\xi=2$ cm, $a=22.86$ cm). Only half of the illuminated area of the mirror is shown.

is independent of φ, and (10) becomes after some reduction

$$2Y/X=A\tan\varphi/(B+C\tan^2\varphi), \quad (11)$$

where

$$A=4e(a-ez)r^2,$$
$$B=(1-e^2)^2(z-ea)a^2-[e^2z-(2-e^2)ea]r^2, \quad (12)$$
$$C=(z-ea)[(1-e^2)^2a^2+e^2r^2].$$

It can be readily shown that $2Y/X$ has the maximum value

$$(2Y/X)_{\max}=\tfrac{1}{2}A/(BC)^{\frac{1}{2}}, \quad (13)$$

when

$$\tan\varphi=\pm(B/C)^{\frac{1}{2}}. \quad (14)$$

Substituting the values (12) for A, B and C into (13), we find after some reduction

$$(2Y/X)_{\max}=2er^2\cdot[(1-e^2)^2a^2-r^2]^{-\frac{1}{2}} \times[(1-e^2)^2a^2+e^2r^2]^{-\frac{1}{2}}. \quad (15)$$

If $2Y$ is denoted by W and X by s, and if the diameter of the mirror, $d=2r$, and the shorter focal length, $f=(1-e)a$, are introduced, Randall and Firestone's formula

$$W/s=2ed^2f^{-2}\cdot[4(1+e)^2-d^2/f^2]^{-\frac{1}{2}} \times[4(1+e)^2+e^2d^2/f^2]^{-\frac{1}{2}} \quad (16)$$

is obtained.

Inertia Effects in Infra-Red Sensitive Phosphors†

F. R. SCOTT,* R. H. THOMPSON,** AND R. T. ELLICKSON***
Reed College, Portland, Oregon

(Received September 15, 1948)

Measurements are reported on the time required for an infra-red phosphor to acquire maximum brightness when exposed to infra-red radiation. This time becomes smaller as the infra-red intensity is increased, but there seems to be no simple relationship between the two quantities. The data given are for phosphors composed of strontium sulfide or selenide activated with europium and samarium. The brightness of strontium sulfide activated with cerium and samarium reaches its maximum value in something less than 10^{-4} sec., a time too short to be measured by the present apparatus.

Results on some samples seem to indicate the existence of two simultaneous processes. An appreciable fraction, often about one-half, of the final brightness is reached in less than 10^{-4} sec., while the ultimate value is approached in a much more leisurely fashion.

AN infra-red sensitive phosphor is one that, upon excitation with ultraviolet light or by radiation from a radioactive substance, releases only a small fraction of its stored visible light immediately after excitation unless exposed to infra-red radiation of a suitable wave-length. If exposed to infra-red radiation of high intensity, it will release its stored light in a very short time; if stored in the dark at room temperature, some infra-red phosphors will store more than half their light for a week or more.

When an infra-red phosphor that has been excited is exposed to infra-red radiation of constant intensity, the brightness of the surface of the phosphor does not always build up to its maximum value immediately. This lag might well be called inertia, and it is this effect that is dealt with in this paper.

There are about four different infra-red phosphors, most of them sulfides or selenides of strontium and calcium to which have been added small amounts of impurities called activators. These impurities, present to a few parts per million, are usually rare earths. The detailed compositions and methods of preparation are fully described elsewhere[1] and will not be dis-

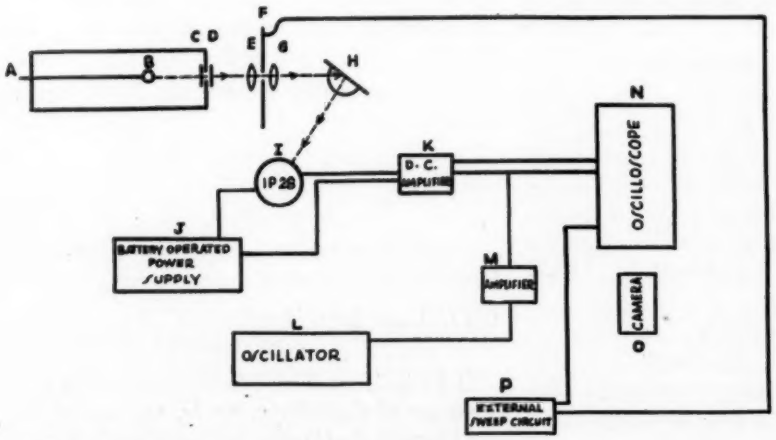

FIG. 1. Schematic diagram of apparatus for measuring inertia effects.

† The work described in this paper was supported by the Office of Naval Research under a contract with Reed College.
* Present address: University of Indiana, Bloomington, Indiana.
** Present address: Rutgers University, New Brunswick, New Jersey.
*** Present address: University of Oregon, Eugene, Oregon.
[1] G. R. Fonda and F. Seitz, *Solid Luminescent Materials* (John Wiley and Sons, Inc., New York, 1948) and references there cited.

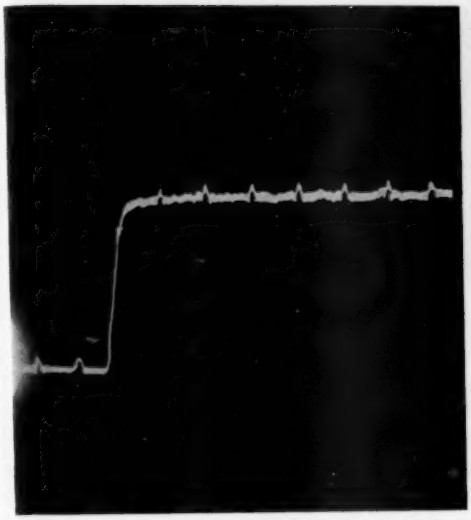

FIG. 2. Photograph using white light. Timing marks 1/2800 sec.

cussed here. The phosphors used in these experiments were kindly furnished to us by Professor Roland Ward of the Polytechnic Institute of Brooklyn, to whom we are deeply indebted for these and other favors.

The experiments described here were performed on three different phosphors the compositions of which were as follows: (1) Standard VI, strontium sulfide activated with samarium and europium, (2) Standard VII, strontium sulfide activated with cerium and samarium, and (3) B-1, strontium selenide activated with samarium and europium. The inertia effect is especially pronounced in the B-1 phosphor. For very low intensity infra-red it may take more than a minute for some samples of this phosphor to reach maximum brightness.[2] For higher infra-red intensities the time to reach maximum brightness is reduced.

The apparatus used is shown schematically in Fig. 1. Light from the tungsten lamp "*B*" was passed through the infra-red transmitting filter "*D*." The lenses "*E*" and "*G*" were introduced to make the light beam as small as possible at the shutter "*F*" and thus to increase the effective speed of the shutter. When the shutter opened,

[2] A. L. Smith, R. D. Rosenstein, and R. Ward, J. Am. Chem. Soc. 69, 1725 (1947).

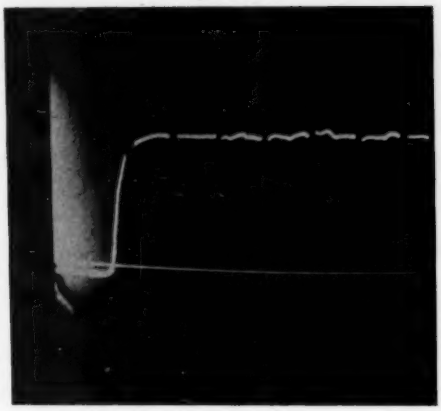

FIG. 3. Standard VII. Timing marks 1/2800 sec.

the infra-red caused the phosphor "*H*" to glow and light from it was picked up by the electron multiplier tube "*I*". The voltage across the load resistor in the final stage of this tube was amplified and impressed across the vertical plates of the oscilloscope. The variable frequency oscillator and its associated amplifier were used to place small, timing "pips" on the output. The external sweep circuit was synchronized with the shutter so that the horizontal sweep began immediately after the shutter opened. Since the whole apparatus was operated in a dark room the camera shutter was not synchronized with the rest of the apparatus, but simply left open for the few seconds it took to take a picture.

The shutter was a simple mechanical one activated by two heavy springs and released by a hand trigger. The speed of the shutter can be estimated from Fig. 2, which shows a picture taken with the infra-red filter removed from the light source and a piece of white paper substituted

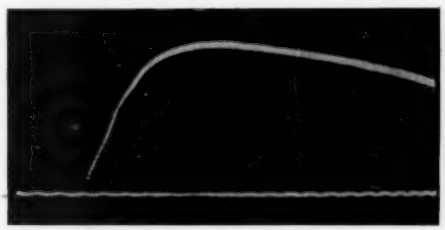

FIG. 4. B-1. Total sweep seven seconds. Infra-red intensity 0.019 lamberts.

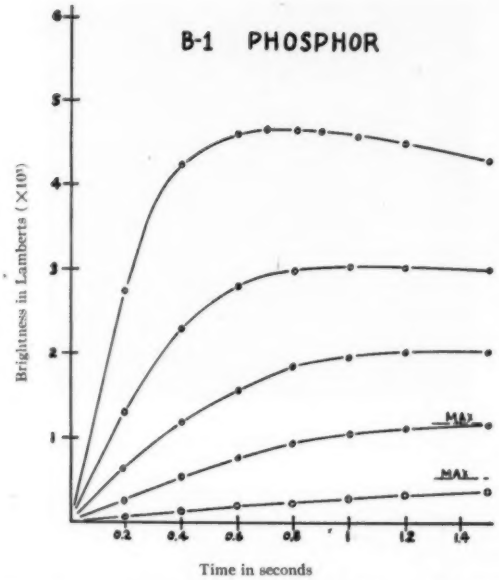

FIG. 5. Inertia curves for B-1. Infra-red intensities 275, 160, 100, 71 and 29 millilamberts.

for the phosphor. The timing pips in this picture are separated by an interval of 1/2800 sec., and one can estimate that the shutter opens in something less than one-fourth of this time or about 10^{-4} sec.

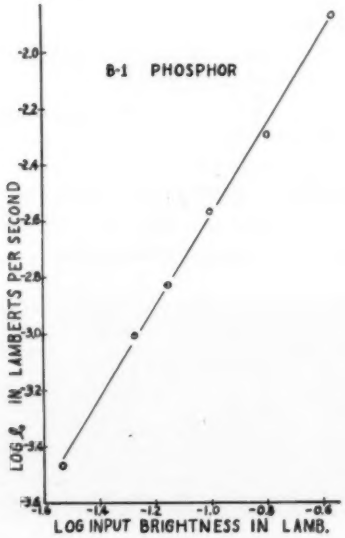

FIG. 6. Variation of the initial slope of the curves of Fig. 5 with infra-red intensity.

The inertia effect is very small in the Standard VII phosphor, as can be seen from Fig. 3. Here the timing "pips" are the same as in Fig. 2, and there is no perceptible difference between the two photographs. We were not able, therefore, to determine the magnitude of the inertia effect in this phosphor except to say that it reaches maximum brightness in less than 10^{-4} sec. even for the weak infra-red intensity we were using.

As mentioned above, the inertia effect in the B-1 phosphor is very pronounced. It is so large that we have been able to measure it for very weak intensities by observing the current from the electron multiplier tube directly in a d.c. galvanometer. A typical build-up curve for this phosphor is shown in Fig. 4. The infra-red intensity for this curve was 19 millilamberts. (Infra-red intensities are given as the brightness of a white surface at the position of the phosphor with the infra-red filter removed from in front of the light source. The brightness of the white surface was measured with a Macbeth Illuminometer.) The total time for the sweep in this picture was seven seconds and the maximum brightness was apparently reached in something over a second.

TABLE I.

Time to reach half-maximum B-1						
Infra-red intensity, millilamberts	275	160	100	71	54	30
Time, seconds	0.18	0.22	0.32	0.44	0.59	0.85

The results of measurements on a number of such photographs are shown in Fig. 5. Here it is quite evident that the time to reach maximum brightness does indeed decrease with increasing infra-red intensity. In Table I the time to reach half-maximum is given for several infra-red intensities. There seems to be no simple relationship between these two quantities.

Curiously enough there does seem to be a quite simple relationship between the initial slope of the brightness *vs.* time curve and the infra-red intensity. Figure 6 shows the log-log plot of these quantities, and the curve is a rather good straight line with a slope of approximately 1.5. We have been unable to give a plausible explanation for this apparently simple relationship.

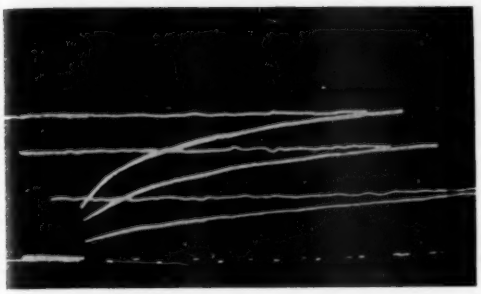

FIG. 7. Inertia effect in Standard VI. Note that a sizeable fraction of the final brightness is reached almost immediately. Infra-red intensities 4.5, 2.9, and 1.3 millilamberts.

The Standard VI phosphor exhibits a peculiar inertia effect as shown in Fig. 7. Apparently a sizable fraction of the final brightness is reached in a time too small to be detected by our present shutter arrangement, something less than 10^{-4} sec. The final brightness value is then approached gradually as in the case of the B-1 phosphor. (The B-1 phosphor shows the same effect to a smaller extent, as shown in Fig. 4, where about one-tenth of the final brightness seems to be reached immediately.

The results of measurements on a number of photographs using Standard VI at different infra-red intensities is shown in Fig. 8. In each case about half the final brightness is reached in a time too small to be detected by our apparatus. We have no explanation to offer for this curious phenomenon except to say that it seems to indicate the presence of two separate processes in the emission of light from this phosphor.

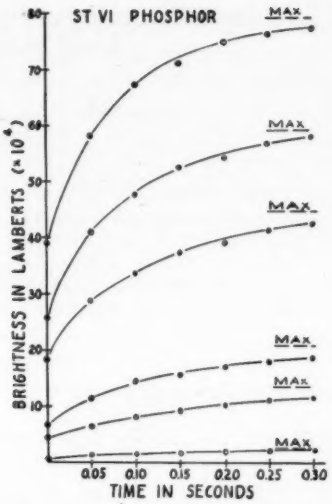

FIG. 8. Inertia curves for Standard VI. Infra-red intensities 17, 13, 9.4, 4.5, 2.9 and 0.56 millilamberts.

The results given in this paper should not be taken as characteristic of every sample of the phosphors described. It is well known, especially in the case of the B-1 phosphor, that some samples show the effect much more than do others. In fact the B-1 samples used in these experiments were chosen because they showed the effect to a greater extent than usual. It is not known at present what causes the effect to be more pronounced in some samples than in others.

We should like to express our thanks to the Office of Naval Research for their generous support of this work and to Professor Roland Ward for furnishing us with samples of phosphors made in his laboratory.

Direct Recording of Spectra in the Region 1.2μ to 3μ Using the Lead Sulfide Photo-Conductive Cell*

R. C. NELSON
Department of Physics, Northwestern University, Evanston, Illinois

(Received September 13, 1948)

The problems arising in the use of the lead sulfide cell for direct recording of spectra have been investigated using a spectrograph designed especially for this work. The inhomogeneity of the surface of these cells, as compared with photo-multipliers, makes for important differences in their use. Using a sharply tuned amplifier, the sensitivity of the cells at room temperature is adequate to permit a resolving power of the order of 40,000 at 1.4μ. Wave-lengths may be determined to about 0.1A, using overlapping orders.

I. INTRODUCTION

THE region 1.2μ to 3μ falls between the region of very sensitive detectors on the short wave-length side and that of large allowable slit widths on the other, and in consequence, has offered considerable experimental difficulties. The recent development by Cashman[1] of lead sulfide (PbS) cells having very high sensitivities over this range, has given it renewed interest, since now resolving powers in wave numbers comparable to those at longer and shorter wave-lengths may be attained easily.

The present paper is a survey of the special problems involved in the direct recording of spectra with the PbS cell, and discusses also the use of the direct recording technique for the accurate measurement of wave-length.

II. THE SPECTROGRAPH

Since it was planned to measure wave-lengths to an accuracy of a few hundredths of an angstrom, the design of a spectrograph especially for this purpose was necessary. The optical arrangement is shown diagrammatically in Fig. 1. It is of the familiar Pfund type with paraboloids of 2-meter focus. The mirrors are aluminized and are carried on kinematic-type supports on a heavy steel frame. The precision bilateral slits are 18 mm long and are made by Gaertner. The grating used in the work reported here was ruled 15,000 lines/inch on speculum metal, $4\frac{7}{8}$-in. wide and $2\frac{7}{8}$-in. high, and was of indifferent quality.

* This work was sponsored by the U. S. Navy Bureau of Ships.

[1] R. J. Cashman, Proc. Nat. Electronics Conf., p. 171 (Chicago, 1946).

III. GRATING DRIVE MECHANISM

The principal design problems arose in connection with the grating table bearings and the grating drive. It was desired to make wave-length determinations to 0.05 A, which would correspond to angular displacements of $\frac{1}{4}''$ of arc. This requirement could be met with a tangent screw accurate to 1 micron operating against an arm 75-cm long. Such a construction requires 2 coaxial bearings for the grating table, one for coarse adjustment, and the other for slow motion. These bearings were made conical, of normalized cast iron, and were lapped and fitted to be parallel to 4″ of arc and concentric to 0.0002 inch.

Since a very slow and very uniform motion was required of the grating drive bearing, its friction had to be reduced to a minimum. This was accomplished by combining with the cone a spring-supported ball thrust bearing which was adjusted so as to carry all but enough weight to locate the cone. The force required at the end of the driving arm to rotate the grating with a 60-pound load on the bearing is a few grams. The driving arm is of tapered I-beam form in welded steel, to give the necessary rigidity. It is linked to the driving nut by means of a steel ball and a hardened steel flat. The drive screw was ground and thoroughly lapped, and is mounted on lapped spherical bearings.

Each driving speed is supplied by a separate gear-head motor, since speeds ranging from 2 r.p.m. to 300 r.p.m. are used, and the design of a gear shift for such a range would be awkward. These motors are linked together with overrunning clutches, with a differential for putting in the reverse. To reduce vibration and heating,

they are mounted outside the spectrograph and the motion is transmitted with selsyns. At the slow speeds, irregularities of the selsyn motion are quite apparent and they are "diluted" with a 22.7 to 1 reduction by lapped herringbone gears between the follower and the drive screw. The total reduction from the drive motors to the grating table is about 100,000 to 1.

A wheel carrying 20 contacts is incorporated into the drive for impressing on the spectrum record a series of marks corresponding to equal displacements of the nut on the screw. Each contact represents a 10-micron motion of the nut but by blocking off part of the contacts this value may be changed. All measurements of wave-length on the chart are made in terms of this scale.

IV. DETECTING AND RECORDING SYSTEM

The design of a suitable amplifier for use with PbS cells has been discussed by Wilson,[2] and an amplifier built by him used for this work. A chopper disk at the entrance slit interrupts the light of 1080 c.p.s.; the signal from the cell is fed into a very sharply tuned amplifier, the over-all gain of which is about 10^8.

For the highest signal to noise ratio at low rates of scanning, it has proved advantageous to operate the amplifier with a band-pass as narrow as 0.5 c.p.s. To do this, the synchronous chopper motor must be supplied with closely regulated frequency, in this case from a tuning fork oscillator. A filter with a time constant of about two seconds is used on the input to the Speedomax recorder, which is here used as a microammeter, with an input resistance of 500 ohms. For higher scanning rates, the overall response time must be kept low, and the sensitivity will be less.

The highest attainable sensitivities with PbS cells are no doubt those of certain minute areas or "hot spots" which are found in many cells. These areas may be a millimeter or two long and about 0.02 mm or less in width, and have 10 to 20 times the response of the general area of the cell. Best practice requires that as much of the light as possible be concentrated on these spots. For this reason, an ellipsoidal mirror is used to focus an image of the exit slit upon the PbS cell at a $\frac{1}{3}$ reduction. The adjustments are rather critical, and a high degree of stability must be provided in the mounting of the cell and ellipsoid.

This is perhaps the most salient difference between direct recording with photo-multipliers and with PbS cells. In the former instance, for the average case, the relative aperture of the spectrograph does not limit the sensitivity since longer slits may be used for equal resolution with instruments of smaller aperture. With PbS cells, as with photography, the relative aperture of the optics assumes primary importance. An advantage arising from this fact is that it is unnecessary to illuminate more than 5 or 6 mm of the entrance slit, a convenient circumstance permitting the use of small brilliant sources to best advantage.

The inhomogeneity of the surface of the cell may be troublesome when the image of the slit on the cell is much wider than the hot spot. In combination with the time lag of the recorder, it has the effect of displacing the recorded peak of the line toward longer or shorter wave-length by an amount proportional to the maximum deflection. Since the hot spot usually occurs at one edge of the cell, it will cause the profile of the line to be asymmetrical; that is, the leading edge will rise more sharply than the trailing edge falls if the image crosses the hot spot before the general area of the cell. If the image is very wide, a spurious triple structure may be seen, consisting of a central peak with an inflection on either side. Such effects as these disappear with slit widths of 0.15 mm or less.

When the spectrograph is used in the manner indicated here, it is possible to obtain at 15,000A a signal 100 times the noise with slits 0.4A-wide using a 70-watt incandescent lamp with a straight helix filament as a source. The work reported

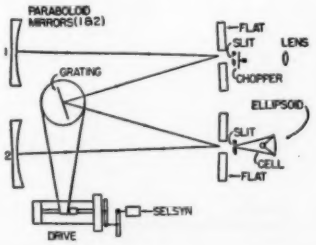

FIG. 1. Diagram of spectrograph.

[2] W. R. Wilson, Astrophys. J. 106, 243 (1947).

here has all been done using PbS cells at room temperature, and it is probable that substantial increases in sensitivity can be had by cooling to dry ice temperatures.

V. RESOLVING POWER

A resolving power of about 45,000 has been reached with this spectrograph, based on resolution of fine structure in the water vapor absorption band at about 13,800A. The limiting factor in this case was apparently the actual width of the lines themselves, although the limit imposed by the amount of energy available from a tungsten source was also being approached. The best resolution attained on the water band at 18,700A is about 25,000. The difference is due largely to the fact that the PbS cell has a minimum of sensitivity near this point.

VI. WAVE-LENGTH MEASUREMENT

Good resolving power in a photographic spectrograph is in a high degree dependent on the constancy of ambient conditions, while precision of wave-length determination is relatively independent of such effects. In a direct recording instrument these are reversed, and while only very rapid changes in the instrument can affect the resolution, the precision of wave-length measurement is affected to the same degree as the resolving power of the photographic instrument. Since the grating must be driven at very low speed for precise wave-length measurements, the time required to cover a useful range of wave-length becomes large, and the difficulty of maintaining constancy of ambient conditions is quite severe.

Wave-length determinations are made in general by the use of overlapping orders. The record is planned so that a line of higher order and accurately known wave-length is found near its beginning, another near its end, and a third not too far from its midpoint. A second order equation expressing wave-length in terms of readings on the impressed scale is calculated from the known wave-lengths of the three lines, and used to compute the wave-lengths of the remaining lines. It is often more convenient to use neon or argon lines from a separate source for the reference points at the beginning and end of the record.

The second order term lumps together corrections for all the sources of non-linearity, such as the changing dispersion of the grating, the changing rate of angular drive due to the use of the tangent screw, the errors arising at the contact between the nut and driving arm (if they are progressive), and a slow progressive drift of temperature (if it is present).

Measurements have been made on absorption lines by a modification of this technique. First a neon spectrum covering the desired range is recorded, after which the instrument is immediately set back to the starting point, and the first neon line again recorded. Without stopping the drive, sources are changed, and the absorption spectrum is recorded, followed by the final neon line. The spectrum of neon alone is used to deter-

FIG. 2. Water vapor absorption near 13,825A. The scanning rate was 3.5A/min., and the slit was 0.4A wide.

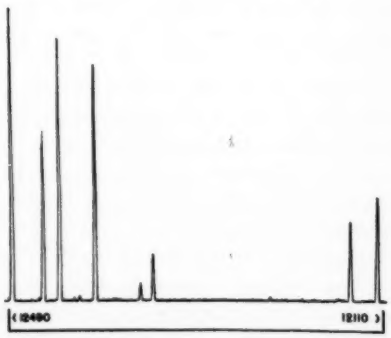

FIG. 3. Argon spectrum from hollow cathode source at 75-watt power. Scanning rate, 50A/min.; slit width 2.5A.

mine the constant of the second order term, which is then applied to the absorption spectrum, the initial and final neon lines determining the first order term constant. The accuracy is about as good as in the procedure using 3 lines on the working record.

Table I shows four common modes of operating the spectrograph. The conditions of highest dispersion do not seem to give any worth-while improvement in precision of wave-length determination, probably because of insufficiently good control of ambient conditions.

The instrument has been used for the examination of the water-vapor absorption bands at 1.4μ and 1.8μ, suitable filters being utilized to remove higher order radiation. Much new detail has been found in these bands, and this work will be published elsewhere. Figure 2 shows a part of the 1.4-μ-band. Figure 3 shows a portion of the infra-red emission spectrum of argon observed in a hollow cathode type source. A number of lines not previously observed have been recorded. In general, sources are the greatest cause of difficulty in the examination of emission spectra in this region, since they must not only be brilliant but must also be capable of maintaining constant excitation conditions for considerable periods while a record is being made.

TABLE I. Typical operating conditions of spectrograph.

Angstroms per hour	Slit width in angstroms	Dispersion on paper	Angstroms per scale division	Standard deviation of a single determination
15,000	5.0	7.0A/mm	...	5.0A
3,000	2.5	1.5A/mm	1.7	0.5A
1,000	1.0	0.5A/mm	1.7	0.13A
200	0.8	0.2A/mm	0.4	0.10A

VII. REMARKS

The work reported here was done as part of a projected survey of spectra and sources suitable for use in light beam communication in the near infra-red. The use of the instrument with continuous sources is limited to the region below 2.2μ at present, as a result of lack of suitable filters for removing overlapping orders.

It may be possible eventually to extend the range of the instrument beyond 4μ, if lead selenide cells of sufficiently high sensitivity are developed. This should be of considerable interest for the study of absorption spectra in this region. In any case, the speed and convenience of recording with photo-conductive cells indicate their use whenever a problem can be attacked in a region where they are sensitive.

ACKNOWLEDGMENT

A great many people have contributed to this work, of whom should be mentioned especially Dr. W. S. Huxford, director of the project under which the work was done; Dr. E. R. Peck, who undertook the early planning of the spectrograph; Dr. R. J. Cashman, who gave us the benefit of his vast experience with the use of photo-conductive cells; Mr. W. R. Sittner, who had had earlier experience using PbS for recording flash spectra; Mr. Wallace Wilson, who built the amplifier and advised on its use; Mr. Arnold Svebilius, in whose shop most of the machine work on the spectrograph was done, and Howard Sonderman and Dana Storch, who assisted in the setting up of the spectrograph.

JOURNAL OF THE OPTICAL SOCIETY OF AMERICA VOLUME 39, NUMBER 1 JANUARY, 1949

New "Offset" Method of Interpreting Spectrophotometric Curves

W. A. SHURCLIFF* AND E. I. STEARNS
Research Department, Calco Chemical Division, American Cyanamid Company, Bound Brook, New Jersey
(Received March 24, 1948)

Qualitative and quantitative analyses of light-absorbing solutes may be carried out rapidly and accurately by direct visual comparison of "offset" spectrophotometric curves linear in log log$1/T$ and plotted on transparent paper. Only the final chemical analytical data are read; no explicit account is taken of optical parameters, and the curves may be plotted on gridless paper.

INTRODUCTION

THIS article describes a general method whereby light-absorbing chemicals may be spectrophotometrically analyzed qualitatively and quantitatively without reading any numerical data whatsoever from the graph paper. All results desired are obtained by direct visual comparison of shapes and displacements of curves on transparent superposed sheets. In most analytical problems the method provides reliability, accuracy, and speed not possible by other methods.

Strictly speaking, the offset method described here is not new. In the writers' laboratory the method, worked out shortly before 1935 by the late O. W. Pineo, has been in continual use since 1936 in solving research and production problems of a wide variety. In this laboratory, the method is used in practically all photometric analyses where the interest lies in chemical determinations.

Automatically recording absorption spectrophotometers,[1] when first placed on the market, were almost invariably used to plot percent transmittance (T). To a physicist interested in optical phenomena such plots were logical enough. Chemists and physical chemists, although interested only in chemical analysis of materials under test, fell into the habit of dealing with transmittance values. Using slide-rules or other devices they could fairly readily compute optical density and, in simple cases, chemical concentration.

O. W. Pineo was the first to develop a spectrophotometer[2] which would plot a function immediately and directly usable in terms of quality and quantity of light-absorbing chemical. The spectrophotometer which used the optics and the electrical components of a commercial spectrophotometer had fitted thereto a cam which causes the spectrophotometer to plot curves of light-absorbing chemicals in solution which use log log$1/T$ as an ordinate. Such curves, over the concentration limits within which Beer's law applies, have shapes independent of concentration and cell length. The shapes are dependent only on specific extinction coefficients and are thus diagnostic of a particular chemical. The vertical position of the curve is, most conveniently, dependent only on concentration (assuming a constant cell thickness).

The offset method, in addition to requiring plots with an ordinate linear in log log$1/T$, requires that the spectrophotometric data be plotted on transparent paper, and that a transparent logarithmic scale be available, this scale having the same modulus or log cycle as was used in plotting the curves. But it should be noted that while it is necessary that the ordinate be linear in log log$1/T$, no actual ordinate grid need be provided on the paper, and the entire sheet may be entirely blank except for the curves themselves and one or two fiducial marks to show that the sheet was positioned properly on the recording drum. On the other hand, there may be included a printed-on grid explicit in one of several parameters; we have found it convenient to label the (unequally spaced) ordinate lines in terms of transmittance, although

* Now with Polaroid Corporation, Cambridge, Massachusetts.

[1] O. W. Pineo, to American Cyanamid Company, U. S. Patent No. 2,107,836 (1938).

[2] O. W. Pineo, to American Cyanamid Company, U. S. Patent No. 2,176,013 (1939).

this grid is entirely ignored in the great majority of analyses.

DETERMINATION OF CHEMICAL IDENTITY

Curves *A* and *B* of Fig. 1 represent the log log1/*T* curves of two solutions of colored solutes. It is desired to know if the solutes are qualitatively identical. In the offset method, in which each log log1/*T* curve has been drawn on a separate sheet of transparent paper, the determination can be made in two or three seconds. One sheet is placed on top of the other and lined up laterally. Then the upper sheet is slid vertically until the two curves coincide at one point, say, at the wave-length of the absorption maximum. If the two curves now coincide throughout their entire length, the absorbing chemicals are identical; otherwise they are different.

Of course, the solutions should be prepared under very similar conditions except for concentration. If for water solutions, for example, such factors as pH are not controlled, the curve shapes may differ for this reason rather than because of a qualitative difference in the solutes themselves. It has also been found desirable to adjust the solution's concentration roughly so that the minimum transmittance value falls in the range from 10 to 30 percent. This serves two purposes; it brings both solutions within a range over which Beer's law is usually obeyed, and it insures that a long segment of the curve will be plotted and hence be available for establishing chemical identity. The assurance of chemical identity is greater the longer the curve segments that coincide.[3]

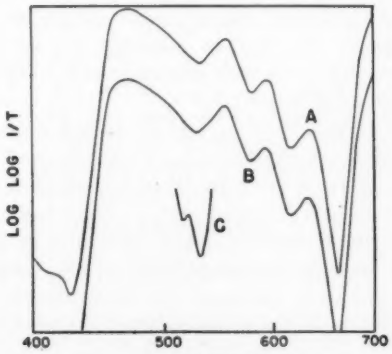

FIG. 1. Chemical identification: *A*—known curve of chlorophyll; *B*—curve of unknown substance; *C*—segment of didymium filter curve.

DETERMINATION OF CONCENTRATION

As a first step in making a quantitative calculation, the curve of the sample is placed on the curve of the standard and adjusted vertically so that the curve shapes may be compared. If the curve shapes are identical, most of the common gross errors have been avoided. For instance, the material has been correctly labeled as to identity, the solutions have been properly prepared and measured, and there is no contamination with foreign light-absorbing materials. If the curve shapes do not agree, then the calculation of concentration should not be made.[4]

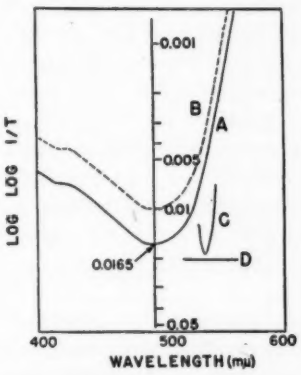

FIG. 2. Quantitative analysis: *A*—Orange II at 16.5 mg/l *p*H 5 in water; *B*—Orange II at unknown concentration; *C*—segment of didymium filter curve; *D*—segment of "gray" filter curve.

[3] Since plotting paper sheets may vary somewhat from sheet to sheet (because of such factors as printing errors and humidity changes), and since different sheets may be mounted slightly imperfectly on the recording drum, internal calibration or fiducial marks should be used for most accurate determination—whether offset or other method is to be used. By means of a clutch in the wave-length drive mechanism, and by means of calibration filters mounted mechanically in a filter slide so that the filters may be correctly positioned in the light beam of the instrument at the push of a button, segments of the transmission curves of a near-horizontal (gray) filter and a near-vertical (didymium) filter may be plotted on a sheet with an elapsed time of less than twenty seconds without ever touching or even seeing the filters in question (see Fig. 2). Only the didymium calibration segment is needed for determination of chemical identity (See Fig. 1).

[4] This is one of the great advantages of spectrophotometry over filter photometry. In the commonest type of filter photometer only one transmittancy value is measured and the concentration calculated. If the calculated concentration is unexpectedly high or low, one may suspect an error of some kind, such as the solution's having

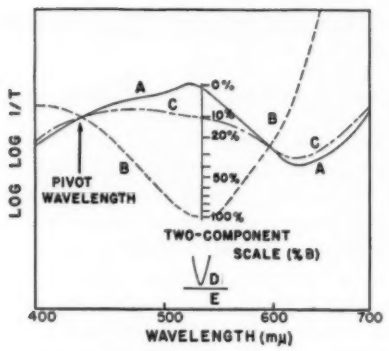

FIG. 3. Two—Component analysis: *A*—diamine green *B*; *B*—diamine violet *N*; *C*—mix of *A* and *B* in unknown proportion; *D*—segment of didymium filter; *E*—segment of "gray" filter.

The relative concentration of the two samples may be determined in a few seconds. The first step is aligning the two sheets according to their fiducial marks—preferably, the internal-standard filter curves drawn on each sheet. The log scale is then superimposed vertically and slid vertically until its 1 mark falls on the curve of the reference solution. The reading on the log scale at the intersection with the curve of the sample solution is then the relative concentration of the sample solution.

The *absolute* concentration is often not needed. But if it is needed, it may be determined readily (if a reference curve of the material at a known concentration is available) by the general method described in the preceding paragraph if the log scale reading at the intersection with the reference curve is made to be the known concentration instead of 1. Figure 2 illustrates the method. Curve *A* is the standard curve, representing a standard 16.5-mg/l solution of Orange II. Curve *B* is that of the unknown. The log scale shows at once that the unknown's concentration is 10 mg/l. This same value is obtained regardless of the wave-length at which the displacement is measured.

ANALYSIS OF TWO-COMPONENT MIXTURES

The analysis of an unknown mixture of two known dyes *A* and *B* by the offset method is very simple if there is a wave-length ("pivot wave-length") at which the curves of *A* and *B* separately cross—and cross at an appreciable angle.

The first step is making a mat, which is a sheet on which is drawn a curve of dye *A* and a curve of dye *B* (at the same concentration) and a vertical two-component scale. The scale connects the two curves at a wave-length where the curves are well seperated.[5] The scale is made by placing the log scale at this wave-length and sliding it until the readings at the intersections with curves *A* and *B* differ by a number readily divisible by 10 (such as 0.37 and 1.37 which differ by 1.00). Then the dye-*B*-percentage marks 0 percent, 10 percent, 20 percent, etc., of the two-component scale are drawn in opposite the log scale marks (in the illustration given) 0.37, 0.47, 0.57, etc. Interpolated marks may be added as desired, the whole process taking only a minute or so and the mat being useful over an indefinite period.

The unknown mixture is analyzed by sliding its curve vertically (on the mat) until it passes through the pivot point. Then the intersection with the two-component scale indicates directly the dye *B* percentage in the unknown, as illustrated in Fig. 3. The aggregate concentration of the two dyes can be found directly by applying the method of the previous section to the data at the pivot wave-length. An important application of this rapid and accurate method of two-component analysis to mixtures of oxy- and met-hemoglobin has been reported by Hamblin and Mangelsdorff.[6]

When the curves *A* and *B* do not cross, the method is varied slightly. With curve *B* held fixed, curve *A* may be displaced until a good intersection is achieved. The *absolute* concentration of dye *B* (but not dye *A*) may now be determined exactly as before.To find the absolute

been prepared at incorrect pH, but this cannot be verified readily, especially if the doubt arises after the solutions have been thrown away. Using spectrophotometric curves linear in log log$1/T$, however, the preliminary curve shape comparison would immediately show up any significant error of this kind. Thus any quantitative analysis is routinely preceded by a qualitative analysis to make sure that the quantitative comparison is legitimate.

[5] In theory, the choice of wave-length at which the scale is drawn is immaterial. In practice, several factors should be kept in mind if greatest accuracy is desired. Separation of the curves and freedom from steep slope are two factors of especial importance.

[6] D. O. Hamblin and A. F. Mangelsdorff, J. Ind. Hygiene Tox. **20**, 523–30 (1938).

concentration of dye *A*, the process is reversed; another mat is prepared in which the curve of dye *A* is held fixed and the curve of dye *B* is shifted arbitrarily. Alternatively (but with same departure from a pure offset method), a sort of nomogram may be prepared whereby the absolute concentration of dye *A*, for example, is determined directly by superposing the unknown's curve on the mat, reading the intersection points with two vertical nomogram scales and adding the two readings. Details of such methods are outside the scope of this discussion of the major uses of the offset method *per se*.

DISCUSSION

None of the procedures described require making any actual readings of transmission or wave-length—or density or specific extinction coefficient. Nothing is read off except the chemical information desired: identity and concentration.

To demonstrate the complete freedom from wave-length and transmission values an instance may be cited when the supply of printed paper was exhausted; instead of shutting down operation, operation continued unabated using common blank onion skin paper, and with no sacrifice of accuracy or speed of analysis.

The method can, of course, be used in analyzing materials absorbing only ultraviolet or infrared light; using appropriately modified plotting techniques it can be used with reflecting samples like colored cloth or paper.

The method is so striking and so little-known that we believe it deserves a distinct name. The name "offset" seemed appropriate, being suggestive of the offset comparison of photographs or maps as in detecting topographic changes.

JOURNAL OF THE OPTICAL SOCIETY OF AMERICA VOLUME 39, NUMBER 1 JANUARY, 1949

Absorption Spectrum of 1,2,4-Trichlorobenzene in the Near Ultraviolet

HEDWIG KOHN
Department of Physics, Wellesley College, Wellesley, Massachusetts

AND

H. SPONER
Department of Physics, Duke University, Durham, North Carolina

(Received September 13, 1948)

The absorption spectrum of 1,2,4-trichlorobenzene at 2960–2600A has been investigated using a medium Hilger quartz spectrograph. The band system corresponds to a transition $A'-A'$ (1,2,4-$C_6H_3Cl_3$ belongs to symmetry group C_s) with the transition moment lying in the molecular plane. The transition is allowed. In agreement with this assignment the 0—0 band appears strongly. Several progressions of symmetric vibrations and many combinations between them have been observed. A number of vibrational frequencies were identified with Raman frequencies. Characteristic of the spectrum is that its bands are spaced very regularly apart from each other, with a difference of about 30 cm^{-1} being most prominent. These differences represent $v-v$ transitions of low frequency vibrations.

INTRODUCTION

THE near ultraviolet absorption of 1,2,4-trichlorobenzene, together with that of 1,3,5- and 1,2,3-trichlorobenzene has been studied in hexane solution by Conrad-Billroth.[1] The general region of the spectra is 2600–2950A. They show three distinct maxima which are sharpest in the 1,2,4-compound. Also, the absorption coefficient is about three times larger in the 1,2,4-derivative than in the other two derivatives. The absorption strength of the latter two substances is very similar to that of benzene under comparable conditions. In agreement with

[1] H. Conrad-Billroth, Zeits. f. physik. Chemie **B19**, 76 (1932); K. L. Wolf and O. Strasser, Zeits. f. physik. Chemie **B21**, 389 (1933).

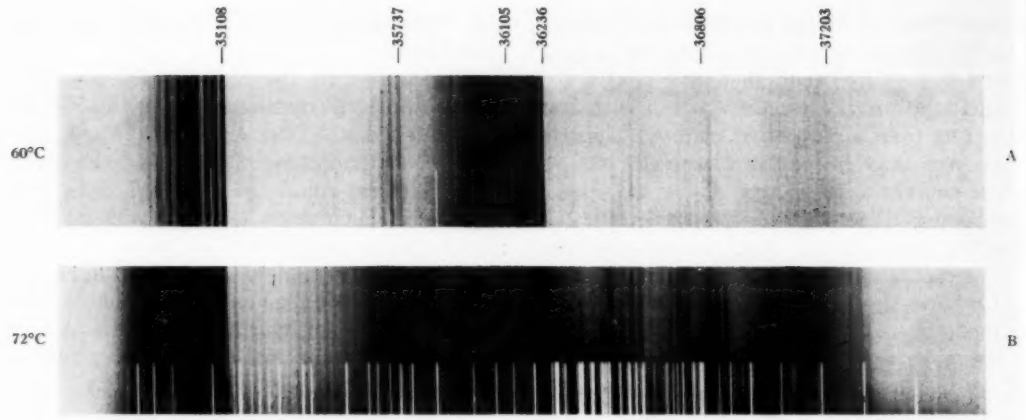

FIG. 1. Absorption spectrum of 1,2,4-trichlorobenzene at different temperatures of the reservoir.

this, their absorption spectra represent forbidden transitions whereas the spectrum of the 1,2,4-trichlorobenzene belongs to an allowed transition.

The vapor spectrum of 1,3,5-trichlorobenzene has been analyzed[2] and the analysis conforms to the requirements of a forbidden transition. In this paper the results are given on the near ultraviolet absorption of gaseous 1,2,4-trichlorobenzene at various pressures of the substance. A brief comparison between the spectra of the trichlorobenzenes in solution and in the vapor phase and among the three vapor spectra has been published recently.[3]

EXPERIMENTAL

The optical arrangement was of the conventional type: A low voltage hydrogen arc[4] used as continuous light source was focused by means of two converging quartz lenses onto the slit of a medium Hilger quartz spectrograph; the light passed the absorption tube approximately parallel. The average dispersion of the Hilger spectrograph is 9.8A/mm at 2600A; 11.5A/mm at 2750A; 14.2A/mm at 2950A. An iron arc of the Pfund type was used as source of the comparison spectrum. All spectrograms were taken on Eastman spectroscopic plates II-0.

The absorption tube was of opaque quartz, 25 cm long and 2 cm in diameter, and it had transparent plane parallel windows fused on to the ends. It was provided with a side arm to contain the body substance. Two separate furnaces regulated the temperatures of the main tube and the appendix, the latter always being at a slightly lower temperature than any other part of the tube.

The 1,2,4-trichlorobenzene was obtained from Eastman Kodak. The substance has a melting point of 17°C and a boiling point of 213°C. It was filled into the absorption tube by vacuum distillation. The first fraction was distilled away at a pressure of a few cm and at a temperature of about 160°C and then the middle fraction, which was used, was distilled under high vacuum into the tube somewhat below 100°C. The whole distillation was carried out with great care.*

Most spectrograms were taken at temperatures between 45° and 90°C, i.e., above the melting point of the substance. Exposure times varied between 1 and 30 minutes. The wave-length measurements were made with a Hilger comparator which allows readings of 0.001 mm. The accuracy of these measurements depends largely on the definition of the band heads. It ranges from several tenths of a wave number (cm^{-1}) for the best defined heads to several (even 6) whole

[2] H. Sponer and Maurice B. Hall, article in Volume commémoratif Victor Henri: *Contribution à l'Etude de la Structure Moléculaire* (Maison Desoer, Liège, 1947–48).

[3] H. Sponer, Chem. Rev. **41**, 281 (1947).

[4] The lamp was of the type described by A. J. Allen and R. G. Franklin, J. Opt. Soc. Am. **29**, 453 (1939) and was obtained from A. G. Nestor of the Bartol Foundation.

* We wish to acknowledge the help of Dr. Stanley Siegel in carrying out the distillation.

units for broad and diffuse bands and for overlapping bands of not sufficient resolution. The accuracy was also decreased in cases of strong background absorption.

RESULTS

Figure 1 is an illustration how the absorption spectrum of 1,2,4-trichlorobenzene develops with increasing pressure. The temperatures are those of the side arm. Many plates have been taken with different variations in pressure and temperature, and the measurements were made from quite a variety of plates. At the lowest temperature of 45°C there may be distinguished three groups of bands. The bands at the violet end of the groups have the wave numbers 35108, 35737, and 36236 cm^{-1} (see Fig. 1). The first group, counting from longer wave-lengths, is the strongest although at higher pressures the first and third group appear to have comparable intensities, as spectrogram *B* shows clearly. At the same time more groups become visible on the violet side of the spectrum which now extends to about 37340 cm^{-1}. The characteristic features of the entire absorption system are a number of groups consisting of apparently equally spaced bands (about 30 cm^{-1} apart) of varying intensities. At about 70°C the absorption has become so strong that the bands in some groups begin to merge into each other, and many more bands can be seen towards longer wave-lengths from the groups. At still higher temperatures the middle portion of the spectrum shows eventually complete absorption with new bands appearing on both wave-length sides of the spectrum. The bands are degraded to the red and many of them are quite sharp. This can be seen much better from the original plates which, of course, show more details than the prints. A few plates taken at a later time** in the large Hilger quartz spectrograph confirm the sharpness of many heads. From these plates the doublet nature of a few bands, i.e., the bands 35108, 36182, 36236, may be clearly recognized. Very distinct is the doubling of the band 35004/010 showing two narrow bands of equal intensity.

The experimental data are collected in Table I. The intensity classification adopted in this paper is the following: est = extremely strong, vst = very strong, st = strong, m = medium, w = weak, vw = very weak, and ew = extremely weak. In some places intermediate steps have been used. Intensities could be estimated over a large range of the spectrum from a single exposure. Most estimates given in Table I refer to plates taken with the reservoir at 65° and 70°C, while the main tube was at 74° and 79°C, respectively. The intensities of the bands at the red and violet ends of the spectrum were estimated from a plate taken at 82°C of the reservoir. Although the intensity notation is the same as in the main region it refers to much weaker bands so that a direct comparison among the three regions should not be made. The bands of the violet and red ends are, for themselves, so different in intensities that a separate scale applies to each region. Most of the outstanding bands of the spectrum remained sharp over a considerable temperature interval and therefore are measured most accurately. Diffuse and broad bands are labeled with *d*. Bands with apparent overlapping could be measured with less accuracy only. A bracket unites their wave numbers. The wave number figures of most bands of Table I represent mean values calculated from plates taken under different conditions. The long and short wave-length ends of the table have been taken from exposure at higher pressures only. The third column of Table I gives the separation of the different bands from the 0−0 band, i.e., from the pure electronic transition.

The fourth column of Table I contains the assignments. The 0−0 band is abbreviated by 0. Wave numbers subtracted or added to 0 correspond to energies of vibrations which occur in the ground or excited electronic state, respectively. The subtracted small numbers of 30, 60, 90, 98 represent differences between vibrational frequencies in the upper and lower electronic states.

1,2,4-trichlorobenzene has a second stronger absorption system below 2500A. No structure has been found in this region. This absorption extends towards longer wave-lengths with increasing pressure but even at 100°C when the near ultraviolet absorption is almost completely continuous, there is a transmission region between the two systems.

** We are indebted to Mr. Casimir Nawrocki for taking these plates.

TABLE I. Absorption bands of 1,2,4-trichlorobenzene.

Wave numbers	Intensity	Separation from 0−0 band	Assignments	Remarks
33,824	ew	−1284		Reservoir at 82°C. Bands from 33824 to 34605 are very weak and very difficult to measure. Hence these wave number values are less reliable than those above 34605.
856	ew	−1252	0−1161−90	
887	ew	−1221	0−1161−60; 0−1132−90	
916	ew	−1192	0−1161−30; 0−1132−60; 0−1101−90	
947	ew	−1161	0−1161; 0−1101−60; 0−1132−30	*R* 1155
976	ew	−1132	0−1132; 0−1101−30	*R* 1132
34,007	ew	−1101	0−1101	*R* 1098
042	ew	−1066	0−1035−30; 0−680−388	
	observed		0−1035	*R* 1035
130	ew	−978	0−3×326; 0−sep. 878−98	
165	ew	−943	0−sep. 878−60	
196	ew	−912	0−sep. 878−30	
230	vw	−878	0−200−680	
268	vw	−840	0−808−30	
300	w	−808	0−808?	*R* 815
335	w	−773	0−680−90; 0−2×388	Very uncertain.
53		−755		
368	m	−740	0−680−60; 0−sep. 653−90	
394	m	−714	0−680−30; 0−sep. 653−60	
408	m	−700		
428	m	−680	0−680; 0−sep. 653−30; 0−sep. 591−90	*R* 676
455	w	−653	0−2×326	
471		−637		
501	m	−607		
517		−591	0−200−388; 0−sep. 530−60	
539	m	−569	0−sep. 530−30; 0−680+108	
565	st	−543		
578		−530	0−200−326	
605	st	−503		Uncertain value.
				Reservoir at 65°C and 70°C. Change in intensity scale.
630	ewd	−478	0−388−90	Uncertain value.
647	ewd	−461	0−461	Uncertain value. *R* 458
686	ewd	−422	0−388−30; 0−326−98	
696		−412	0−326−90	
720	ew	−388	0−388; 0−326−60	Inaccurate, difficult to measure. *R* 397
749	vw	−359	0−326−30	
782	w-m	−326	0−326	*R* 329
808	w-m	−300	0−300?	*R* 308
838	w-m	−270		
876	m	−232	0−200−30	
891*	st	−217		
908*		−200	0−200	*R* 196
				Bands with an asterisk were also measured from plate taken in large Hilger. 34891/908 are probably two different bands, measured as single at 34909 in medium Hilger.
939*	w-m	−169		Bands from 34908 to 35108 are the sharpest in the spectrum.
948*		−160	0−461+301	
981	st	−127	0−461+333	
35,004*	st	−104		Probably two different bands.
010*		−98	0−98	
043*	vst	−65		Probably two heads of same band. Measured single at 35050 in medium Hilger.
048*		−60	0−60	
072*	vst	−36		Probably two heads of same band. Measured single at 35080 in medium Hilger.
078*		−30	0−30	
093*	st	−15		
102*	vst	− 6	0−0 band	Probably two heads of same band. Measured single at 35108 in medium Hilger.
108*	est	0	main edge	
148	vw-w	+40	0−326+364	
183	ew	+75	0+108−30	
216	vw	108	0+108	

TABLE I. Absorption bands of 1,2,4-trichlorobenzene.—*Continued.*

Wave numbers	Intensity	Separation from 0−0 band	Assignments	Remarks
35,249	vw	141	0+sep. 169−30	
277	ewd	169	0−200+364; 0−461+629	* Uncertain, difficult to measure.
310	ew	202	0−200−326+2×364	
341	ew	233	0−388+629; 0+333−98	
374	vw	266	0+301−30; 0+333−60; 0+364−98; 0−461+2×364	
409	vw	301	0+301; 0+333−30; 0+364−60; 0−326+629	
441	vw	333	0+333; 0+364−30	
472	vw-w	364	0+364	
503	vw	395		
515		407	0+108+301	
538		430	0−200+629	Perhaps three overlapping bands.
42	vwd	434		
46		438	0+108+333	
575	vw	467	0+108+364; 0−sep. 160+629	
606	w	498	0−sep. 127+629	
641	w-m	533	0+629−98; 0−461+sep. 997	
676	w-m	568	0+629−60	
706	m	598	0+629−30; 0+2×301; 0−388+364+629; 0−388+997	
737	m-s	629	0+629; 0+301+333	
751	w	643	0−200+2×108+629	
772	ewd	664	0+2×333; 0+301+364; 0−326+997	Bands from 35772 to 35863 very difficult to measure because of strong background absorption.
803	ewd	695	0+333+364; 0−680+301+1074; 0−300+997	
834	ewd	726	0+2×364; 0−680+333+1074; 0−680+301+1100	
863	ewd	755	0−680+333+1100; 0−680+301+1128; 0−680+364+1074	
888	vwd	780	0−326+108+997	
919	wd	811	0+997−98−90	Perhaps two bands overlapping.
945	vwd	837	0+997−98−60	
979	m	871	0+997−98−30; 0−sep. 127+997	
36,011	m-s	903	0+997−98; 0−200+1100	
044	m-s	936	0+997−60; 0+301+629	
075	s	967	0+997−30; 0+333+629	
105	vs	997	0+997; 0+364+629; 0+1100−104	
121	m-s	1013	0+1074−60; 0+1100−90	
148	m-s	1040	0+1074−30; 0+1100−60;	Possibly two heads of same band.
154	s	1046	0+1128−90	
178*	es	1070	0+1074; 0+1100−30;	Probably two heads of same band. Bands with an asterisk have been measured from plates in large and medium Hilger.
182*		1074	0+1128−60	
208*	vs	1100	0+1100; 0+108+997; 0+1128−30	
228*	s	1120	0+1128	Probably two heads of same band.
236*		1128		
251	vw	1143	0+sep. 1205−60; 0+sep. 1235−90	
280	ewd	1172	0+sep. 1205−30; 0+sep. 1235−60; 0+sep. 1263−90; 0+sep. 169+997	Bands from 36280 to 36343 measured from one plate only since very weak and diffuse.
313	vwd	1205	0+sep. 1235−30; 0+sep. 1263−60; 0+sep. 202+997; 0+108+1100	
343	ewd	1235	0+sep. 1263−30; 0+sep. 233+997; 0+108+1128	
371	vwd	1263	0+sep. 1296−30;	

TABLE I. Absorption bands of 1,2,4-trichlorobenzene.—*Continued.*

Wave numbers	Intensity	Separation from 0−0 band	Assignments	Remarks
36,371			0+sep. 266+997; 0+2×629	
404	ewd	1296	0+sep. 1329−30; 0+301+997	
437	vw	1329	0+sep. 1359−30; 0+333+997	
467	m-w	1359	0+364+997; 0+2×364+629	
478	w	1370	0+sep. 1401−30; 0+sep. 1433−60; 0+sep. 1463−90; 0+301+1074	
509	vw	1401	0+sep. 1433−30; 0+sep. 1463−60; 0+sep. 407+997; 0+301+1100; 0+333+1074	
541	m-w	1433	0+sep. 1463−30; 0+sep. 1495−60; 0+sep. 434+997; 0+301+1128; 0+333+1100; 0+364+1074	
571	m-w	1463	0+sep. 1495−30; 0+sep. 467+997; 0+333+1128; 0+364+1100	
603	vwd	1495	0+sep. 1595−98; 0+sep. 498+997; 0+364+1128	
640	vwd	1532	0+sep. 1564−30; 0+sep. 1595−60; 0+sep. 1624−90; 0+sep. 533+997	
672	w	1564	0+sep. 1595−30; 0+sep. 1624−60; 0+sep. 568+997; 0+301+2×629	
703	w	1595	0+sep. 1624−30; 0+sep. 598+997; 0+333+2×629	
732	w	1624	0+629+997; 0+364+2×629	
761	w	1653	0+sep. 1754−98	
777		1669	0+sep. 1698−30; 0+sep. 1726−60	
806	w-m	1698	0+sep. 1726−30; 0+sep. 1754−60; 0+629+1074	
834	w	1726	0+sep. 1754−30; 0+629+1100	
862	vw	1754	0+629+1128	Bands from 36862 to 36989 are very difficult to measure, inaccurate.
883	ewd	1775	0+333+364+1074; 0+sep. 780+997	
910	ewd	1802	0+2×364+1074; 0+333+364+1100	
——	observed	——		Too weak and diffuse for measurement.
965	ewd	1857	0+2×364+1128	
989	ewd	1881	0+3×629	
37,016	ewd	1908	0+2×997−90	
045	vwd	1937	0+sep. 936+997	
075	vwd	1967	0+sep. 967+997	
097		1989	0+sep. 997+997	Perhaps two heads of same band and overlapping of others.
104	wd	1996		
115		2007	0+sep. 2038−30; 0+sep. 2067−60; 0+sep. 2095−90	
146	w-m	2038	0+sep. 2067−30; 0+sep. 2095−60; 0+333+629+1074	
175	w-m	2067	0+sep. 2095−30;	

TABLE I. Absorption bands of 1,2,4-trichlorobenzene.—*Continued.*

Wave numbers	Intensity	Separation from 0−0 band	Assignments	Remarks
37,175			0+997+1074; 0+333+629+1100	
203	w-m	2095	0+997+1100; 0+333+629+1128	
228	vwd	2120	0+sep. 2147−30; 0+sep. 2175−60; 0+sep. 2206−90; 0+997+1128	
255	vw	2147	0+sep. 2175−30; 0+sep. 2206−60; 0+2×1074	
283	w	2175	0+sep. 2206−30; 0+1074+1100	
314	w	2206	0+2×1100; 0+1074+1128	
339	md	2231	0+sep. 2293−60; 0+sep. 1235+997; 0+1100+1128	Reservoir at 82°C. Change in intensity scale.
——	observed	——		Too diffuse for measurement.
382	m-sd	2274	0+sep. 2367−90	Bands from 37382 to 37457 are very diffuse; strong background absorption.
401	m-sd	2293	0+sep. 1296+997; 0+sep. 2324−30	
432	m-sd	2324	0+sep. 1329+997	
457	m-sd	2349	0+sep. 1359+997	
475	md	2367	0+sep. 1370+997; 0+sep. 2464−98	
509	md	2401	0+sep. 1401+997; 0+sep. 2464−60; 0+sep. 2430−30	
538	md	2430	0+sep. 1433+997; 0+sep. 2464−30	
547	md	2439	0+sep. 2501−60	
572	w-md	2464	0+sep. 1463+997; 0+sep. 2563−98	
609	m	2501	0+sep. 2532−30; 0+sep. 2563−60; 0+sep. 2592−90; 0+4×629	
640	w-m	2532	0+sep. 1532+997; 0+sep. 2563−30; 0+sep. 2592−60; 0+333+2×1100	
671	w-m	2563	0+333+1100+1128; 0+364+1074+1128; 0+364+2×1100; 0+sep. 1564+997; 0+sep. 2592−30	
700	w-m	2592	0+364+1100+1128; 0+sep. 1595+997; 0+sep. 2685−90	
——	observed	——		Too diffuse to measure.
729	vwd	2621	0+sep. 2685−60; 0+sep. 2714−90; 0+sep. 1624+997	
765	wd	2657	0+sep. 2685−30; 0+sep. 2714−60; 0+301+2×629+1100; 0+333+2×629+1074	
793	wd	2685	0+301+2×629+1128; 0+333+2×629+1100; 0+sep. 2714−30	
822	vwd	2714	0+333+2×629+1128	
845	ewd	2737	0+sep. 2796−60; 0+2×333+997+1074	
868	ewd	2760	0+sep. 2857−98; 0+2×333+997+1100	
904	wd	2796	0+sep. 2829−30; 0+sep. 2857−60;	

TABLE I. Absorption bands of 1,2,4-trichlorobenzene.—*Continued.*

Wave numbers	Intensity	Separation from 0−0 band	Assignments	Remarks
37,904			0+sep. 1802+997;	
			0+2×333+997+1128	
937	wd	2829	0+sep. 2857−30;	
			0+629+2×1100;	
			0+629+1074+1128	
965	wd	2857	0+sep. 1857+997;	
			0+629+1100+1128	
38,000	vwd	2892	0+sep. 2988−98;	
			0+629+2×1128	
033	vwd	2925	0+sep. 2988−60	
067	vwd	2959	0+sep. 1967+997;	
			0+sep. 2988−30;	
			0+2×301+2×629+1100;	
096	vwd	2988	0+3×997	Perhaps two heads of same band.
103	wd	2995		
137	wd	3029	0+sep. 2038+997;	
			0−200+997+1100+1128	
171	wd	3063	0+sep. 2067+997	
213	vwd	3105	0+sep. 3137−30;	
			0+sep. 3166−60;	
			0−200+1074+1100+1128	
245	vw	3137	0+sep. 2147+997;	
			0+sep. 3166−30;	
			0+5×629	
274	vw	3166	0+sep. 2175+997;	
			0+sep. 3230−60	
307	ewd	3199	0+sep. 3230−30;	Bands from 38307 to the end are inaccurate.
			0+sep. 2206+997	
338	ewd	3230	0+3×1074;	
			0+sep. 2231+997	
——	observed	——		Too weak and diffuse for measurement.
383	ewd	3275	0+1074+2×1100	
420	ewd	3312	0+3×1100	

DISCUSSION AND ANALYSIS OF THE SPECTRUM

The 1,2,4-trichlorobenzene has the lowest symmetry of the halogenated benzenes. Its only symmetry element is the molecular plane σ_z perpendicular to the z axis. The molecule belongs to the symmetry groups C_s which provides only two types of electronic and vibrational levels that are symmetrical or antisymmetrical to the molecular plane. The distribution of the molecule's thirty vibrations among the two kinds of symmetry classes is given in Table II. The symbols T_z, etc. indicate, as usual, which symmetry types (or classes) correspond to translations along the coordinate axes. All vibrations are allowed in the Raman and infra-red spectrum.

Both electronic states involved in the spectrum are of symmetry A'. The symmetry class A' in the group C_s corresponds to all classes in the group D_{6h} of benzene that are symmetrical to the molecular plane. In benzene the corresponding spectrum arises from a transition $A_{1g}-B_{2u}$, and both states are symmetric to the molecular plane. The transition $A'-A'$ (see Table II) is allowed; the transition moment lies in the molecular plane. It arises from a destruction of the sixfold symmetry of benzene when substituting three halogen atoms for hydrogens in the 1, 2, and 4 positions. A transition with a moment perpendicular to the molecular plane may be found in bands in which vibrations[5] of type α'' occur singly excited.

From these simple group theoretical rules one should expect that the spectrum, resulting from an allowed transition, will have a strong 0−0 band, and numerous progressions of different symmetric vibrations and combinations between them causing bands of shorter wave-lengths than the 0−0 band. On the long wave-length side of the principal bands we expect a number of v−v transitions since the variety of low frequency vibrations with favorable Boltzmann factors is large in the trichlorobenzenes. Further towards

[5] Greek letters are used if the symbol refers to the symmetry of a vibration.

longer wave-lengths there may occur bands resulting from these vibrations excited in the ground state only. Symmetric vibrations should give rise to stronger bands than unsymmetric vibrations of similar frequencies because the former correspond to transition moments in the molecule's plane. In brief: we should expect a rather complicated spectrum. Whereas in benzene there are only two totally symmetric vibrations and in symmetric trichlorobenzene four, their number has increased to 21 in 1,2,4-trichlorobenzene. This means that the possibilities of interpreting the bands will be great, and many bands may be caused by a superposition of several different transitions.

A knowledge of the vibrational spectrum of 1,2,4-trichlorobenzene would, of course, facilitate the analysis of the ultraviolet absorption system. At present, the vibrational spectrum is incompletely known. The Raman lines given by Dadieu, Pongratz, and Kohlrausch[6] are 183(3*b*), 194(4*b*), 308(3), 329(5), 396(3), 458(4), 676(6), 814(2), 1035(5), 1098(3), 1132(3), 1152(5), 1243(1), 1564(8), 3070(3). An uncertain line at 575 is omitted because it was not confirmed by Murray and Andrews.[7] They found new, mostly very weak lines at 216(1), 489(0), 515(0), 868(0), 1375(2), 2523(2*v*), 3115(1) and 3132(1). A correlation of the observed frequencies to modes of vibration was attempted using mechanical models.[8]

In analyzing the spectrum, it is obvious that the 0−0 band (pure electronic transition) must be present in the first group toward longer waves. We assign to it the band 35108 cm^{-1} on the short wave-length side of this group. Towards longer waves, a number of bands may be found whose separations from the 0−0 band coincide fairly well with Raman frequencies. They appear under different conditions because of their different Boltzmann factors. Bands have been observed at the following separations: 200, 326, 461, 680, 1035, 1101, 1132, 1161 cm^{-1}. The band with a separation of 1035 cm^{-1} was only observed but not measured. All bands in the 1000 cm^{-1} region are extremely weak. The separations of other bands like 300, 388, 808 coincide less well with observed Raman frequencies.

Going back to the 0−0 band 35108 we should expect superimposed on the pure electronic transition vibrational transitions of symmetric carbon ring vibrations in the 1000 cm^{-1} region in analogy to the spectra of benzene and other benzene derivatives. Indeed, by comparing the first and third group of the spectrum it can be seen that the pattern of the third group is not a simple repetition of the first group but that it rather looks like a superposition of at least two repetitions but may be three or even four. It is believed that one repetition begins with the band 36105 and another with 36236, both times starting with the bands on the short wave-length side of the pattern. The intensity of the band 36182 (third band of the third group from the violet end) suggests a third repetition. The separations of these bands, in the order they have been mentioned, from the 0−0 band are 997, 1128, and 1074 cm^{-1} and they represent wave numbers of symmetric vibrations. Some of them will be mostly carbon vibrations in nature. The 997 and 1074 occur doubly and possibly trebly excited as well as in combination with each other and with the 1128 as may be seen from Table I. We have not been able to trace a progression of the 1128 because it falls in a region of many weak diffuse bands. It is plausible to assign the differences 997, 1074, and 1128 to vibrations whose frequency values in the ground state correspond to the Raman lines 1035, 1098, and 1132. Of course, a correlation of the 1128 to the Raman line 1152 cannot be excluded, particularly since it is not impossible that the band 36208 contains, among other possibilities, the transition of a 1100 cm^{-1} vibration which might correspond to the 1132 Raman line. However, such detailed decisions cannot be made with certainty.

The appearance of the second weaker group

TABLE II. Types of electronic and vibrational levels of group C_s: 1,2,4-$C_6H_3Cl_3$.

Symmetry type	Essential elements of symmetry σ_s	Number of vibrations	Selection rules Raman	Selection rules Infra-red
A'	+	21 $T_s T_y$	+	+
A''	−	9 T_s	+	+

[6] A. Dadieu, A. Pongratz, and K. W. F. Kohlrausch, Monats. f. Chem. **61**, 426 (1932).
[7] J. W. Murray and D. H. Andrews, J. Chem. Phys. **2**, 119 (1934).
[8] J. W. Murray, V. Deitz, and D. H. Andrews, J. Chem. Phys. **3**, 180 (1935).

is ascribed to the excitation of the carbon-chlorine valence vibration. Its wave number is taken from the first band at the violet end as 629. The value in the ground state is 680 (Raman value 676 cm^{-1}). The interpretation is reasonable because a vibrational frequency in this region has been found in many substances with one or more C−Cl bonds. The vibration 629 occurs in a progression, five members of which may be recognized. Combinations with the vibrations in the 1000–1100 region may be found in Table I.

The pattern of an individual group may best be studied from the first group. The measurements reveal that the distances between adjacent bands are mostly about 30 cm^{-1} and that a prominent separation from the 0−0 band is about 98 cm^{-1}. It is obvious that such small frequency separations must represent differences between vibrations in the ground and upper electronic states. These vibrations must have small frequencies because of the great intensity of the bands. It was mentioned before that a number of such vibrations appears excited in the ground state. The bands of the "group" are much stronger than these bands. This means, that 1−1, 2−2, etc. (v−v) transitions of these vibrations must be stronger than 1−0 or 0−1 transitions of the same vibrations. This can be understood from the Franck-Condon principle if the "potential curves" of these vibrations in the two electronic states have their minima practically one above the other. That the minima lie one above the other is a requirement for non-symmetric vibrations, and in 1,3,5-trichlorobenzene, for example, these small vibrations are non-symmetric. It is plausible to assume similar conditions in the 1,2,4 derivative. Which vibrations are involved in the v−v transitions cannot be decided from the group pattern alone. Additional information may be expected from the bands between the first and second group since they should contain these vibrations excited in the upper electronic state. As to the nature of these vibrations, it is plausible to associate them mostly with motions of the chlorine atoms.

The bands between the mentioned groups are weak, but some of them stand out more than others, namely the bands 35148, 35216, 35249, 35374, 35409, 35441, and 35471. These bands are distant from the 0−0 band by 40, 108, 141, 266, 301, 333, 364 cm^{-1}, respectively. If we tentatively correlate the 364 with the 461 vibration in the ground state, this would mean a drop of 97 cm^{-1} (94 if the Raman value 458 is used) in the upper electronic state. The interpretation would gain support if bands could be found displaced by 97 (or 94) cm^{-1} to the red from the main bands. Indeed, a strong band is observed 98 cm^{-1} away from the 0−0 band and similar bands can be found on the long wave side of many strong bands. The 2−2 transition of the 461 vibration (2×98) falls on top of the band 34909 with the separation 200 cm^{-1} which was considered before as a ground state vibration. A band appears also where the twofold excitation of the 364 vibration is expected, furthermore in places calculated from combinations of the 364 with the 1000–1100 and 629 vibrations.

In a similar way we may pick the band 35409 (0+301) and correlate it with the ground state vibration of 326 cm^{-1} (Raman value 329), thus obtaining a 1−1 transition of about 30 cm^{-1}. Many bands with separations of about 30 cm^{-1} to the red from strong bands may be interpreted in this fashion. Differences of about 60 cm^{-1} may be considered as 2×30 or 2−2 transitions.

A 60 difference may be derived also from the band 35441 (0+333) by correlating it with the ground state vibration 388 (Raman value 396). The necessity of a 60 difference cannot be concluded from the group pattern because the intensities of the bands are only rough estimates.

An observed difference of 90 cm^{-1} may result from 3−3 transitions involving the separation of 30 cm^{-1}, or from a combination of the 30 and 60 differences, or may represent a new difference.

Attempts of interpretation of the kind just mentioned must be regarded as possibilities only but not as certainties. Differences of 30, 60, 90, 98 cm^{-1} can be obtained in various ways by using different vibrations in connection with the bands between the first and second group. They may represent 1−1, 1−2, 2−1, etc. transitions of the same or different vibrations. Also, many bands between the first two groups can be obtained simply by superposing the symmetric vibrations of 629, 997, etc. on the very weak bands (0−326 for example, and others) of the red end of the spectrum, or by superposing different small ground state vibrations on the

transitions constituting the second and third groups. The interesting fact is that, once the first group and the bands between the first and second groups are explained, the remainder of the spectrum is obtained by superposing on these bands the first discussed symmetric vibrations of larger wave numbers. Of course, there will be some bands which may represent a single vibrational transition of another symmetric vibration not yet used, as perhaps the band 36467. This band may correspond to the excitation of a 1359 vibration besides involving other transitions. But on the whole the bands beyond the third group toward shorter waves result from the before mentioned superpositions.

The results of our analysis are included in Table I under Assignments. In cases where a band is interpreted, in one or more ways, as a combination of several frequencies it was often found convenient to abbreviate these combinations by just giving the separation from the 0−0 band as sep. . . . when it occurs combined with still other frequencies (for example, 0+sep. 2095 in band 37175 stands for the assignments 0+997+1100 and 0+333+629+1128 of band 37203). This is particularly convenient in connection with the repeatedly occurring differences of 30, 60, 90, and 98 cm^{-1}. In the calculations the frequency values found from the spectrum have been used and not the Raman values. We consider the interpretations as reasonably safe in which the 629 vibration and the vibrations in the 1000–1100 cm^{-1} region are used, furthermore interpretations in which ground state vibrations known from Raman lines are used. Ambiguities arise when it comes to an explanation of the 30 and 98 cm^{-1}, etc. differences, and of the weak bands between the first and second groups. Possible effects of anharmonicities have been neglected in the numerical calculations.

TABLE III. Differences between frequencies of some low vibrations in the lower and upper electronic states.

Ground state \ Upper state	108	301	333	364
200 (*R*196)	*− 92*	+101	+133	*+164*
326 (*R*329)	−218	*− 25*	+ *7*	*+ 38*
388 (*R*397)	−280	*− 87*	*− 55*	*− 24*
461 (*R*458)	−353	*−160*	*−128*	*− 97*

In the assignments presented here only a few vibrations of small frequency values have been used. The correlation between their values in the two electronic states may be seen from Table III. The numbers in italics refer to interpretations used in Table I. We wish to emphasize again that the correlation scheme in Table III is one among other possibilities. It is given here as an interesting example that a complicated spectrum like the one treated here may be interpreted using relatively few different vibrations. More information might be obtained from exposures using higher dispersion combined with better intensity measurements, and from a comparison with the dichlorobenzene spectra some of which are also rather regular in appearance.

The experimental part of this research was carried out during the summers of 1941 and 1942. We gratefully acknowledge its support by grant-in-aids from the Rockefeller Foundation and from the Duke University Research Fund.

JOURNAL OF THE OPTICAL SOCIETY OF AMERICA VOLUME 39, NUMBER 1 JANUARY, 1949

Preparation and Application of Reproducible Gloss Standards*

DANIEL SMITH AND MARIE M. MAHONEY
Interchemical Corporation, Research Laboratories, New York, New York

(Received October 11, 1948)

A polystyrene replica technique, similar to that employed in electron microscopy, has been used to prepare extremely thin films of identical surface structure. These thin transparent films can be transferred to any desirable surface. Replicas made from gloss standards are shown to be reproducible in surface structure and spatial reflectance characteristics.

A PROGRAM has been undertaken to determine and study the factors involved in the visual evaluation of gloss. Some of the more obvious factors, other than the microscopic structure of the surface, which might influence visual evaluation of gloss are surface chromaticity, total luminous reflectance, mode of illumination and viewing, and luminant chromaticity. Any insight into the mental integration of these factors, which precedes the observer's statement of evaluation of gloss, must necessarily remain for that time in the future when each of the influencing factors will have been studied in detail from a physical point of view and statistical comparison made with visual evaluations.

It would be desirable to establish a psychophysical basis for the quantitative evaluation and specification of gloss, somewhat similar to what has been done in the field of color evaluation and specification.

The sample preparation techniques developed by the authors will facilitate the design of experiments directed toward the achievement of a useful psychophysical correlation. It would be desirable to be able to change the dominant wave-length, excitation purity, and/or total luminous reflectance over the whole visible range while maintaining some aspect of the gloss of the samples constant. A polystyrene replica technique similar to that being used extensively by the electron microscopists for surface studies, provides this flexibility to the present method for sample preparation. These surface replicas may be transferred and mounted on any base having the desired spectral reflectance characteristics.

PREPARATION OF ORIGINAL SURFACES AND REPLICAS

Several black Carrara glass blocks were ground together in pairs, using levigated FFF carborundum, until the surfaces were completely uniform. These ground blocks were then individually polished on a polishing wheel until the desired degree of gloss was obtained on the basis of either instrumental or visual evaluation.

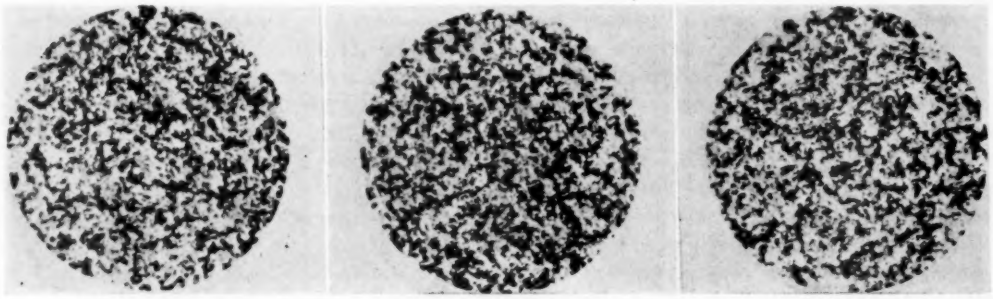

Original Replica on Black Replica on Gray

FIG. 1. Photomicrographs (epi illumination). Original gloss standard and two polystyrene replicas. ASTM gloss index "A" of black glass original = 7.9

* Presented at the O. S. A. Meeting in Cincinnati, October, 1947.

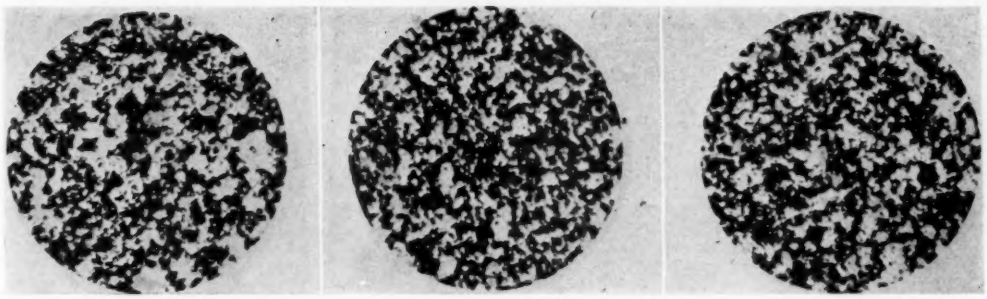

Original Replica on Black Replica on Gray

FIG. 2. Photomicrographs (epi illumination). Original gloss standard and two polystyrene replicas. ASTM gloss index "A" of black glass original = 20.6

Replicas of the surfaces of these blocks were prepared by whirler coating with a solution of approximately 4 percent Dow polystyrene YAR K77 CLEAR in xylene. The final concentration was adjusted by the addition of solvent until smooth films free of striations and orange peel were obtainable. The replica films so prepared were about two ten thousandths of an inch thick.

A special holder was made for rotating the individual blocks on the shaft of the polishing wheel motor. The polystyrene solution was poured in sufficient amounts to completely cover the surface of the block. During the subsequent spinning, the block was completely enclosed to maintain a dust-free atmosphere.

The blocks were spun and stopped alternately for 15-second intervals during a period of 2 minutes, after which they were spun continuously for 5 minutes, and then they were uncovered to dry at least an additional 10 minutes without spinning.

The removal of the dried polystyrene replica from the original was accomplished with great facility by scoring the edge of the replica and immersing the composite in a dilute aqueous solution of Aerosol OT. This solution enters the interface between the original and the replica to eliminate completely the adhesion between them.

The loosened replica was then turned over onto a suitable base (in this case Carrara glass blocks were used) covered with an aqueous solution of 2 percent gelatin and 1 percent glycerine. The replica surface was uppermost at this stage. Excess gelatin solution was wiped away and the film gently flattened out by swabbing with a dampened blotter from the center of the replica outward to the edges. The replica surface was then wiped with wet cotton and allowed to dry completely.

The gelatin-glycerin solution acts as an adhesive which can be applied very thin so that

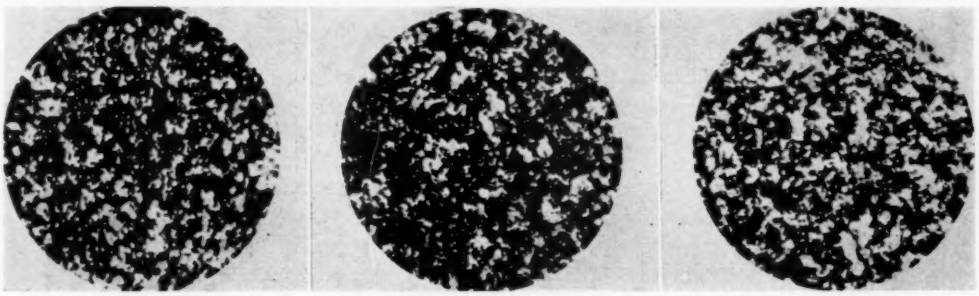

Original Replica on Black Replica on Gray

FIG. 3. Photomicrographs (epi illumination). Original gloss standard and two polystyrene replicas. ASTM gloss index "A" of black glass original = 26.9

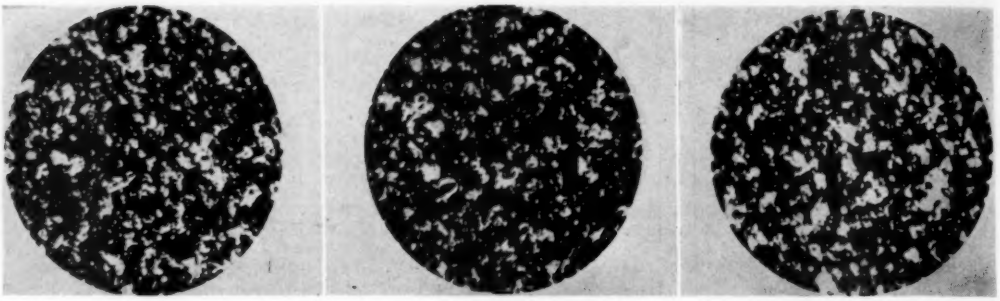

Original Replica on Black Replica on Gray

FIG. 4. Photomicrographs (epi illumination). Original gloss standard and two polystyrene replicas. ASTM gloss index "A" of black glass original = 29.9

the replica surface becomes essentially an integral part of the base to which it is applied.

EVALUATION OF REPRODUCIBILITY

The reflectance characteristics and surface structure of replicas made by this method were evaluated goniophotometrically, and microscopically using epi illumination. The faithfulness with which the original surfaces were reproduced by the replicas was evaluated after simultaneously vacuum aluminizing the surfaces until brightness differences were no longer apparent between black and light gray samples.

Goniophotometry and photomicrography of the aluminized surfaces served to evaluate any differences in surface structure. The replicas, of course, are negatives of the original. These should not be readily distinguishable with epi illumination, but might reasonably be expected to differ somewhat goniophotometrically.

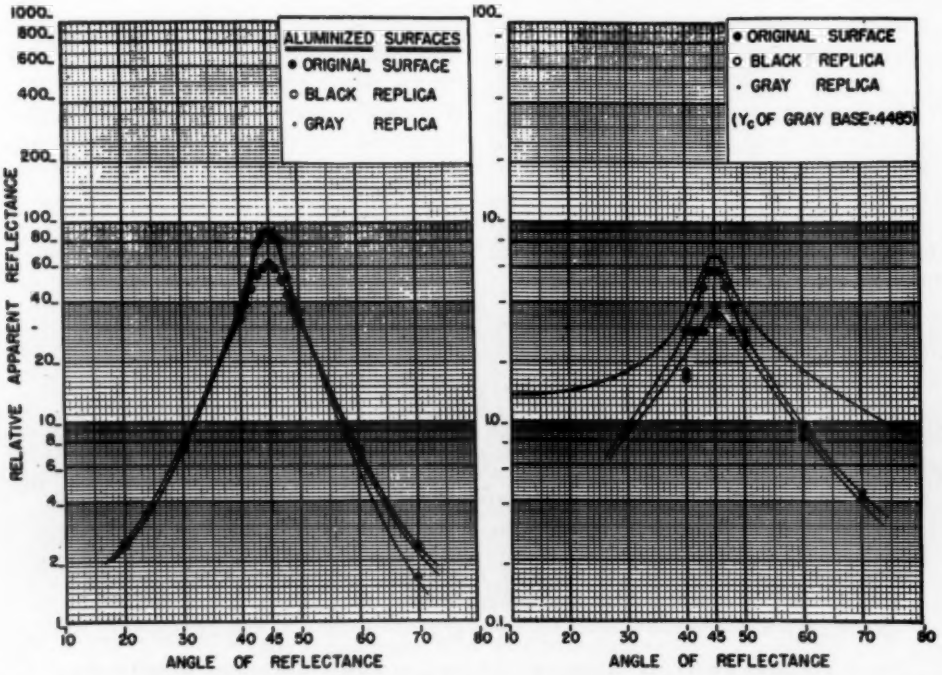

FIG. 5. Goniophotometric curves. 45-degree incident illumination. ASTM gloss index "A" of black glass original = 7.9

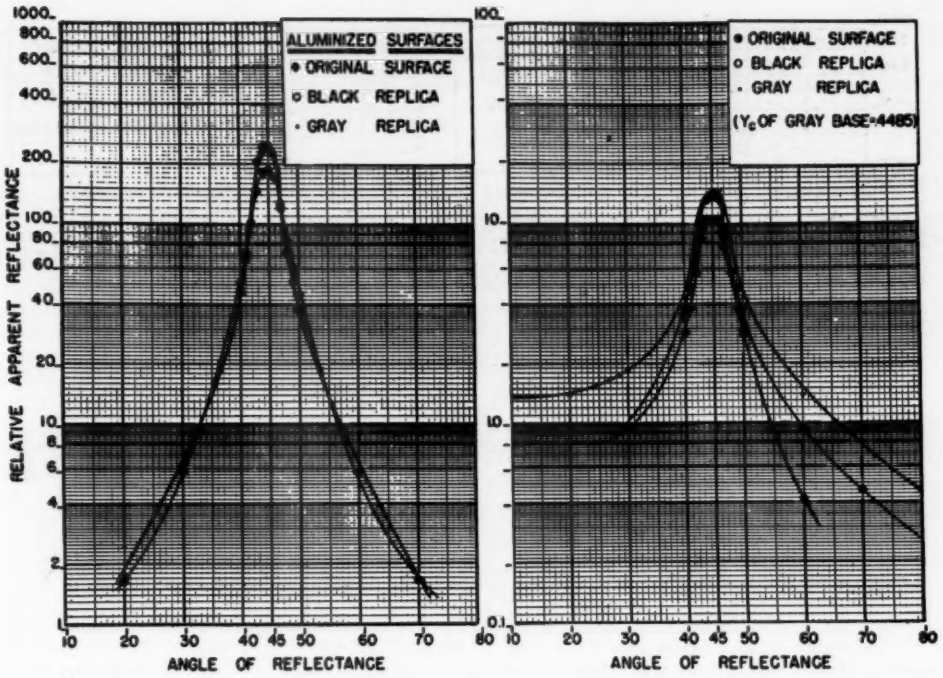

FIG. 6. Goniophotometric curves. 45-degree incident illumination. ASTM gloss index "A" of black glass original = 20.6

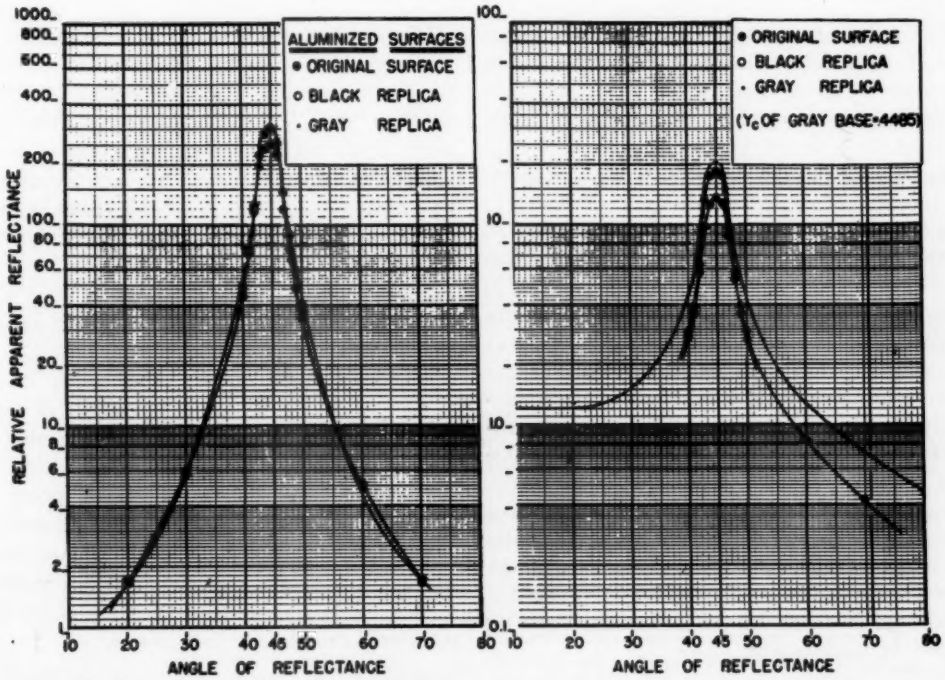

FIG. 7. Goniophotometric curves. 45-degree incident illumination. ASTM gloss index "A" of black glass original = 26.9

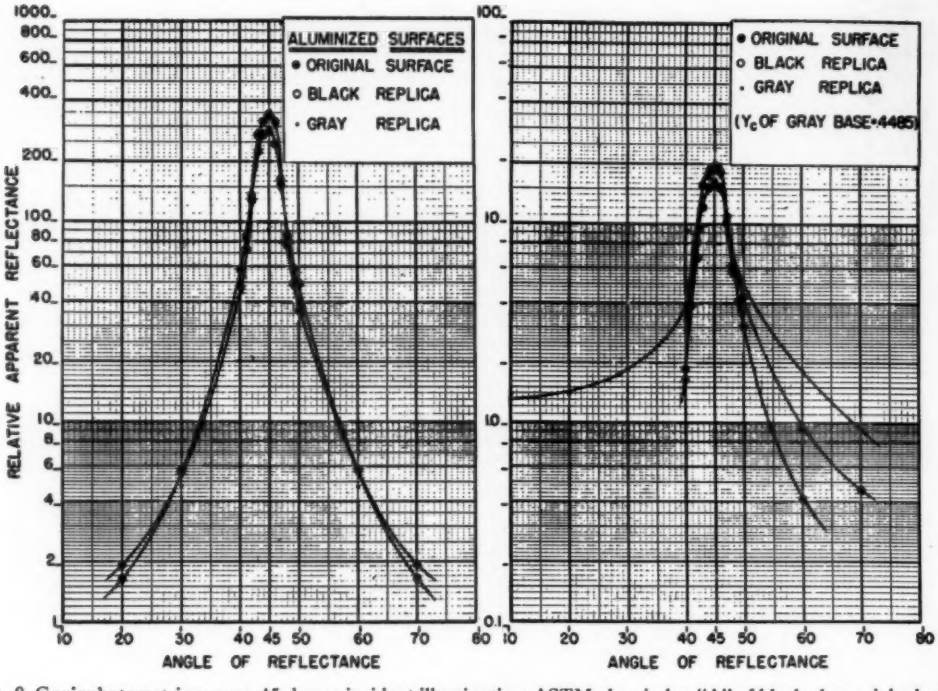

FIG. 8. Goniophotometric curves. 45-degree incident illumination. ASTM gloss index "A" of black glass original = 29.9

The photomicrographs reproduced herewith (Figs. 1, 2, 3, and 4) show the similarity between the original and the replicas.

The goniophotometric measurements were made on an instrument of the type described by Moon and Lawrence** employing slits following the recommendations of A.S.T.M. D 523–44T, Procedure *A*. The area of the sample illuminated by the incident beam at normal incidence was approximately $\frac{1}{16}'' \times \frac{3}{8}''$. This area is about 250 times that shown in the accompanying photomicrographs.

Goniophotometric curves plotted for the aluminized surfaces (Figs. 5, 6, 7, and 8) are practically identical for the pairs of replicas and generally somewhat higher at the peak reflectance than the original from which they were made. Measurements were also made for these surfaces before they were vacuum aluminized to evaluate the effect of the brightness difference. These curves are reproduced along with those for the aluminized surfaces, the latter being of greater interest at the moment.

With this technique, it will be possible to prepare adequate samples for studies leading to the development of a psychophysical correlation between "gloss" and "glossiness", as these terms were employed by Judd.*** Samples having identical geometrical surface characteristics can be prepared and located anywhere on the color mixture diagram, limited only by the availability of the colored base on which to mount the surface replicas. This provides a means for evaluating the influence of chromaticity on visual gloss evaluation.

An immediately useful application of this technique would be the preparation of goniophotometrically identical surfaces in multiple for purposes of instrument calibration.

It is hoped that this technique will prove useful to others interested in the experimental investigations necessary for the ultimate attainment of an adequate psychophysical correlation for the evaluation and specification of the gloss of colored samples.

** Moon and Lawrence, J. Opt. Soc. Am. **31**, 130 (1941).

*** D. B. Judd, Am. Dyest. Reptr. **26**, 234 (1937).

Letters to the Editor

Multibanded Emission Spectra of Zinc-Cadmium Sulfide Phosphors

W. H. BYLER
United States Radium Corporation, New York, New York
October 4, 1948

THE existence of multibanded emission spectra of zinc sulfide and zinc-cadmium sulfide phosphors found by the writer[1] using photographic recording has been questioned by Studer and Larson.[2] They used photocell recording and reported inability to confirm the results of the writer. They also cite the work of others who have reported single band spectra.

We have continued our work and now report qualitative confirmation of our earlier results along with an explanation for the discrepancies between reported spectra.

Emission spectra of zinc sulfide phosphors are subject to a number of variables. In many cases, the color shifts toward blue with increase in intensity of excitation. In most cases, the color shifts toward red with increase of temperature. In specimens in which self-excitation occurs, the color is a function of layer thickness. The type of excitant may cause variation of color. Different workers are not likely to obtain quantitative agreement unless all conditions are duplicated.

But we are concerned here with a significant qualitative difference which seems to be due to difference in method of recording the spectra. It should be mentioned that many published spectra were obtained with cathode-ray excitation, a method which tends to smooth out the curves resulting from internal heating. Also, most published spectra are those of copper or silver-activated phosphors which generally show less separation of bands than the non-activated or gold-activated specimens.

For the present work, light from a Bausch and Lomb spectrophotometer sphere at a color temperature of 2765°K was used as standard light source. Since seven spectra could be recorded conveniently on each film, it was possible to calibrate each film directly with proper matching of densities for unknown and standard.

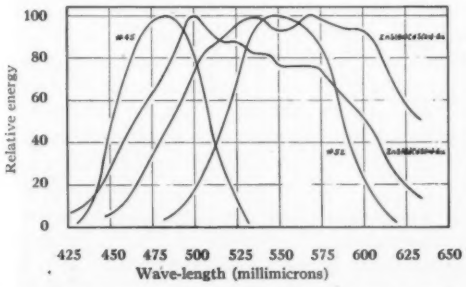

FIG. 1. Relative energy curves of two phosphors and of standard source filtered through two Wratten filters.

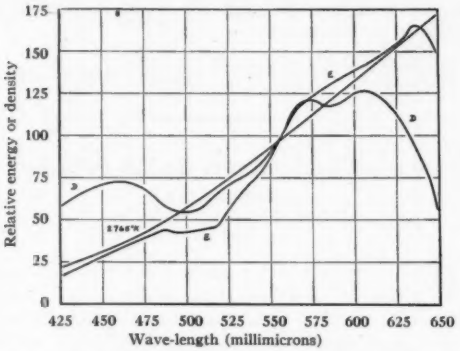

FIG. 2. Effect of variation in density on resultant spectra. Curves are brought together at 5550A. *D* is the relative density curve for standard source (2765°K) yielding density 0.685 at 5550A. *E* is relative energy curve calculated for standard source exposure with density 0.39 at 5550A using calibration from above exposure.

In order to demonstrate the existence of structure in some of the phosphor spectra, the spectra of known structureless sources were recorded on the same film. Some of the results are shown in Fig. 1. The known structureless sources were obtained by filtering the standard 2765°K light through selected Wratten filters. Peak densities for the unknown sources were in each case made to correspond closely to the densities for the standard source at those positions. Peak densities for the No. 52 filter and for both phosphors lie near 5700A. Reproduction of the filtered sources is rather faithful with slight distortion of the No. 52 source around 5700A. It is clear that there is structure in the phosphor spectra.

The photographic method is able to reveal structure which may be overlooked with the photo-cell method because the film fault which is responsible for low density failure of the reciprocity law is responsible here for amplication of the secondary peaks. This effect is shown in Fig. 2. The film was calibrated on the basis of the relative density curve shown, for which the net density at 5550A was 0.685. The calibration is the ratio of the 2765°K energy curve to the density curve. When treated as an unknown, an exposure on the same film yielding density 0.39 at 5550A gives the curve shown. This shows why densities for unknown and standard should be kept in the same range. It shows also that whenever the unknown densities are below those used in the calibration, the high density regions are amplified relative to neighboring low density regions. This effect is apparently independent of variations in film sensitivity as such (Tri-X panchromatic).

It is obvious that variations of film sensitivity cannot account for the structure in the phosphor spectra of Fig. 1. However, it is found in some cases that this does cause distortion, especially in the region of the 5700A sensitivity peak. Use of a standard source with spectrum similar to

that of the unknown would be the ideal arrangement. In any case, whenever there is a question about the reality of an indicated inflection in the unknown source, it can be checked against a calibration for which the density for the standard source is about the same as that for the unknown in that region.

[1] W. H. Byler, J. Opt. Soc. Am. **37**, 920 (1947).
[2] F. J. Studer and D. A. Larson, J. Opt. Soc. Am. **38**, 480 (1948).

On the Mechanism of Optical Polishing

KAMALESH RAY
831 Pearl Street, Boulder, Colorado
September 16, 1948

THE question whether rouge polishes by its cutting action or by softening the superficial skin of the glass still remains open since the time of Herschel. Interesting discourses have been published on the subject, some of which are referred to at the end of this note.

The chemical examination of spent rouge shows some amount of silica coming out of glass, but not enough to account for the total polish. Other experiments indicate that "filling up" process through softening of the glass surface is definitely involved, and calculations show that a sufficient amount of heat through polishing friction is available for the purpose. It has been said that rouge is softer than glass, and therefore cannot "cut" the glass in the usual sense of the term. Further the polishing laps (pitch, resin compound, felt, etc.) play important part both in speed and quality of the polish.

If rouge particles act as tiny cutters, the surface of a rouge-polished glass is likely to show fine scratches under a powerful microscope. Lord Rayleigh tried microscope at 500× but failed to detect such structure on the surface. The present author tried replica of a half-polished glass under an electron microscope but no scratches were revealed at magnifications of 8000 to 20,000 of the polished facets (no gold shadow used). It was also observed that the unpolished pits, left by the fine abrasive, had more rounded look at their edges.

Examination of fresh and spent rouge samples under the electron microscope did not tell much in the conclusive. However, the spent rouge seemed to be better dispersed and had more rounded corners than the fresh ones. The particle sizes vary, but mostly around $\frac{1}{4}\mu$.

Both the samples of rouge were found to contain some light flaky particles, hexagonal in shape, which were usually much larger than the rouge particles. It would be a little too drastic to identify them as silica particles coming from the glass or extraneous sources.

It would be interesting to mention some of the observations (unpublished) made by Dr. J. A. Anderson of the Mt. Wilson Observatory. Some of the Mt. Wilson's old lenses showed surface cracks which were extremely fine. Dr. Anderson measured the depths of these hair-cracks optically and found them to be about 30-wave-lengths deep. Such hair-cracks have also bee observed on old telescope lenses in different parts of the world, and it is thought that the periodic (diurnal, especially) heating and cooling over span of years might have caused them. This effect may possibly be ascribed to fatigue-failure of the surface layer if the layer was rendered weaker in the process of polishing.

Dr. Anderson reproduced such surface cracks in the laboratory by heating ordinary lenses to 100–120°C and subsequently chilling them on a cool metal plate. The depths of such cracks were also found to be of the same order as the natural cracks.

These observations suggest that the skin of a rouge-polished lens has physical properties different from the bulk of the lens body. This may be possible if the polishing takes place through thermal (softening) action at the superficial layer.

My thanks are due Dr. J. A. Anderson, Astrophysics Department, California Institute of Technology, for his valuable discussions, and to Mr. B. L. Henke, Physics Department, for his kind cooperation in taking the electron microscope pictures.

BIBLIOGRAPHY: (1) G. J. Beilby "Flow theory," Trans. Opt. Soc. London **9**, 22 (1907).
(2) J. W. French "Flow of beta layer," Trans. Opt. Soc., 1916 (1917).
(3) Lord Rayleigh "Microscopic study of optical surface," *Collected Papers*, Vol. 4, p. 542.
(4) Selby and Lowers "Chemical examination of spent rouge," Sci. Am., pp. 336–38 (December, 1938).
(5) E. Thomson "Round bottom scratch by rouge," J. Opt. Soc. Am. **6**, 843 (1922).
(6) General discussions of the polishing theories—Amateur Telescope Making, Sci. Am. pp. 326–333.